SW Spain Ore Deposits
Field Guide

ETH zürich

UNIVERSITÉ TOULOUSE III PAUL SABATIER

SEG Student Chapter ETH Zürich

Field guide

SW Spain Ore Deposits

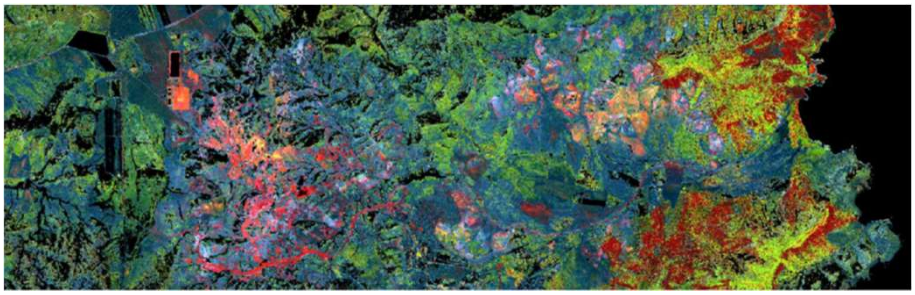

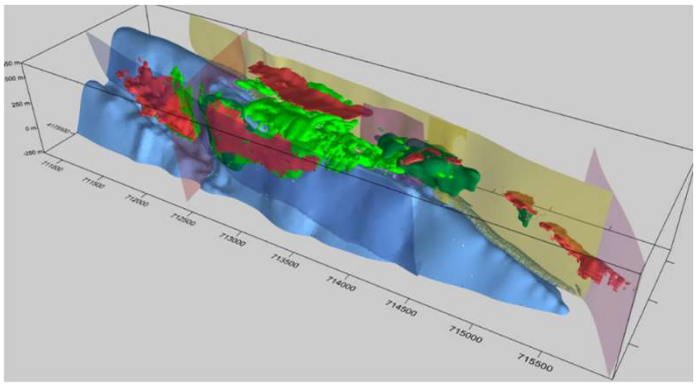

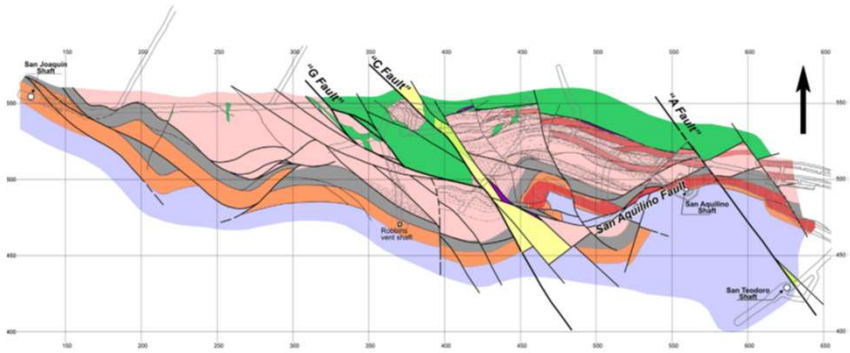

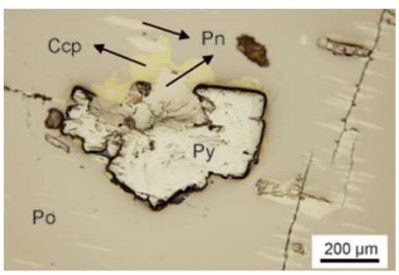

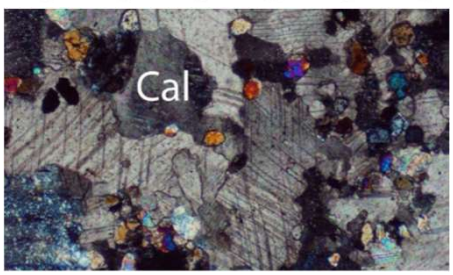

Edited by Julian Reyes and Cyrielle Bernard
Institute of Geochemistry and Petrology
19 – 28 April, 2019

Acknowledgements

matsa
A MUBADALA & TRAFIGURA COMPANY

Atalaya MINING

valoriza minería

Figures of (top-left to bottom-right): **1.** Absorption depths of the 1st, 2nd and 3rd feature, displayed in an RGB color composite. From van der Meer, F., et al. (2018). "Wavelength feature mapping as a proxy to mineral chemistry for investigating geologic systems: An example from the Rodalquilar epithermal system." International Journal of Applied Earth Observation and Geoinformation 64: 237-248. **2.** Native gold on quartz matrix from Rodalquilar, Níjar, Almeria, Andalusia, Spain. From https://www.minfind.com/mineral-591663.html (retrieved on 11.03.2019). **3.** Chromitite on the Ronda ultramafic complex from González-Jiménez, Jose & Griffin, W & Proenza, J & Gervilla, Fernando & O'Reilly, Suzanne & Akbulut, Mehmet & J. Pearson, Norman & Arai, Shoji. (2014). Chromitites in ophiolites: How, where, when, why? Part II. The crystallization of chromitites. Lithos. 189. 140-158. 10.1016/j.lithos.2013.09.008. **4.** 3D geological model of the Rio Tinto VMS deposits. From Martin-Izard, A., et al. (2016). "Ore deposit types and tectonic evolution of the Iberian Pyrite Belt: From transtensional basins and magmatism to transpression and inversion tectonics." Ore Geology Reviews 79: 254-267. **5.** Goethite from Cerro Colorado, Rio Tinto Mines, Huelva, Andalusia, Spain. From https://www.mindat.org/photo-397110.html (retrieved on 11.03.2019). **6.** Mercury on cinnabar from Almadén Mine, Almadén, Ciudad Real, Castile-La Mancha, Spain. From https://www.mindat.org/photo-226733.html (retrieved on 11.03.2019). **7.** Geological map of western part of 14th Level, Almadén Mine. From Palero-Fernandez, F. J., et al. (2015). "Geological context and plumbotectonic evolution of the giant Almaden Mercury Deposit." Ore Geology Reviews 64: 71-88. **8.** Epidote, quartz and andradite from Aguablanca Mine, Monesterio, Badajoz, Extremadura, Spain. From https://www.mindat.org/photo-225928.html (retrieved on 11.03.2019). **9.** Reflected-light optical micrographs in semi-massive ore samples from the Aguablanca Ni-Cu sulphide deposit; Py, pyrite; Po, pyrrhotite; Pn, pentlandite; Ccp, chalcopyrite. From Pina, R., et al. (2013). "Platinum-group elements-bearing pyrite from the Aguablanca Ni-Cu sulphide deposit (SW Spain): a LA-ICP-MS study." European Journal of Mineralogy 25(2): 241-252. **10.** Photomicrographs of a marble (cross-polarized light). From Ganino, C., et al. (2014). "Metamorphic degassing of carbonates in the contact aureole of the Aguablanca Cu-Ni-PGE deposit, Spain." Contributions to Mineralogy and Petrology 168(3): 21.

Field Guide:
SW Spain Ore Deposits

Contributions

The contributions to the field guide were compiled from the literature by the students of the society of economic geologists (SEG) student chapter of ETH Zurich and Universite Toulouse III Paul Sabatier, who take responsibility for correct referencing of data sources, to the best of their knowledge. There is no own research beyond the literature study involved.

Support

We gratefully acknowledge the financial support by the Institute of Geochemistry and Petrology of ETH Zurich. We appreciate the logistical and scientific support of Dr. Lola Yesares, Dr. Fernando Tornos and, current Ph.D. student, Leslie Logan.

Published in the ETH Research Collection, April 2019, © ETHZ 2019

ISBN: 978-3-906916-59-0
DOI: 10.3929/ethz-b-000340437

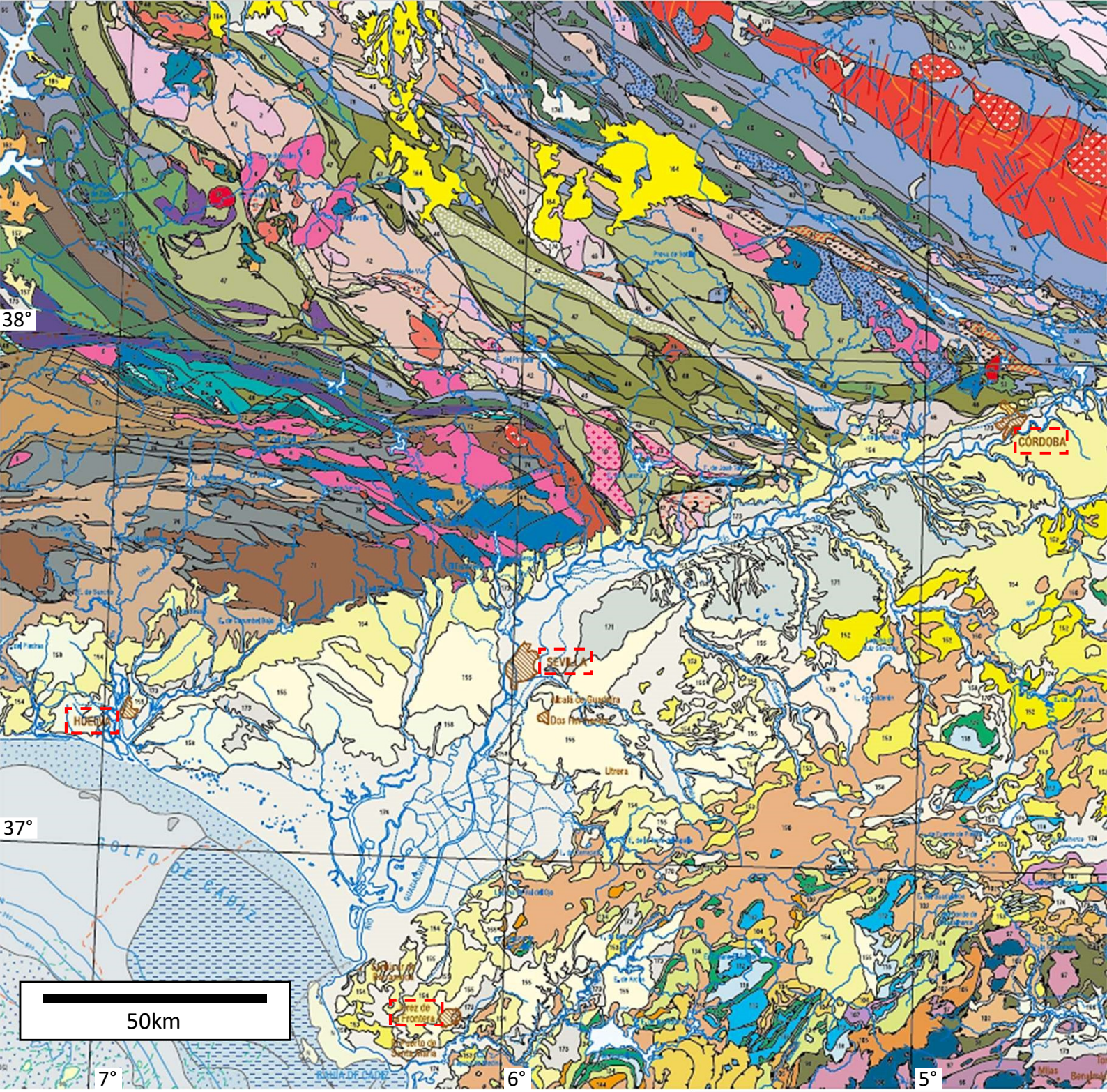

MACIZO VARISCO IBERICO

ZC Zona Cantábrica
ZAOL Zona Asturoccidental-Leonesa
ZCI Zona Centroibérica
ZOM Zona de Ossa Morena
ZSP Zona Surportuguesa
P.C. Pirineos y Catalánides

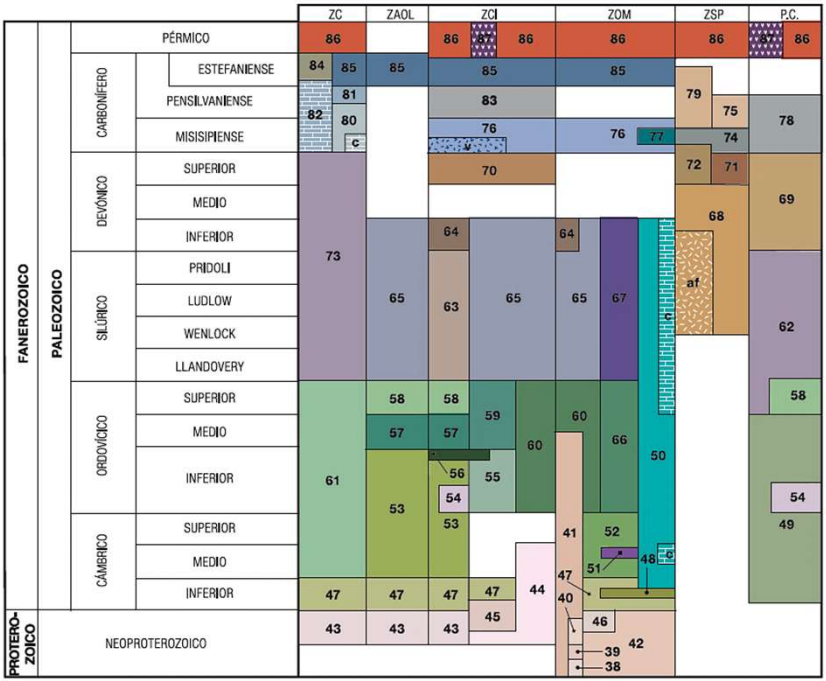

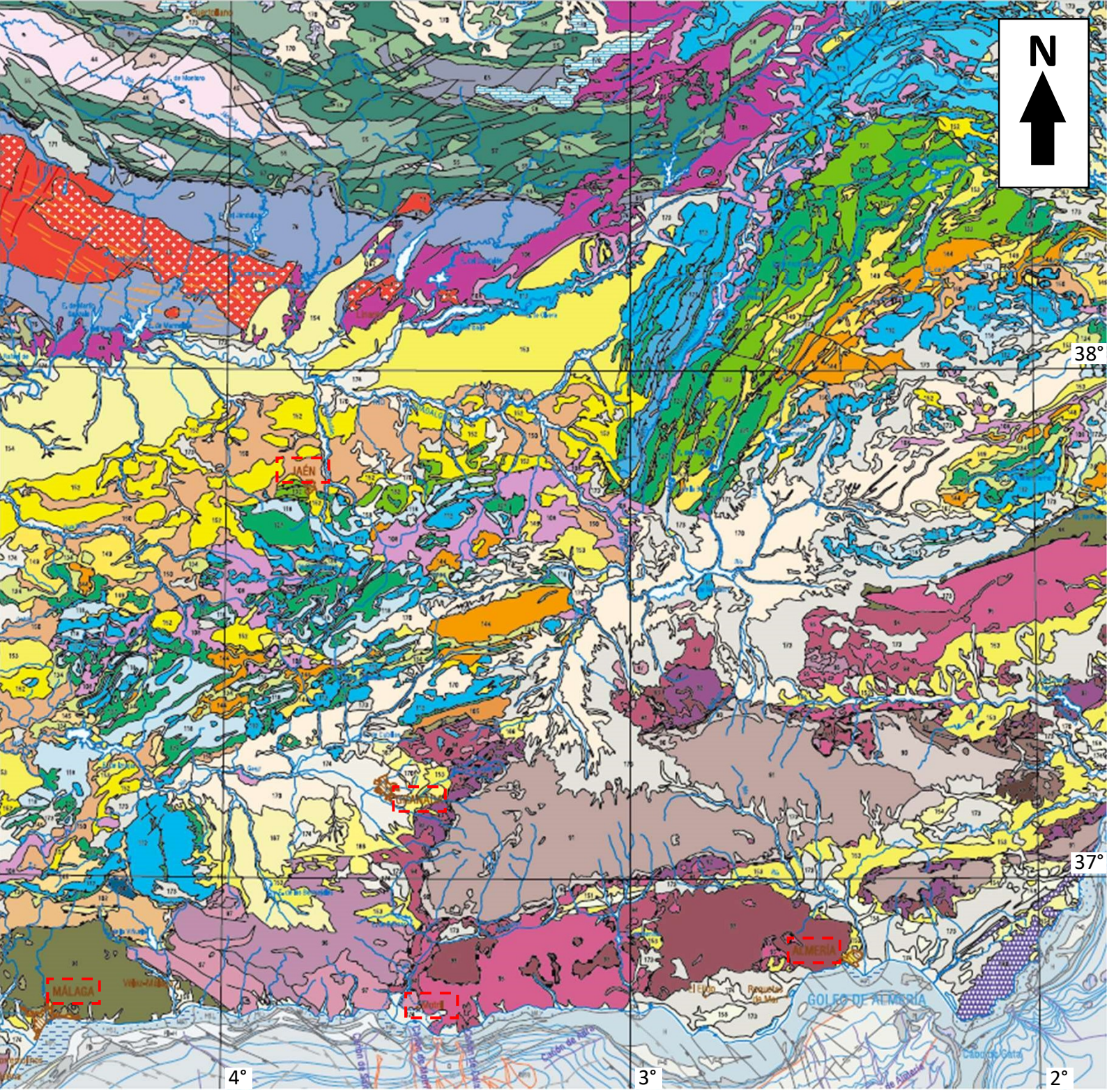

UNIDADES ESPECÍFICAS DE LA CORDILLERA BÉTICA Y DEL RIF

				CAMPO DE GIBRALTAR	ZONAS INTERNAS: COMPLEJO MALÁGUIDE Y GHOMÁRIDE	ZONAS INTERNAS: COMPLEJO ALPUJÁRRIDE Y SÉBTIDE	ZONAS INTERNAS: COMPLEJO NEVADO-FILÁBRIDE
CENOZOICO	NEÓGENO	MIOCENO	MED.				
			INF.	105	99	100	
	PALEÓGENO			104			
				103			
				102			
				101			
MESOZOICO	CRETÁCICO						
	JURÁSICO					97	
	TRIÁSICO	SUPERIOR				96	
		MEDIO				94	
		INFERIOR				92	
PALEOZOICO	PÉRMICO				98	95	91
	CARBONÍFERO	PENSILVANIENSE				93	90
							89
							88

Contents

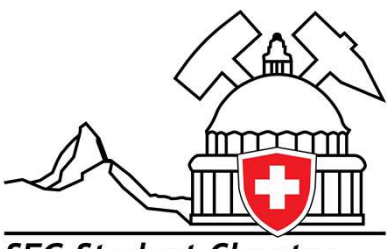

1. Geology of southern Iberian Peninsula

Gaétan Link

Introduction

The Iberian Peninsula, also known as Iberia, is located at the southwest of Europe. It outcrops one of the most complete Paleozoic sedimentary successions in Europe in the western (Iberian Massif) and northern massifs (Cantabrian Massif and Pyrenees) (Gibbons and Moreno, 2002). These rocks have been deformed and metamorphosed during the Variscan orogenesis (380-280 Ma). The center and the eastern Iberia consist of sedimentary basins filled by Mesozoic and Cenozoic sediments. The Peninsula is delimited by the Pyrenees belt at the North, which formed during the collision between Iberia and Europe, and the Betic and Catalan coastal ranges at the East, which formed during the western Mediterranean opening and the collision between Iberia and Africa (fig.2).

Geological evolution

Originally, Iberia was a promontory of the northern margin of Gondwana made of a Proterozoic basement. This particular position formed the Iberian-Armorican arc of the Variscan orogen (fig.1). Gondwana and Laurussia collided in Carboniferous times, which closed the Rheic Ocean and formed the Variscan orogen. The Paleozoic sedimentary succession of Iberia was overthrusted to the north by allochthon nappes and accreted blocs. Iberia is affected by a polyphased deformation and crustal thickening, which induced a barrovian metamorphism. During the Carboniferous-Permian transition, a second LP/HT metamorphism phase induced crustal partial melting and formation of syn-deformation granitoids, related to extension tectonics.

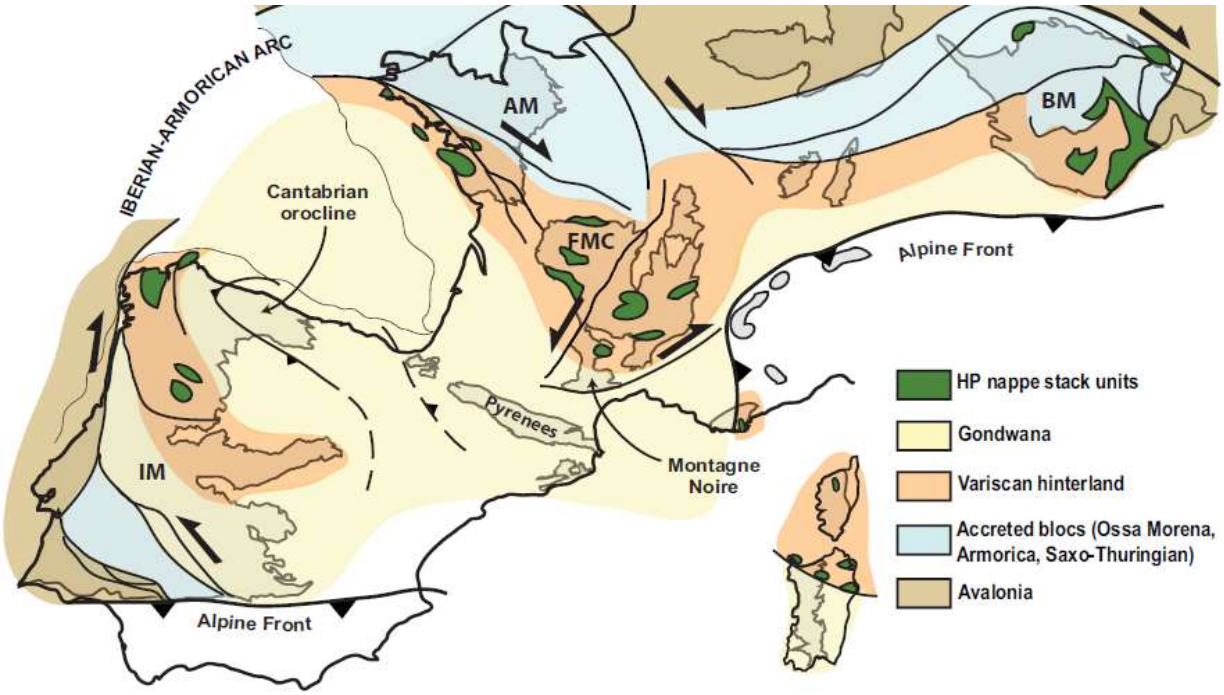

Figure 1: Sketch structural map of Variscan belt of Europe (after Cochelin et al. 2017).

The Variscan belt collapsed during the Permian period and formed fault-related continental sedimentary basins, where acidic volcanism is active. The opening of the Neo-Tethys at the Triassic period separated Iberia to the rest of Gondwana, as it were progressively isolated from Europe by the early rifting of the Bay of Biscay at the beginning of the Jurassic period. During the Mesozoic, Iberia was a subsident area with intracratonic basins that formed epicontinental seas. These basins were mainly filled by marine carbonate deposits. Only a western landmass (the so-called Iberian massif) remained. During the Cretaceous period, Iberia was separated from Europe due to the opening of the Bay of Biscay, following a counterclockwise rotation. As a consequence

of the northward cinematic of Africa, Iberia moved to the North and collided Europa during the Cenozoic and formed the Cantabrian-Pyrenees belt. The collision between former continental blocks of the western Mediterranean and southern Iberia formed the Betic and Rif Cordilleras.

Iberian massif

The Iberian massif is the main geological unit of the western Iberia. The Variscan basement is exhumed and three main structural units have been recognized: the Central Iberian Zone, the Ossa Morena Zone and the South Portugese Zone (fig.3).

Figure 2: Simplified geological map of Iberian peninsula (modified after PePeEfe, Wikimedia Commons, https://commons.wikimedia.org/wiki/File:Iberian_Peninsula_geological_map_EN.svg, CC-BY-SA 4,0)

Central Iberian Zone

The Central Iberian Zone (CIZ) corresponds to the former northern Gondwana margin. The CIZ have been deformed and metamorphosed during the Ediacaran Cadomian orogeny. During the Paleozoic, the area was a

passive margin along a rifting zone, in proximal position, with clastic sedimentation (López-Guijarro et al. 2008). The CIZ was affected by a first Devonian ductile deformation stage, followed by a second deformation stage during the Carboniferous. These deformations stages are related to the Variscan orogeny, where the metamorphic conditions remained in low-greenschist facies conditions (Martínez Poyatos et al. 2001). The CIZ is in tectonic contact with the Ossa Morena Zone through the Badajoz-Córdoba Shear Zone (BCSZ). The BCSZ is interpreted as an Ediacaran suture zone, reactivated during the Variscan orogenesis (López-Guijarro et al. 2008).

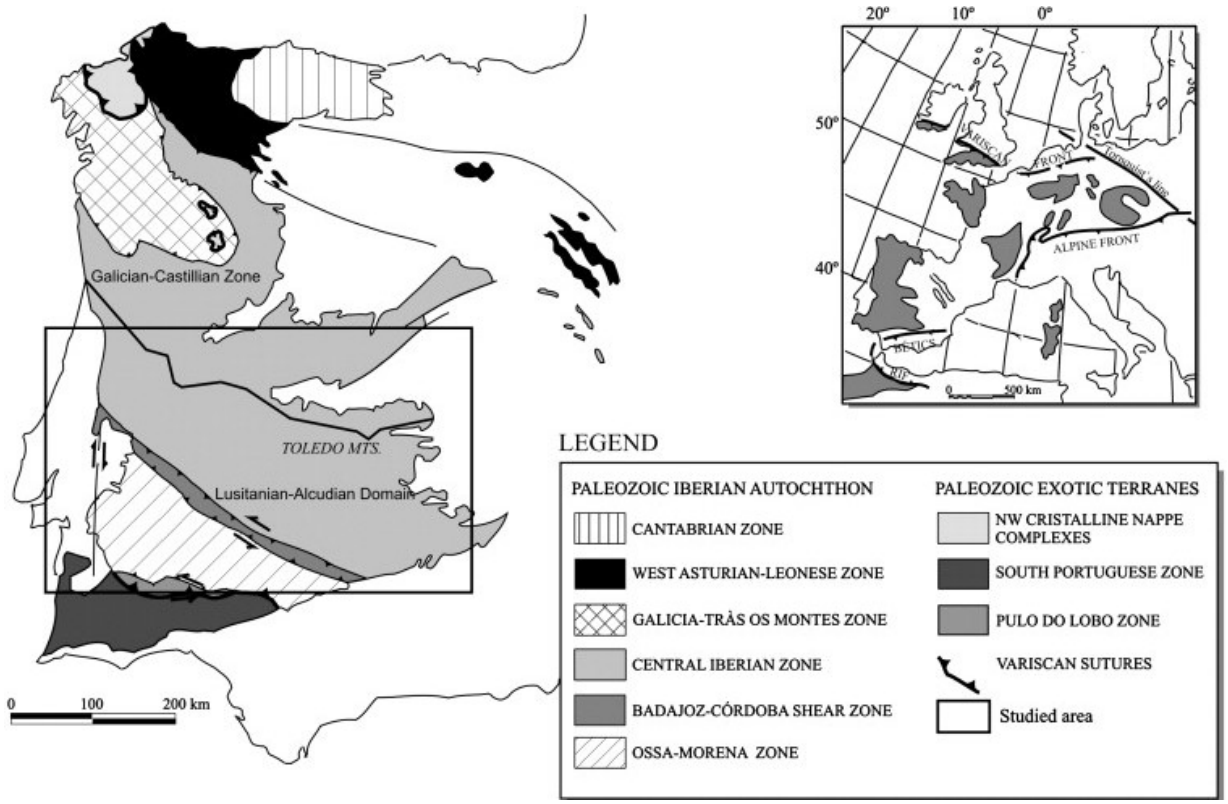

Figure 1: Zonal division of the Iberian Massif (López-Guijarro et al. 2008).

Ossa Morena Zone

The Ossa Morena Zone (OMZ) is a former accreted continental bloc, which was located between Laurussia and Gondwana. The OMZ was affected by the Cadomian orogenesis (620-480 Ma). It corresponds to a former post-collisional volcanic arc with calc-alkaline magmatism (Ordoñez Casado 1998). This event was followed by back-arc extension, tectonic inversion, crustal thickening and cratonization in an Andean-type continental margin. Then, the area recorded an early Paleozoic continental rifting with marine sedimentation. The Cadomian basement and the Paleozoic cover were affected by low-grade tectono-metamorphic events related to the Variscan orogenesis in the 390-300 Ma interval (Eguiluz et al. 2000).

South Portugese Zone

The South Portugese Zone (SPZ) is the southernmost domain of Variscan Iberian massif. It is a part of the Avalonia continental bloc (southern margin of Laurussia). The SPZ is subdivided into three main structural units: the Pulo do Lobo Antiform (PLA), the Iberian Pyrite Belt (IPB) and the Baixo Alentejo Flysch Group (BAFG) (fig.4). The SPZ have been deformed during the continental collision, where the Paleozoic cover was folded and thrusted to the south (thin-skinned tectonics) (fig.). The Pulo do Lobo Antiform is a former accretionary prism, made of turbiditic sedimentary succession, strongly folded and faulted. The Iberian Pyrite Belt is interpreted as a former volcanic arc active during the subduction of Laurussia below the Ossa Morena Zone. The IPB is made of a sedimentary formation with native and exotic material reworked into a fine-grained pelitic

matrix. Volcanic-sedimentary complex are present, associated to caldera structures. Many VMS deposits are also present along the IPB. The Baixo Alentejo Flysch Group formed during the continental collision following the IPB subduction. The BAFG is principally made of flysch sequence of Lower Carboniferous age. The sedimentary succession was folded and thrusted to the south during the thin-skinned tectonics phase.

The South Portugese Zone is accreted to the Ossa Morena Zone along the Beja-Acebuches Ophiolitic Complex. This complex is interpreted as the Rheic Ocean suture, where a former small oceanic crust (back-arc or transtensional basin) is obducted. It is principally made of amphibolites strongly deformed by sub-vertical mylonite. It is thrusted to the north by granulites of the Ossa Morena Zone (Onézime et al. 2003).

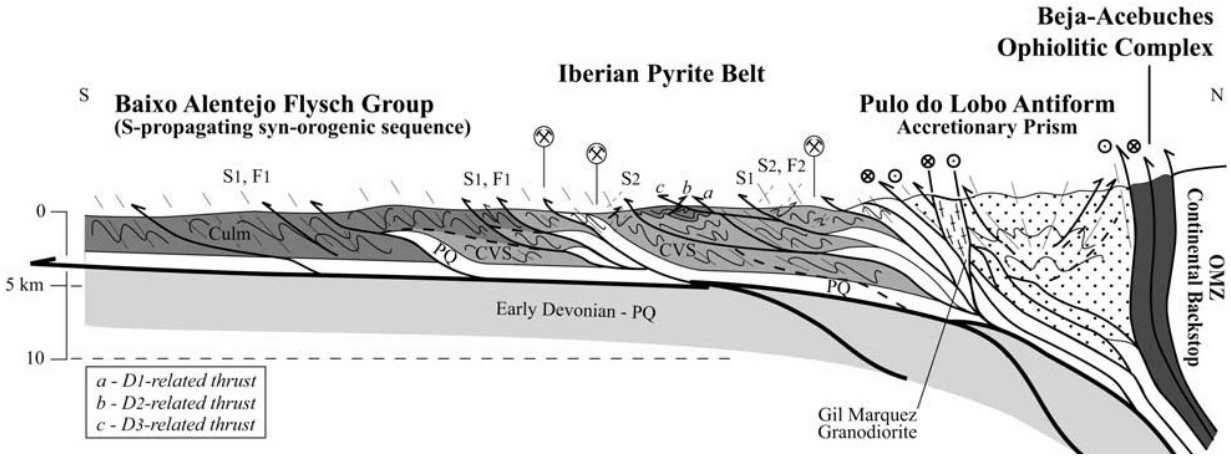

Figure 2. Cross section of the South Portugese Zone (after Onézime et al. 2003).

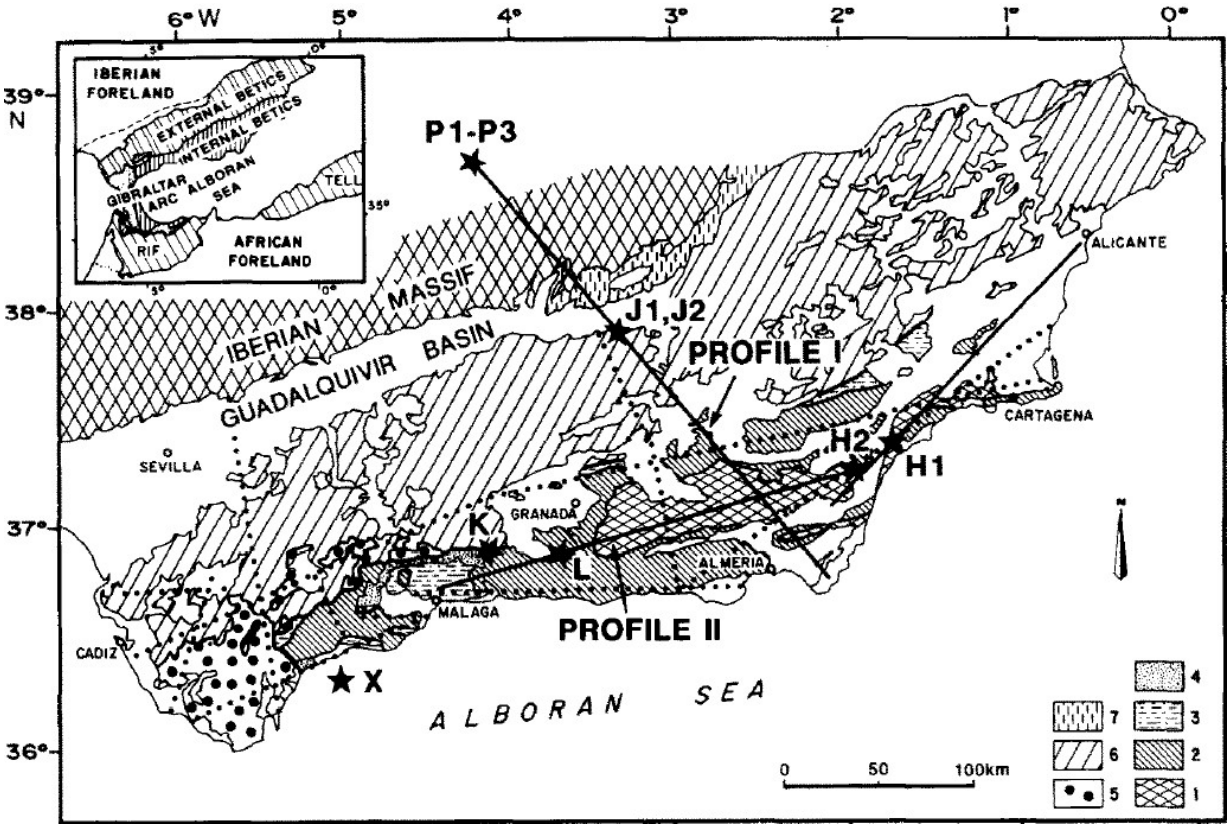

Figure 3. Simplified geological map of the Betic Cordillera and position of the Gadalquivir basin (after Banda et al. 1993). 1 = Nevado-Filbrides nappe. 2 = Alpujarrides complex. 3 = Malaguides complex. 4 = Early Miocene deposits (Alboran domain). 5 = Flysch Trough units. 6 = Sedimentary cover of the external Betics. 7 = Cover of the Iberian massif.

Betic Cordillera and its foreland basins

The Betic Cordillera, as known as Betic Ranges, was formed during the Cenozoic convergence between Africa and Iberia. It is a mountain belt in southeastern Spain, which is a part of the Gibraltar Arc, as the Rif Cordillera (Morocco). The Betic Cordillera was formed by the collision between Iberia and little continental blocs (named as AlKaPeCa), initially located between Africa and Iberia. A continental subduction of the Iberian crust below the Betic Cordillera and the Alborán Sea have been identified by Morales et al. (1999). This subduction is proposed as source of intermediate-depth earthquakes in the area. The Betic Cordillera is divided into two main domains: the Internal Betics (South) and the External Betics (North). The Internal Betics domain is related to AlKaPeca continental block. The External Betics domain is the deformed former Iberian margin. The thickening process induced by the continental collision produced a HP-LT metamorphism coeval with the nappe stacking tectonics. The compressional regime was followed by an extensional regime during the Miocene period (23-12 Ma). The extensional strain was mainly accommodated along detachment faults in the internal domain (Jabaloy et al. 1993).

Guadalquivir basin

The Guadalquivir basin is located to the north of the Betic Cordillera (fig.5). This basin is interpreted as the Betic foreland basin. It is filled by Neogene to Quaternary marine sedimentary rocks. Northward, the sediments of the Guadalquivir basin shows an unconformity with Paleozoic series of the Iberian massif (Azañon et al. 2002).

References

Azañon J.M., Galindo-Zaldívar J., García-Dueñas V. & Jabaloy A. (2002). Alpine tectonics II: Betic Cordillera and Balearic Islands. In: Gibbons W. & Moreno T. (ed), *Geology of Spain*, The Geological Society, London, pp. 401-416.

Banda E., Gallart J., García-Dueñas V., Dañobeitia J.J. & Makris J. (1993). Lateral variation of the crust in the Iberian Peninsula: new evidence from the Betic Cordillera. *Tectonophysics*, 221, 53-66.

Cochelin B., Chardon D., Denèle Y., Gumiaux C. & Le Bayon B. (2017). Vertical strain partitioning in hot Variscan crust: Syn-convergence escape of the Pyrenees in the Iberian-Armorican syntax. *Bull. Soc. Géol. Fr.*, 188, 39.

Eguiluz L., Gil Ibarguchi J.I., Abalos B. & Apraiz A. (2000). Superposed Hercynian and Cadomian orogenic cycles in the Ossa-Morena zone and related areas of the Iberian Massif. *GSA Bulletin*, 112:9, 1398-1413.

Gibbons W. & Moreno T. (2002). Introduction and overview. In: Gibbons W. & Moreno T. (ed), *Geology of Spain*, The Geological Society, London, pp. 1-7.

Jabaloy A., Galindo-Zaldívar J. & González-Lodeiro F. (1993). The Alpujárride-Nevado-Fibábride extensional shear zone, Betic Cordillera, SE Spain. *Journal of Structural Geology*, 15:3-5, 555-569.

López-Guijarro R., Armendáriz M., Quesada C., Fernández-Suárez J., Brendan Murphy J., Pin C. & Bellido F. (2008). Ediacaran-Paleozoic tectonic evolution of the Ossa Morena and Central Iberian zones (SW Iberia) as revealed by Sm-Nd isotope systematics. *Tectonophysics*, 461:4, 202-214.

Martínez Poyatos D., Nieto F., Azor Antonio & Fernando Simancas J. (2001). Relationships between very-low-grade metamorphic and tectonic deformation: examples from the southern Central Iberian Zone (Iberian Massif, Variscan Belt). *Journal of the Geological Society*, 158, 953-968.

Morales J., Serrano I., Jabaloy A., Galindo-Zaldívar J., Zhao D., Torcal D., Vidal F. & González-Lodeira F. (1999). Active continental subduction beneath the Betic Cordillera and the Alborán Sea. *Geology*, 27:8, 735-738.

Onézime J., Charvet J., Faure M., Bourdier J.-L. & Chauvet A. (2003). A new geodynamic interpretation for the South Portugese Zone (SW Iberia) and the Iberian Pyrite Belt genesis. *Tectonics*, 22:4, 1027.

Ordoñez Casado Berta (1998). Geochronological studies of the pre-Mesozoic basement of the Iberian Massif : the Ossa Morena zone and the Allochthonous Complexes within the Central Iberian zone. Thesis, ETH Zürich.

2. Magmatic record in southern Spain

Edgar Alejandro Cortes Calderon

Introduction

Magmatism is a remarkably efficient mechanism to transport and focus elements of economic interest in the crust (Annen and Zellmer, 2008). The nature of magmas (i.e. mixtures of crystals, melts and gases) and their evolutionary trends trigger a selective sieving of elements (Hedenquist and Lowenstern, 1994; Annen and Zellmer, 2008). This element sorting is P-T-fO_2 dependent and follow the degree of compatibility between a chemical element and the vapor, liquid or solid phase in a magma (Annen and Zellmer, 2008). Therefore, understanding how magmas are generated, stored and erupted has important implications in ore genesis and prospection (Arndt and Ganino, 2011).

South Spain

Southern Spain has recorded multiple events of magmatism through the geological time (Onézime et al., 2003; Tornos et al., 2004; Valenzuela et al., 2011). Some of these magmatic products host ore bodies such as the world-class deposit Iberian Pyrite Belt (IPB) (Onézime et al., 2003; Valenzuela et al., 2011). There are two important magmatic episodes during the Paleozoic related to ore deposits: 1) an Early Paleozoic phase linked with the fate of the Cadomian arc (Tornos et al., 2004); 2) a Late Paleozoic phase associated to the accretion of the South Portuguese Zone (SPZ) (Tornos et al., 2004). A third main magmatic pulse occurred during the Cenozoic related to the Alpine orogeny (Arribas et al., 2005). The aim of this chapter is to review the characteristics of the igneous rocks related to the above-mentioned magmatic episodes (Fig. 1).

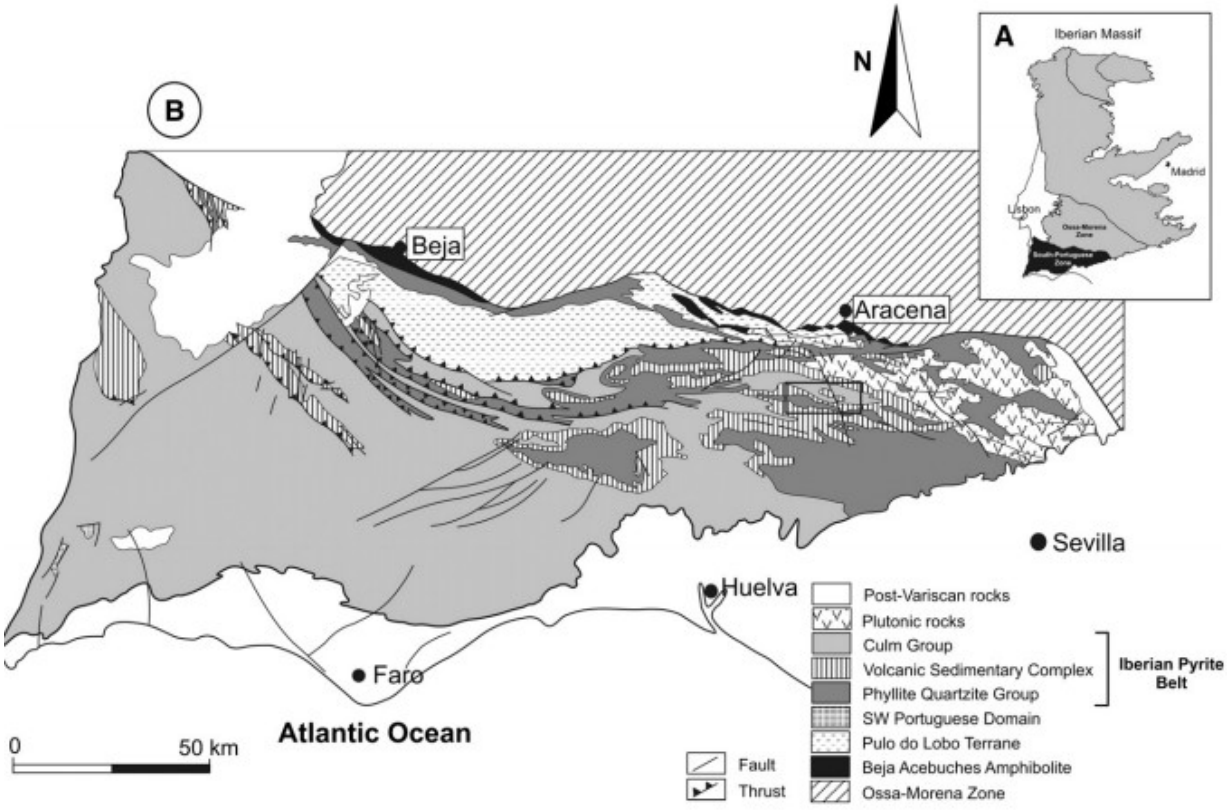

Fig. 1. Geological Map of the South Portuguese Zone and the Ossa-Morena Zone. Location of the IBERIAN Pyrite Belt and the Pre- and Post- Variscan lithologies. Obtained from Valenzuela et al., 2011.

Paleozoic magmatism

The Southern part of the Iberian Peninsula was characterised by series of amalgamation and rifting events during the Paleozoic (Sarrionandia, 2012 and references therein). These tectonic processes led to the formation of magmas by hydration and adiabatic decompression (Tornos et al., 2004; Sarrionandia, 2012). The Ossa-Morena zone (OMZ), a polyphase terrane, records subduction-like magmatism during the Neoproterozoic and extensional magmatism that led the opening of the Rheic Ocean during the Cambrian-Ordovician periods (Tornos et al., 2004; Sarrionandia, 2012). The IPB, a vast Devonian complex, hosts eight giant volcanogenic massive sulphide (VMS) deposits.

The Cadomian terrane

After the amalgamation of the Cadomian arc (i.e. the so-called OMZ) along the NW edge of Gondwana during the Neoproterozoic-Cambrian transition, a major rifting event led the formation of the Rheic Ocean (Sarrionandia, 2012). This continental break-up is recorded by volcanosedimentary rocks that belong to the OMZ (Sarrionandia, 2012). After the rifting event a new accretion processes (i.e. Variscan orogeny) trigger the metamorphism of the OMZ (Tornos et al., 2004). The ore deposits related to this terrane comprise: 1) arc-related VMS and minor porphyry-Copper mineralisation during the formation of the Cadomian arc in the Cadomian orogeny (Tornos et al., 2004); 2) iron oxide stratabound deposits during the opening of the Rheic Ocean (Tornos et al., 2004); 3) orogenic deposits (i.e. Hg, U, Au, Cu-Ni ores) related to transpressional strain during the Variscan orogeny (Tornos et al., 2004).

The Cadomian arc is the result of Andean-type volcanism (i.e. subduction magmatism) with a calc-alkaline chemical evolution (Tornos et al., 2004). Andesitic-dacitic plutons and volcanic desposits are the main constituents of this arc (Tornos et al., 2004). Although the ore deposits related to this arc are scare, a subordinate back-arc represents the main environment for ore accumulation (i.e. VMS and SEDEX) during this period (Tornos et al., 2004). No epithermal deposits have been found to date, and Au-orogenic deposits in the OMZ are more related to the Variscan rather than the Cadomian orogeny (Tornos et al., 2004).

The opening of the Rheic ocean led the formation of a rifting event (Sarrionandia, 2012). The rocks from this stage comprise moderately alkaline ultrabasic to acid units (Sarrionandia, 2012). Geochemical analyses of these units exhibit an OIB-type source (Sarrionandia, 2012). The chemical diversity of this volcanic sequence is attributed to fractional crystallisation of plagioclase, clinopyroxene and amphibole with a minor component of crustal assimilation (Sarrionandia, 2012). There are two types of primitive melts that are characterised by different amounts of partial melting of the sublithospheric mantle (Sarrionandia, 2012). It is noteworthy that this magmatic episode is not related to MORB-type magmatism, but hotspot-type that contribute to the continental break up (Sarrionandia, 2012). The ore bodies in these volcanosedimentary sequences are restricted to iron oxide stratabound deposits that are favoured by rifting conditions (Tornos et al., 2004).

The accretion of the SPZ was charaterised by a subduction regime and metamorphic pulses that altered the units described above in different proportions (Onézime et al., 2003; Tornos et al., 2004). This Late Paleozoic event corresponds to the Variscan orogeny and led the more economic important ore accumulation in the OMZ (Tornos et al., 2004). Magmatic pulses (arc-related) are related to pull-apart basins that were produced due to transpressional-type stresses (Tornos et al., 2004). Calc-alkaline signatures are found in the volcanic sequences and plutons, which confirm the presence of subduction tectonics (Tornos et al., 2004). Variscan intrusions are mainly metalumuous ranging from gabbros to monzogranites (Tornos et al., 2004). The cumulates related to the Variscan plutons in the OMZ host important Ni-Cu ore bodies (Tornos et al., 2004). Subsequent increase in stress rates led to replacement of arc-related deposits triggering the formation of orogenic ore bodies and veins (Tornos et al., 2004).

Accretion of the South Portuguese Zone

The SPZ is a continental fragment that was accreted to the OMZ edge during the Late Paleozoic (i.e. Variscan orogeny) (Onézime et al., 2003; Valenzuela et al., 2011). This terrane hosts the world-class ore deposit IPB, which consists mainly of VMS-like deposits (Valenzuela et al., 2011). The ore bodies are located specifically in

the volcano-sedimentary complex (Fig. 2). Lithofacies analysis through Odiel river section reveals that the sequence records a submarine eruption environment (e.g. ash-poor, thick lava packages, little or no sediments interbedded) (Valenzuela et al., 2011). The presence of mafic facies decreases upwards the section and the massive sulphides are hosted in the upper sedimentary and felsic unit (Valenzuela et al., 2011).

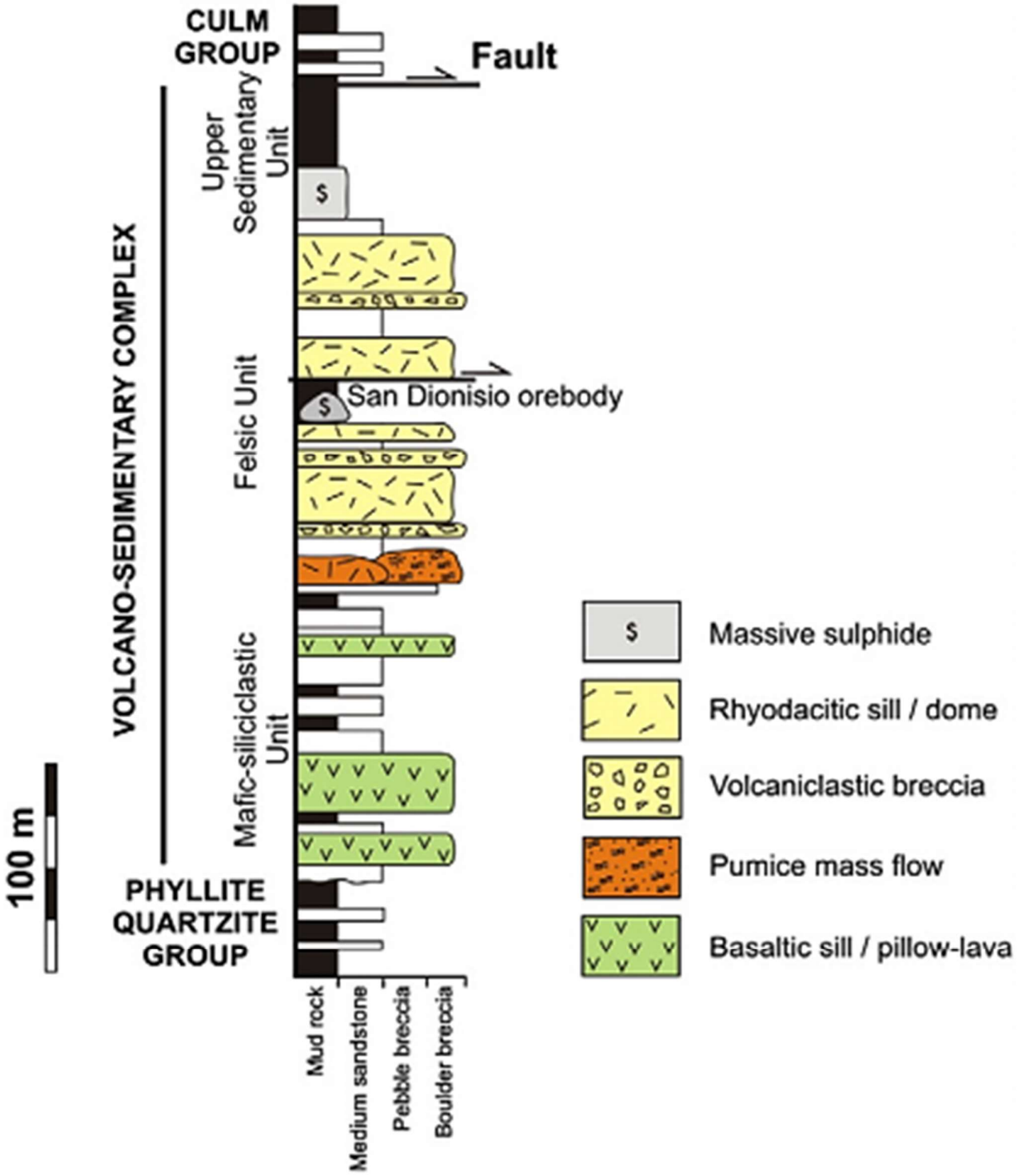

Fig. 2. Odiel section showing the Iberian Pyrite Belt sequence. Obtained from Valenzuela et al. (2011).

The tectonic setting linked to the volcanism in this area is still a matter of debate (Onézime et al., 2003; Valenzuela et al., 2011). Furthermore, there is no agreement whether the genesis of the ore bodies is related to the volcanism or just a consequence of basinal fluids (Onézime et al., 2003; Valenzuela). The works that link the volcanism with massive sulphides genesis argue that the felsic stage should be related to an arc environment, where dome-collapses could be possible. However, the abundance of massive sulphides in this area makes unrealistic the arc-setting as the unique agent for ore accumulation (Valenzuela, et al., 2011).

Cenozoic magmatism

Further accretion events occurred during the Alpine orogeny (López-Ruiz, 1999). Extensional regimes are triggered to compensate the new thickness of the crust. This volcanism formed a caldera above a felsic magma chamber during the Miocene (López-Ruiz, 1999). The development and collapse of this caldera (i.e. Rodalquilar caldera) produced dacitic domes and ignimbrites with a calc-alkaline signature (López-Ruiz, 1999). Economic Au accumulation in the explosive phase of Rodalquilar volcanism (Arribas, et al., 2005). The importance of calderas relies on the creation of fractures, which work as pathways for fluid flow (Arribas, et al., 2005). Therefore, calderas structures are important places for hydrothermal alteration, which is related to ore accumulation (Arribas, et al., 2005).

References

Annen, C., Zellmer, G.F., (2008). Dynamics of crustal magma transfer, storage and differentiation. Geological Society of London, p. 288

Arribas, A., Hernández. F., Fernández, M.A., Gröbner, J., Leal, G., (2005). Bocamina. Revista de Minerales y Yacimientos de España. Vol. 15

Arndt, N., Ganino, C., (2011). Magmatic Ore deposits. In: Metals and Society. Metals and Society. Vol 2. Springer, Heidelberg.

Hedenquist, J., Lowenstern, J.B., (1994). The role of magmas in the formation of hydrothermal ore deposits. Nature. Vol. 370.

Onézime, J., Charvet, J., Faure, M., Bourdier, J-L., Chauvet, A., (2003). A new geodynamic interpretation for the South Portuguese Zone (SW Iberia) and the Iberian Pyrite Belt. Tectonics. Vol. 22.

López-Ruiz, J., (1999) El campo volcánico del neógeno del SE de España. Enseñanza de las ciencias de la tierra.

Sarrionandia, F., Carracedo-Sanchez, M., Eguiluz, L., Ábalos, B., Rodríguez, J., Pin, C., Gill-Ibarguchi, J.I., (2012). Cambrian rift-related magmatism in the Ossa-Morena Zone (Iberian Massif): Geochemical and geophysical evidence of Gondwana break-up. Tectonophysics. Vol. 570-571. p, 135-150.

Tornos, F., Inverno, M.C., Casquet, C., Mateus, A., Ortiz, G., Oliviera, V., (2004). The metallogenic evolution of the Ossa-Morena Zone. Journal of Iberian Geology, Vol. 30. p. 143-181.

Valenzuela, A., Donaire, T., González-Roldán, M.J., Toscano, M., Pascual, E., (2011). Volcanic architecture in the Odiel river área and the volcanic environment in the Riotinto-Nerva Unit, Iberian Pyrite Belt, Spain. Vol. 202. P.29-46.

3. The Rodalquilar epithermal gold-deposit

Jeremias Arnold

Mining history

Mining of galena-quartz veins began in the second half of the eighteenth century. Gold was discovered in 1883 and subsequently mined from small operations. Significant gold mineralization in the present mining area has been outlined by geochemical methods in 1942, with estimated reserves of four million tons with ore grades of 4.5 ppm gold. Opencast and underground mining was carried out from 1956 to 1966. During this period some three million tons of rock have been removed, of which 1.5 million tons had an average grade of 6.5 - 7 ppm gold (Oepen et al. 1989; Rytuba et al. 1990).

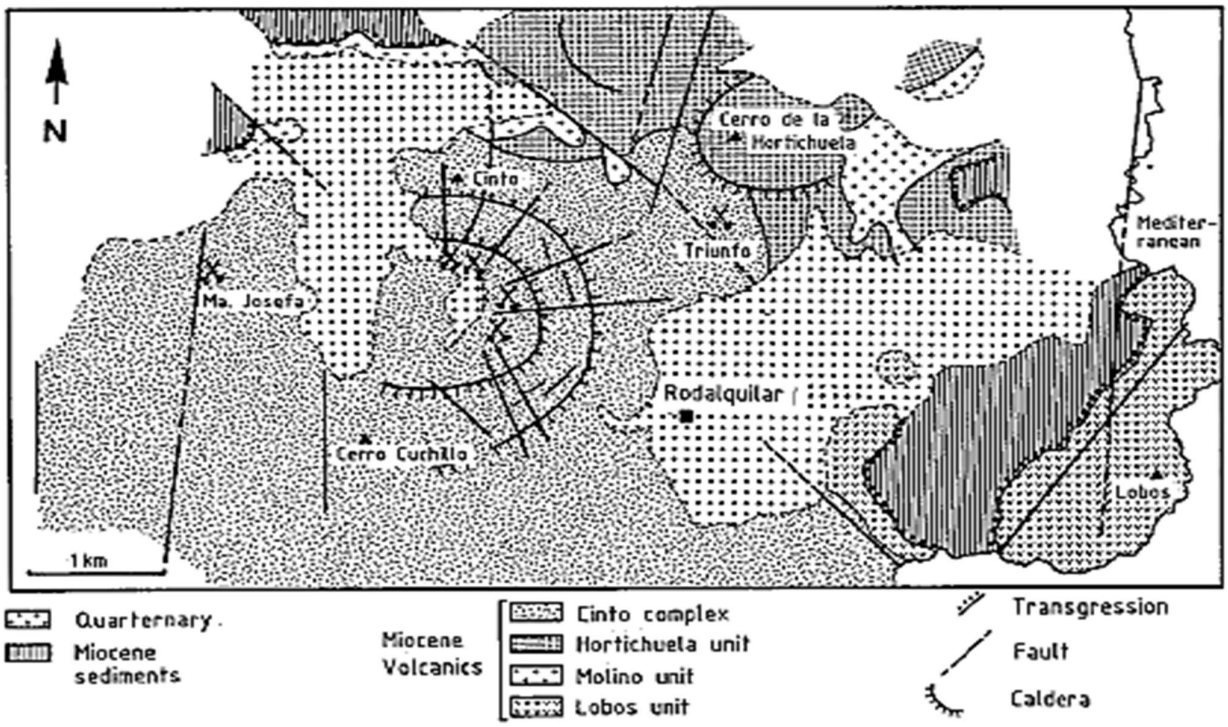

Figure 1: Simplified geology of the Rodalquilar district, showing deposits associated with the caldera-related radial and concentric faults. Obtained from Oepen (1989).

Geological Setting

The area between Almeria and Cartagena shows a wide spectrum of posttectonic Neogene magmatic activity, ranging from calc-alkaline andesite via ultrapotassic rocks to alkali basalts (Lopez-Ruiz and Rodriguez Badiola 1980; Bellon et al. 1983; Venturelli et al. 1984; Bordet 1985; Torres-Roldan et al. 1986). The volcanic rocks of the Sierra del Cabo de Gata (SCG) ranging 14-18 Ma were grouped into four major phases. Complex A consists in pyroxene- and hornblende-bearing andesite with age-equivalent tuffs overlained by hornblende-andesites of complex B. Dacites and rhyolites of complex C are found in the central SCG. The final volcanic phase, complex D, consists of dark pyroxene andesites. Gold mineralization is hosted in the rhyolites and rhyodacites of complex C, in the so called Cinto complex, and found in the eastern wall of the Lomilla caldera. The tectonic pattern is dominated by radial and ring fractures towards the Cerro Cinto and gold mineralization is largely confined to these caldera-related faults (Oepen et al. 1989).

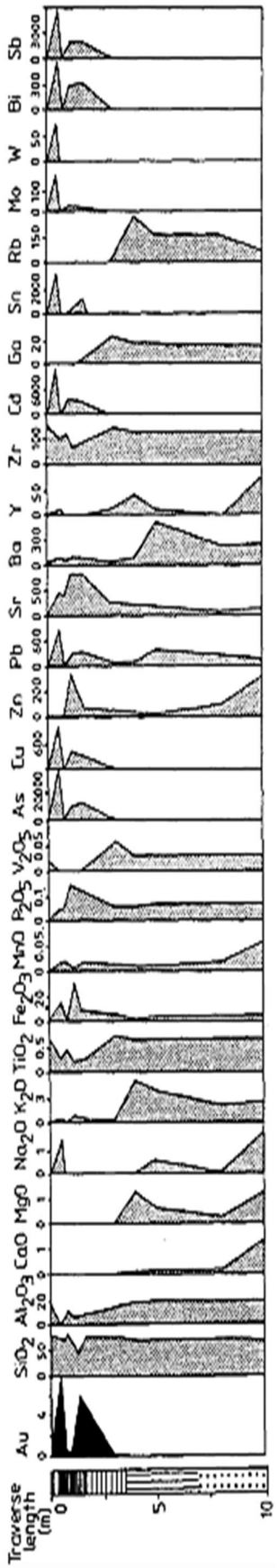

Figure 2: Lithogeochemical profiles perpendicular to the vein structure. Oxides are given in wt%, elements in ppm. Obtained from Oepen (1989).

Alteration

Intensive alteration of volcanic host rocks have transformed the primary mineral paragenesis to the extent that only primary quartz phenocrysts remained unaffected. Altered rocks consist of quartz, alunite, kaolinite, jarosite, pyrophyllite and hematite. Zoning ranges from advanced argillic alteration in and close to gold-mineralized structures towards argillic and more regionally developed propylitic alteration (Lodder 1966). In some areas, pockets of extremely high grade gold mineralization exceeding 500 ppm can be found (Martin-Vivaldi et al. 1971). Supergene replacement reactions can be observed and form very fine gold (Oepen et al. 1989).

Fluids

Two fluids with different origins and compositions were distinguished. A hypersaline, acid fluid of magmatic origin can be characterized by its NaCl and KCl content, hematite and other unidentified daughter minerals. When overpressured and overheated, fluids escaped from the parental magma through caldera-related fractures, violent boiling lead to variable liquid contents and different amounts of salt crystals in those inclusions. A low-salinity fluid with 3-5 equiv. wt% NaCl is assumed to derive from seawater.*Fluid inclusions*

Fluid inclusions

In order to get information on vertical changes in P-T-X conditions of hydrothermal fluids, micro-thermometric investigations were performed on drill core samples over a depth of 650 m. Based on phase relationships, two-phase, liquid-rich fluid inclusions (type 1), multiphase fluid inclusions with up to four daughter minerals (type 2) and vapor-rich or vapor-filled inclusions (type 3) were described by Oepen et al. (1989). Vapor-rich inclusions of type 3 can be linked to either type-1 or type-2 inclusions on the basis of comparable salinities or similar daughter crystals. Microthermometric investigations also revealed widespread evidence of boiling throughout the investigated depth interval. From pressure, a paleosurface of 50 m above the present is estimated, which also agrees with geologically inferred evidence (Hernandez 1988).

Generic model

Timing

The mineralization is closely associated with hornblende-andesite intrusives and flows, which corresponds to the youngest volcanic activity within the Rodalquilar caldera. Only some of the hornblende-andesites are altered and mineralized, indicating that mineralization occurred during the early phase of andesitic volcanism but ended before the last flows emplaced, at 9.0±0.6 Ma. Potassium-argon dating of alunite and illite from the alteration zones associated with gold deposits range from 9.5±0.5 Ma to 11.3±0.4 Ma for Illite and 10.3±0.4 Ma to 10.6±0.5 Ma for alunite (Arribas et al. 1989).

Gold mineralization

The Rodalquilar gold-alunite deposits are closely related in time and space to porphyritic, intermediate composition magma emplaced along caldera

structures, but unrelated to the caldera forming the magmatic system (Rytuba et al. 1990). Gold mineralization and advanced alteration are considered to have evolved from hyper saline and overpressured solutions in the near-surface environment. Episodic pressure releases due to fracturing of rocks or widening of conduits must have caused fluids to boil. Low-salinity fluids of marine origin flowed into the fractured system and interacted with both the wallrock and the magmatic fluids. High-grade gold mineralization occurs within the upper 50 m below surface, with decreasing Au contents down to about 120 m. This corresponds to the depth interval at which low-salinity fluids maintained homogenization temperatures of 175°C.

It is suggested that fluid boiling was accompanied by a H_2S loss as vapor. Subsequent oxidation of H_2O to H_2SO_4 in superjacent fluids caused an important decrease in pH (Henley 1985; Fournier 1985; Hayba et al. 1985). Reactions between acid fluids and silicates from wallrocks may have released silica into the fluids, causing significant supersaturation with respect to quartz or even formation of calcedony. The leaching of wallrock was connected with volcanogenic activity (Hedenquist et al. 1988). This physiochemical environment during acid alteration was favorable to the formation of gold mineralization since the decrease in pH and increase in fO_2 favor gold precipitation when transported as a bisulfide complex (Seward 1984).

References

Arribas Jr, A., Rytuba, J. J., Rye, R. O., Cunningham, C. G., Podwysocki, M. H., Kelly, W. C., ... & Smith, J. G. (1989). *Preliminary study of the ore deposits and hydrothermal alteration in the Rodalquilar caldera complex, southeastern Spain* (No. 89-327). US Dept. of the Interior, US Geological Survey,.

Bellon, H., Bordet, P., & Montenat, C. (1983). Chronologie du magmatisme néogène des Cordillères bétiques (Espagne méridionale). *Bulletin de la Société géologique de France*, *7*(2), 205-217.

Bordet, P. (1985). Le volcanisme Miocène des Sierras de Gata et de Carboneras, Espagne du Sud-Est (No. 8). Institut géologique Albert de Lapparent.

Fournier, R. O. (1985). The behavior of silica in hydrothermal solutions. *Review in Economic Geology, v.*, *2*, 45-60.

HAYBA, B. (1985). Geologic, mineralogic and geochemical characteristics of volcanic hosted epithermal precious metal deposits. In Geology and geochemistry of epithermal systems. *Rev. Econ. Geol.*, *2*, 129-167.

Hedenquist, J. (1988). Epithermal gold mineralization of acid-leached rocks in the Nansatsu district of southern Kyushu, Japan. In *Gold 1988 Conference* (pp. 183-190). Geol. Soc..

Henley, R. W. (1985). The geothermal framework of epithermal deposits. *Geology and geochemistry of epithermal systems*, 1-24.

Lodder, W. (1966). Gold-alunite deposits and zonal wall-rock alteration near Rodalquilar. *Univ. Amsterdam, Geol. Inst., Medeling*, (318), 93.

López Ruiz, J., & Rodríguez Badiola, E. (1980). La región volcánica neógena del sureste de España.

Oepen, P. S. V., Friedrich, G., & Vogt, J. H. (1989). Fluid evolution, wallrock alteration, and ore mineralization associated with the Rodalquilar epithermal gold-deposit in southeast Spain. *Mineralium Deposita*, *24*(4), 235-243.

Rytuba, J. J., Arribas, A., Cunningham, C. G., McKee, E. H., Podwysocki, M. H., Smith, J. G., & Kelly, W. C. (1990). Mineralized and unmineralized calderas in Spain; Part II, evolution of the Rodalquilar caldera complex and associated gold-alunite deposits. *Mineralium Deposita*, *25*(1), S29-S35.

Seward, T. M. (1984). The transport and deposition of gold in hydrothermal systems. *Gold'82: The geology, geochemistry and genesis of gold deposits*, 165-181.

Torres-Roldán, R. L., Poli, G., & Peccerillo, A. (1986). An Early Miocene arc-tholeiitic magmatic dike event from the Alboran Sea—Evidence for precollisional subduction and back-arc crustal extension in the westernmost Mediterranean. *Geologische Rundschau*, *75*(1), 219-234.

Venturelli, G., Capedri, S., Di Battistini, G., Crawford, A., Kogarko, L. N., & Celestini, S. (1984). The ultrapotassic rocks from southeastern Spain. *Lithos*, *17*, 37-54.

Vivaldi, J. M., Sierra, J., & Leal, G. (1971). Some Aspects of the Mineralization and Wall-rock Alteration in the Rodalquilar Gold-Field, SE Spain. Society of Mining Geologists of Japan

4. Podiform chromite in the Serrania Ronda, Southern Spain

Jean-Marc Benz

Introduction

Chromite is a Cr-bearing ore ($FeCr_2O_4$) that contains mainly Cr- and Al-rich spinel (González-Jiménez et al., 2014). Significant amounts of chromite can be found either in stratiform or podiform chromitite deposits. Podiform chromitite deposits display high chromium numbers (Cr # = Cr/[Cr + Al] atomic ratio), mostly higher than 0.4, with common values ranging between 0.7 and 0.8 (Arai, 1997). Usually chromitite deposit are restricted to ophiolites, tectonically emplaced oceanic crust and upper mantle sequences over a continental crust. Therein the chromite hosting zones are in the upper mantle or close to the crust-mantle boundary (González-Jiménez et al., 2014). Economically viable chromitite deposits contain approximately 30% Cr. The podiform Ronda chromite deposits are in the Betic-Rifean orgenic belt in Southern Spain (Crespo et al., 2006).

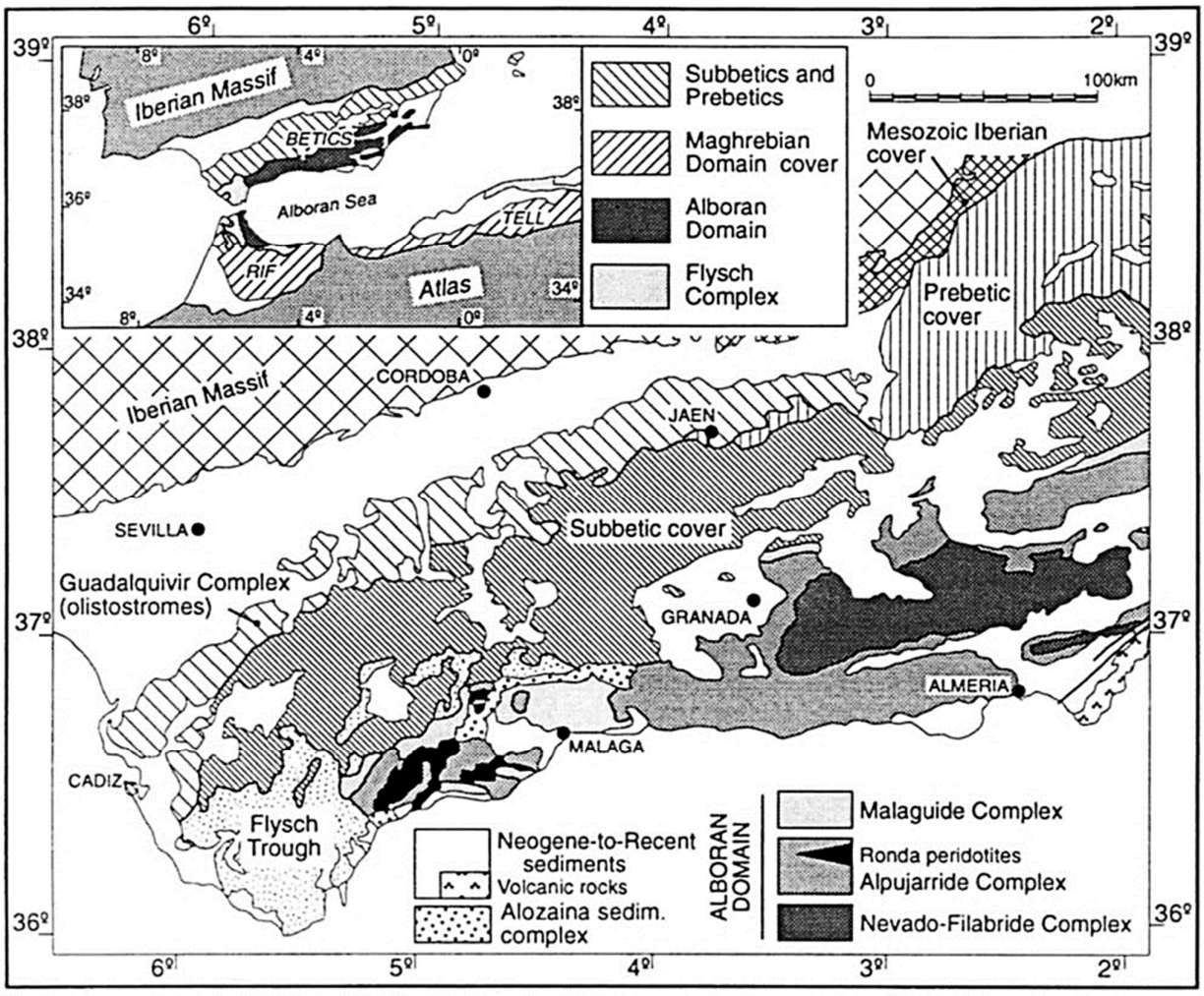

Figure 4: Tectonic map of the Betic Chain with the indicated position of the Ronda peridotites in the Alpujarride Complex. Obtained from Crespo-blanc (1997).

Geological Setting

The Betic and Rif mountain chains form an arc-shaped mountain belt around the Straits of Gibraltar north and south of the Alboran Sea. The mountain chain is made up by four major tectonic domains, namely the Alboran, Sub Iberian, Maghrebian domains, and the allochthonous Flysch trough (Crespo-blanc, 1997, Platt et al., 2013). Within the internal zone of the Gibraltar Arc the Alpujarride complex is located. The *Serrania de Ronda* is in the western Alpujarride units of the Betic-Rifean orgogenic belt, the western most part of the Mediterranean Alpine belt in southern Spain (Fig. 1) (Crespo-blanc, 1997). The ultramafic rocks of *Serrania de Ronda* crop out in three separated mounts, namely the Ronda, Ojén and Carratraca massifs. The Ronda mount host the world's largest exposed orogenic lherzolites. All three ultramafic mounts are portions of an old (Proterozoic) subcontinental lithospheric mantle tectonically emplaced in the lower crust 22 Ma ago (Crespo et al., 2006).

Formation of podiform chromitite deposits

Podiform or alpine-type chromitites are exclusively found in the mantle and/or the mantle-crust transition zone of ophiolitic complexes or their dismembered equivalents. The best-documented podiform chromitite deposits are in Cyprus and Oman. The crustal thickness at Cyprus is 8 km and at Oman 6 km, the chromitites were formed at a lithostatic pressure of 0.2 GPa including the seawater, lithostatic, pressure.

The name 'podiform' is given by the shape of pods of the chromitite enveloped in a dunite. However, they can also cut the surrounding structure of the mantle peridotites (Arai, 1997). Podiform chromite deposits were claimed to be related to mid-ocean ridges, where huge basaltic magma chambers are produced. More recent studies suggest a genesis in a supra-subduction zone environment because of the hydrous character of involved basaltic melts (e.g. Rollinson & Adetunji, 2013; Matveev & Ballhaus, 2002).

Chromium is a compatible lithophile element that gets enriched in the mafic silicate melt fraction with increasing degree of partial melting of primitive mantle. Primitive mantle melts have a chromium concentration of 200-500ppm, so to achieve 30% Cr in bulk ore two enrichment mechanisms are needed. The first mechanism acts at a small scale and leads to physical separation of olivine and chromite at magmatic temperatures, where primitive melts are normally saturated in both species. Chromite concentration is controlled by surface processes where oxides are better wetted by water-rich fluid phase than by silicate melt. Since the opposite is true for the silicate minerals, chromite-bearing water-rich bubbles coalesce and migrate upward. Accumulation of these bubbles leads to the formation of chromite pools. The second mechanism leads to a large-scale concentration of chromite. The main driving mechanism is the density contrast between chromite-laden fluid pools and silicate melt. Sinking of accumulated chromite bearing bubbles occurs when chromite concentration reaches over 50%. Fast down sinking and insulation by the remaining water-rich fluid phase prevents the chromite from melting. The sheet likes structure is a result from the accumulation by sinking process (Matveev & Ballhaus, 2002).

Figure 5: Genetic model of chromite formation. Left figure shows the ascension of Cr-rich bubbles after exsolution. Right figure shows the descent of aggregated Cr-rich bubbles when attaining a state of negative buoyancy. Obtained from Matveev & Ballhaus (2002).

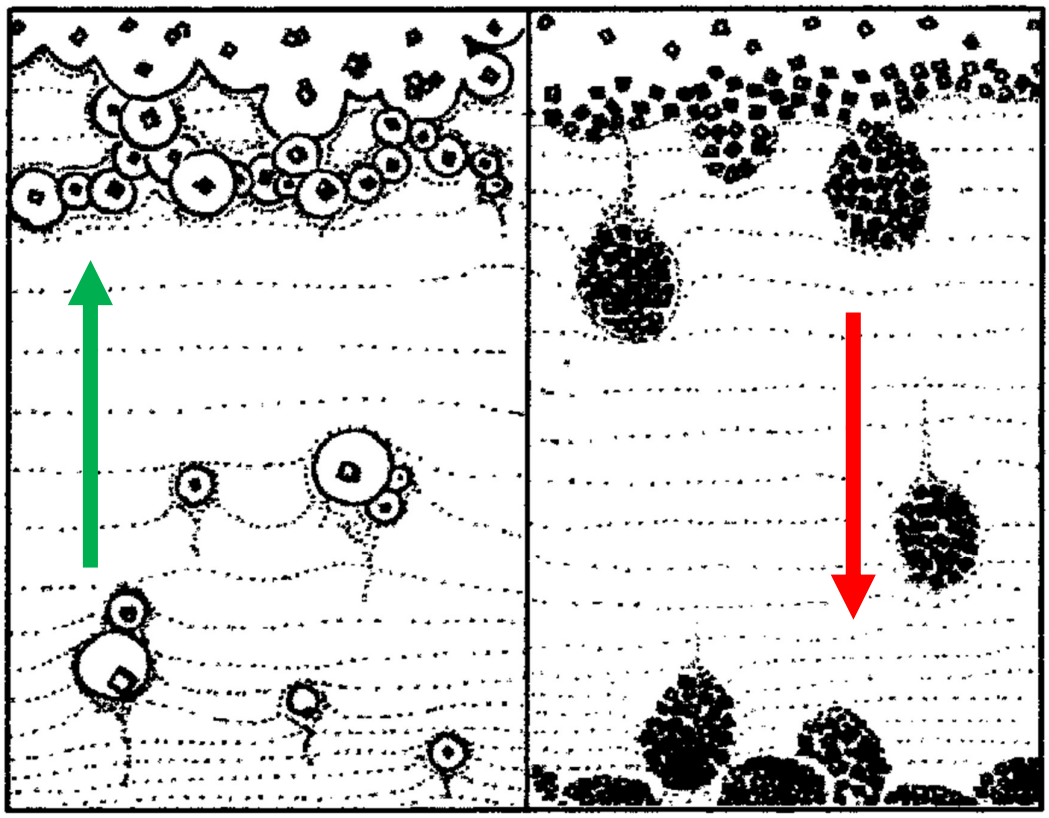

References

Arai, S. (1997). Origin of podiform chromitites. *Journal of Asian Earth Sciences*, *15*(2-3), 303-310.

Crespo-blanc, A. (1997). Continental collision, crustal thinning and nappe forming during the pre-Miocene evolution of the Alpujarride Complex (Alboran Domain, Betics). Journal of Structural Geology, 19(8), 1055-1071.

Crespo, E., Luque, F. J., Rodas, M., Wada, H., & Gervilla, F. (2006). Graphite–sulfide deposits in Ronda and Beni Bousera peridotites (Spain and Morocco) and the origin of carbon in mantle-derived rocks. *Gondwana Research*, *9*(3), 279-290.

Gonzalez-Jimenez, J. M., Griffin, W. L., Proenza, J. A., Gervilla, F., O'Reilly, S. Y., Akbulut, M., Pearson, N. J. & Arai, S. (2014). Chromitites in ophiolites: How, where, when, why? Part II. The crystallization of chromitites. *Lithos*, *189*, 140-158.

Gutierrez-Narbona, R., Lorand, J. P., Gervilla, F., & Gros, M. (2003). New data on base metal mineralogy and platinum-group minerals in the Ojen chromitites (Serrania de Ronda, Betic Cordillera, southern Spain). *Neues Jahrbuch für Mineralogie-Abhandlungen: Journal of Mineralogy and Geochemistry*, *179*(2), 143-173.

Matveev, S., & Ballhaus, C. (2002). Role of water in the origin of podiform chromitite deposits. *Earth and Planetary Science Letters*, *203*(1), 235-243.

Marchesi, C., Griffin, W. L., Garrido, C. J., Bodinier, J. L., O'Reilly, S. Y., & Pearson, N. J. (2010). Persistence of mantle lithospheric Re–Os signature during asthenospherization of the subcontinental lithospheric mantle: insights from in situ isotopic analysis of sulfides from the Ronda peridotite (Southern Spain). *Contributions to Mineralogy and Petrology*, *159*(3), 315-330.

Platt, J. P., Behr, W. M., Johanesen, K., & Williams, J. R. (2013). The Betic-Rif arc and its orogenic hinterland: a review. Annual Review of Earth and Planetary Sciences, 41, 313-357.

Rollinson, H., & Adetunji, J. (2013). Mantle podiform chromitites do not form beneath mid-ocean ridges: A case study from the Moho transition zone of the Oman ophiolite. *Lithos*, *177*, 314-327.

Torres-Ruiz, J., Garuti, G., Gazzotti, M., Gervilla, F., & Hach-Ali, P. F. (1996). Platinum-group minerals in chromitites from the Ojen lherzolite massif (Serrania de Ronda, Betic Cordillera, Southern Spain). *Mineralogy and Petrology*, *56*(1-2), 25-50.

5. Iberian Pyrite Belt geology

Cyrielle Bernard

Introduction

The Iberian Pyrite Belt (IPB) is a part of the South Portuguese Zone, located in southern Spain and Portugal. It is made from base to top of the Phyllite-Quartzite Formation (PQF), the Volcano-Sedimentary Complex (VSC), and finally a turbidite named the Culm Group (CG). They all have been deformed during the Variscan orogeny; their timing of formation is detailed in the next section and summarized in Fig. 1.

The Phyllite-Quartzite Formation (PQF)

The basement of the IPB is made of the PQF, of Late Devonian age (385±2.6 to 359±2.5 Ma), made of an alternation of meter thick quartzites, limestones and dark shales. This unit is the most deformed, however sedimentary structures such as parallel laminations, ripples and bioturbation indicates this unit emplaced in a shallow water environment, probably an epicontinental sea. The summit of the PQF is made of a 30 m thick shales layer, which contains lenses of bioclastic limestones. Fossils such as trilobites, brachyopods and conodonts were found in this top section.

The Volcano-Sedimentary Complex (VSC)

The VSC is made of a mix between sedimentary and volcanic rocks and is 0 to 1300 m thick depending on its proximity to volcanic centres. It is dated as Late Fammenian (~359 Ma) to Late Viséan (~328 Ma) and its contact with the PQF is mainly tectonic. The VSC hosts all volcanic-hosted massive sulphide (VHMS) deposits. Three main volcanic episodes have been recognized and dated between 351±0.4 and 345±0.6 Ma (Valenzuela et al., 2011). From the youngest to the oldest episode, the complex is divided in: (1) rhyolitic pyroclasts and lavas; (2) rhyolitic to rhyodacitic lavas and pyroclasts; and (3) tuffs and siliceous shales (Dallmeyer and Garcia, 2012; Soriano and Casas, 2002). The whole sequence is intruded by sills and dikes, comprised by gabbros, diorites, tonalities and granites. Most plutons emplaced after the extension event that affected the IPB. The magmatic evolution is linked to melting of progressively shallower crustal levels and is interpreted as having occurred in an extensional context linked with a mantle plume. This plume was probably mostly active between 355 and 335 Ma (Valenzuela et al., 2011).

The VSC is also divided into a lower autochthonous and an upper allochthonous sections. The autochthonous section is highly deformed and includes several major anticlinal folds such as Alcoutim and Cercal. On the other hand, the allochthonous segment is comprised by the Galé-Cela and Mértola Nappes (Dallmeyer and Garcia, 2012). Both sections have experienced hydrothermal alteration.

The Culm Group (CG)

Finally, the top of the IPB is made of the CG, a Late Viséan to Middle-Late Pennsylvanian (~300 Ma) turbidite. It consists of shale, litharenite and conglomerate. This flysh is partly made of rocks from the VSC and is interpreted as a consequence of the Variscan orogeny.

Deformation of IPB

Deformation that affects the whole IPB is known to have occurred in three phases. D1 is made of cleavages, folds verging SSW and associated north-dipping thrusts. D2 are the most widespread structures. Cleavages dip NNE, folds are asymmetric and verge to the south, and thrusts dip NNE. Folds are meters to decimeters scale. These D2 structures affect the D1 event. D3 structures are not well developed and do not interact with D1 and D2 structures. Cleavages can dip to the SSW as well as to the NNE and folds display and E-W trend (Soriano and Casas, 2002). All these deformations are the result of an extensive context and have been used again during the inversion to a compressive context during the Variscan orogeny shaping the actual landscape (Fig. 2). VHMS deposits formed using the preexisting thrusts, that were ideal channels for the circulation of metalliferous hydrothermal fluids (Leistel et al., 1997).

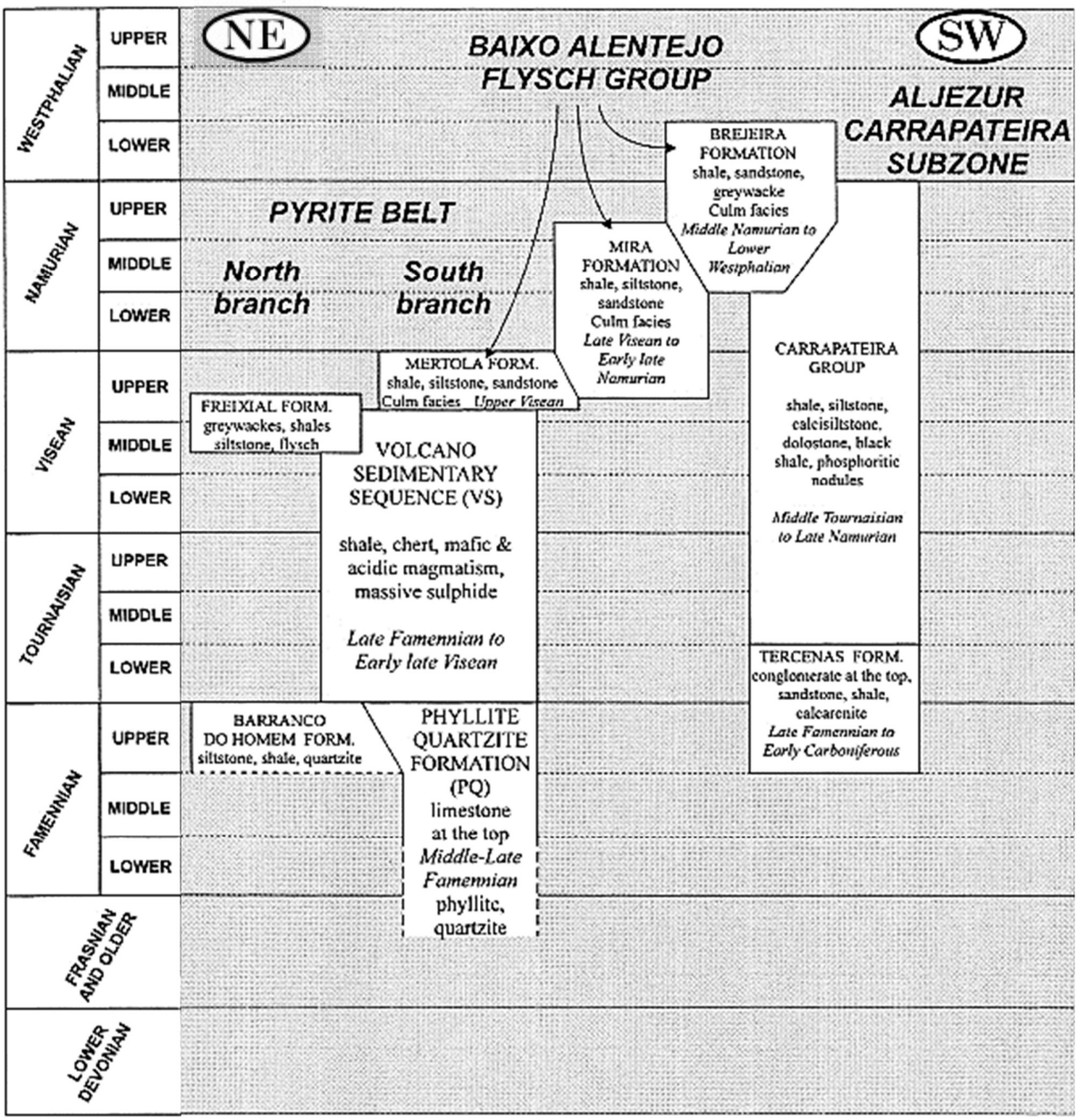

Figure 1: Summary of chrono-lithostratigraphic relations inside the South Portuguese, modified from Leistel et al. (1997).

Conclusion

Finally, the proposed scenario for the IBP formation is the following: (1) Rupture of the shallow water detritic platform (PQF) during Upper Famennian to Middle Visean. This resulted in the formation of a rift, which then split in half grabens and began volcanism, probably in relation with a mantellic plume; (2) Following subduction and collision between the southern branch and the Ossa-Morena Zone during the Variscan orogenesis, the extensional regime turned into a compressive one; and (3) gave birth to flysh sedimentation of the Culm Group.

Figure 2: (a) Paleogeographic context of the South Portuguese Zone at the Devonian-Carboniferous transition. (b) Paleogeographic context of the South Portuguese Zone during Upper Viséan. Modified from Onézime et al., 2003. (c) Cross section of the South Portuguese Zone. Obtained from Onézime et al. (2003).

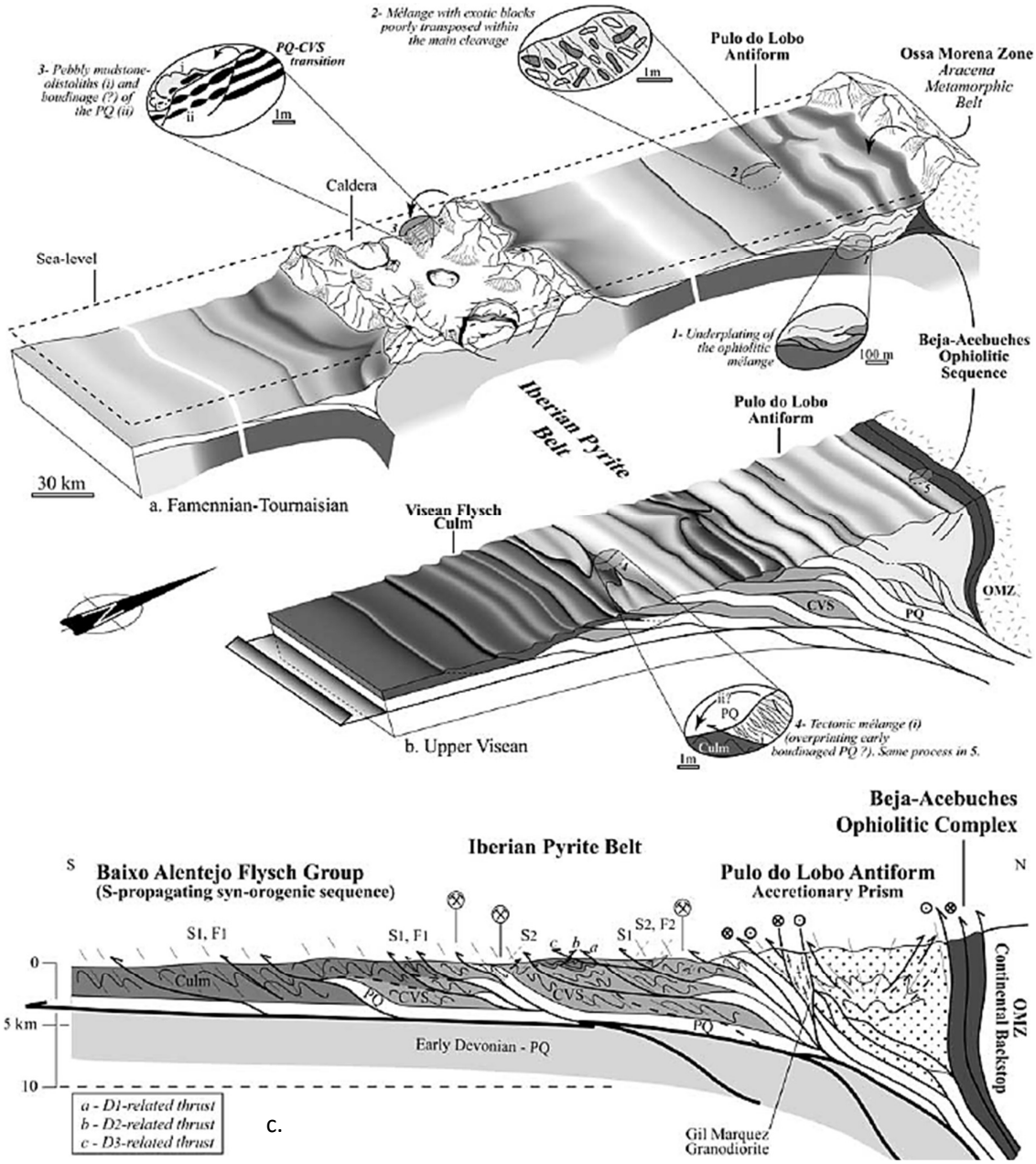

References

Dallmeyer, R.D., Garcia, E.M., 2012. Pre-mesozoic geology of Iberia. Springer Science & Business Media.

Leistel, J.M., Marcoux, E., Thiéblemont, D., Quesada, C., Sánchez, A., Almodóvar, G.R., Pascual, E., Sáez, R., 1997. The volcanic-hosted massive sulphide deposits of the Iberian Pyrite BeltReview and preface to the Thematic Issue. Miner. Deposita 33, 2–30. https://doi.org/10.1007/s001260050130

Onézime, J., Charvet, J., Faure, M., Bourdier, J.-L., Chauvet, A., 2003. A new geodynamic interpretation for the South Portuguese Zone (SW Iberia) and the Iberian Pyrite Belt genesis. Tectonics 22.

Soriano, C., Casas, J., 2002. Variscan tectonics in the Iberian Pyrite Belt, South Portuguese Zone. Int. J. Earth Sci. 91, 882–896. https://doi.org/10.1007/s00531-001-0253-8

Valenzuela, A., Donaire, T., Pin, C., Toscano, M., Hamilton, M.A., Pascual, E., 2011. Geochemistry and U–Pb dating of felsic volcanic rocks in the Riotinto–Nerva unit, Iberian Pyrite Belt, Spain: crustal thinning, progressive crustal melting and massive sulphide genesis. J. Geol. Soc. 168, 717–732. https://doi.org/10.1144/0016-76492010-081

6. Tharsis VMS deposits: Shale Hosted Massive Sulfide

Julian Mauricio Reyes Alvarez

Introduction

The Tharsis deposit is composed by 16 orebodies of very variable size with more than 133 Mt of ore, hosted in 5 open pits (Filón Norte, Filón Sur, Sierra Bullones, Filón Centro and Esperanza). The biggest mine is Filón Norte open pit, including the Filón Norte, San Guillermo and Sierra Bullones lenses, with at least 88 Mt of ore grading 46.5 wt% S, 2.7 wt% Zn + Pb, and 0.7 wt% Cu. While the gossan at Filón Sur mine contained 15.5 Mt of ore grading 1.7 g/t Au and 29 g/t Ag (Velasco et al., 2013). The district has felsic volcanic and shale rocks that have experienced major hydrothermal alteration with semimassive sulfides, stockwork and disseminated textures (Tornos et al. 2008). In the district, the mineralization could be hosted in volcanic (e.g. Almagrera, Lagunazo, La Lapilla, Filón Sur) and shale (e.g. Filón Norte, Fig. 3a) rocks.

Geological Setting

The main ore bodies are in a ~ 50–300 m thick tectonically complex area, in between tectonic sheets in a shale bearing unit (Lower unit). The bottom tectonic, thrust, contact is with the Phyllite-Quartzite (PQ) Group, located below the Volcanic Sedimentary Complex (VSC). The top contact of the main ore bodies is a tectonic sheet of dark shale with minor jasper intruded by basaltic sills of the VSC (Intermediate unit). The Lower and Intermediate units are the hanging wall of the Puebla de Guzman Nappe, in contact with a mylonitic zone on top, overlain by rhyodacitic subvolvanic sills within dark shales interbedded with felsic volcanoclastics, and microgabro sills of the VSC (Upper unit; Fig. 1, 2) (Conde et al. 2010; Tornos et al. 2008).

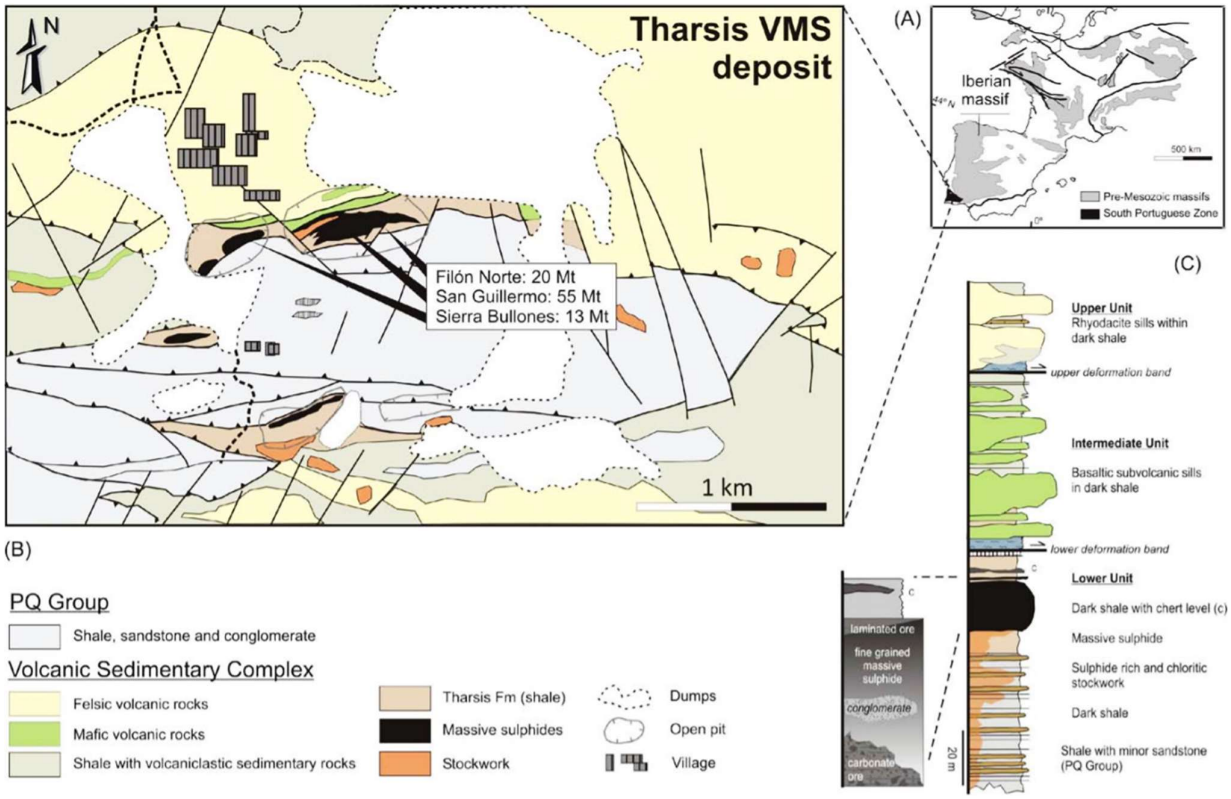

Figure 1: Geological setting of the Tharsis VMS deposit. (A) Schematic map of the Variscan Fold Belt in Europe (Oliveira and Quesada, 1998). (B) Detailed geological map of the Tharsis area and location of Filón Norte, San Guillermo and Sierra Bullones lenses (modified from Tornos et al., 2008). (C) General stratigraphic column of Filón Norte open pit, Tharsis, showing the distribution of the different types of mineralization within the orebody (modified from Tornos and Conde, 2002; Tornos et al., 2008). Obtained from Conde et al. (2010).

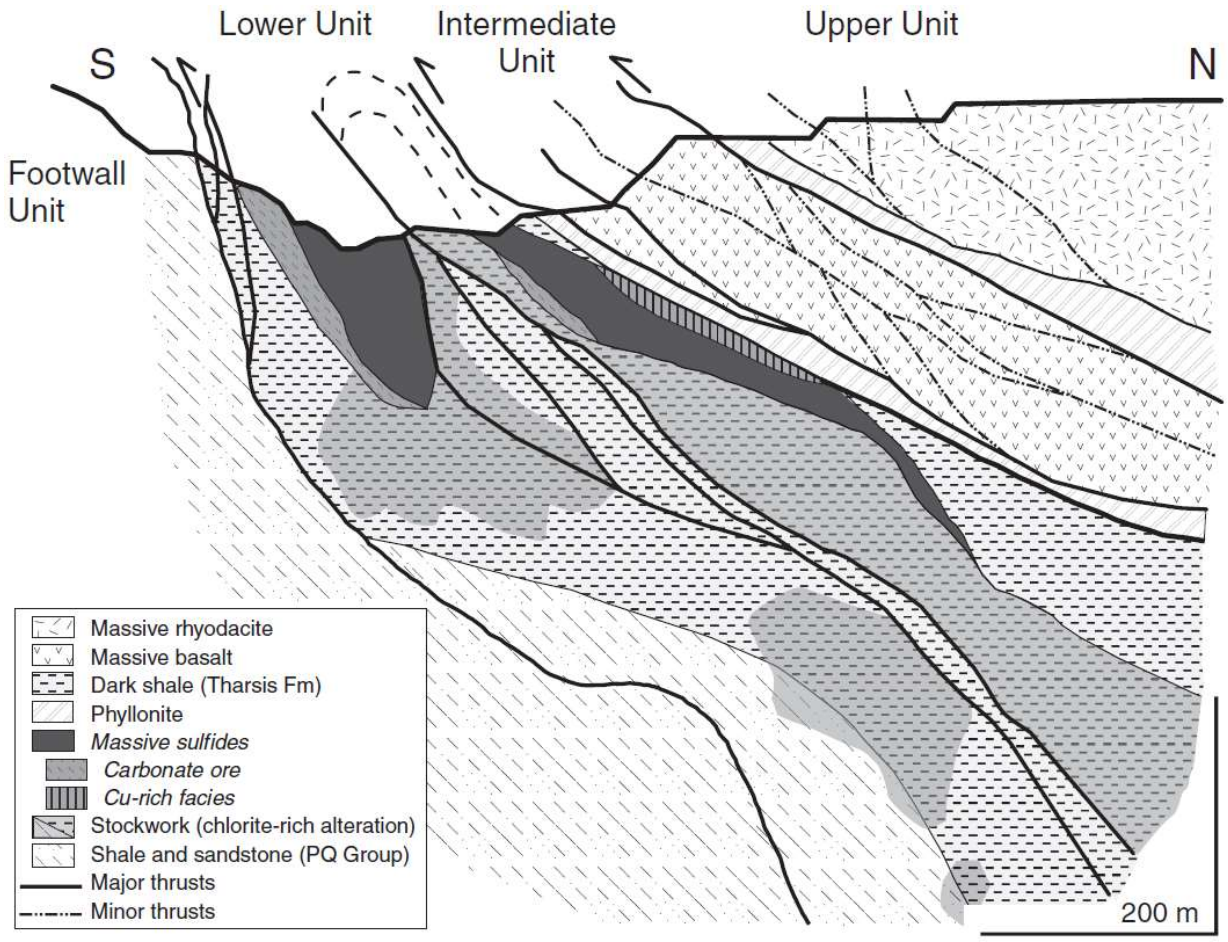

Figure 2: Cross section of the Filon Norte deposit from Tornos et al. (2008)

Filón Norte deposit

The igneous and sedimentary sequence adjacent to the orebodies, excluding the microgabbro sills in the Upper unit, has experienced pervasive hydrothermal alteration. Alteration in the Intermediate unit is evidenced as ankeritization, on the other hand, the Upper unit as sporadic sericitization and silicification (Tornos et al. 2008). From palynological dating of the shale hosting the Filón Norte deposit it is interpreted that the age of the Tharsis orebody is late Famennian (González et al., 2002), moreover, this age has been linked to other shale-hosted deposits in the southern Iberian Pyrite Belt (Aznalcóllar: Pereira et al., 1996; Neves Corvo: Oliveira et al., 2004) and is consistent with the 353±44 Ma and 348.6±12.3 Ma Re–Os ages by Mathur et al. (1999) and Nieto et al. (2000).

Shale-hosted stockwork mineralization

Chlorite alteration is developed in the stockwork zone, up to 200m, below the massive sulfides affecting the shale of the PQ Group and VSC. The stockwork is characterized by none structural control, with minor siderite, quartz and sulfides in the Fe-rich chloritization overprinting the shale (Tornos et al., 1998, Fig. 3f, 4a). In the interbedded volcaniclastic layers there is albite replacement (Tornos et al. 2008). The veins are 0.5- to 2-cm-wide of pyrite ± Co-As-Fe-S minerals (pyrrhotite, arsenopyrite, cobaltite, alloclasite, löellingite) ± quartz (± Bi-Pb-Cu-(Sb) sulfosalts ± tellurides (joseite, tetradymite) ± native gold) (Marcoux et el., 1996; Tornos et al., 1998). There is a clear evolution from Co-As-Fe-S minerals to younger pyrite in the core (Tornos et al. 2008). Afterwards, in the Variscan deformation pyrite, quartz, ankerite, and siderite veins precipitate and ductile minerals, including gold, are remobilized (Tornos et al., 1997, 1998; Marignac et al., 2003).

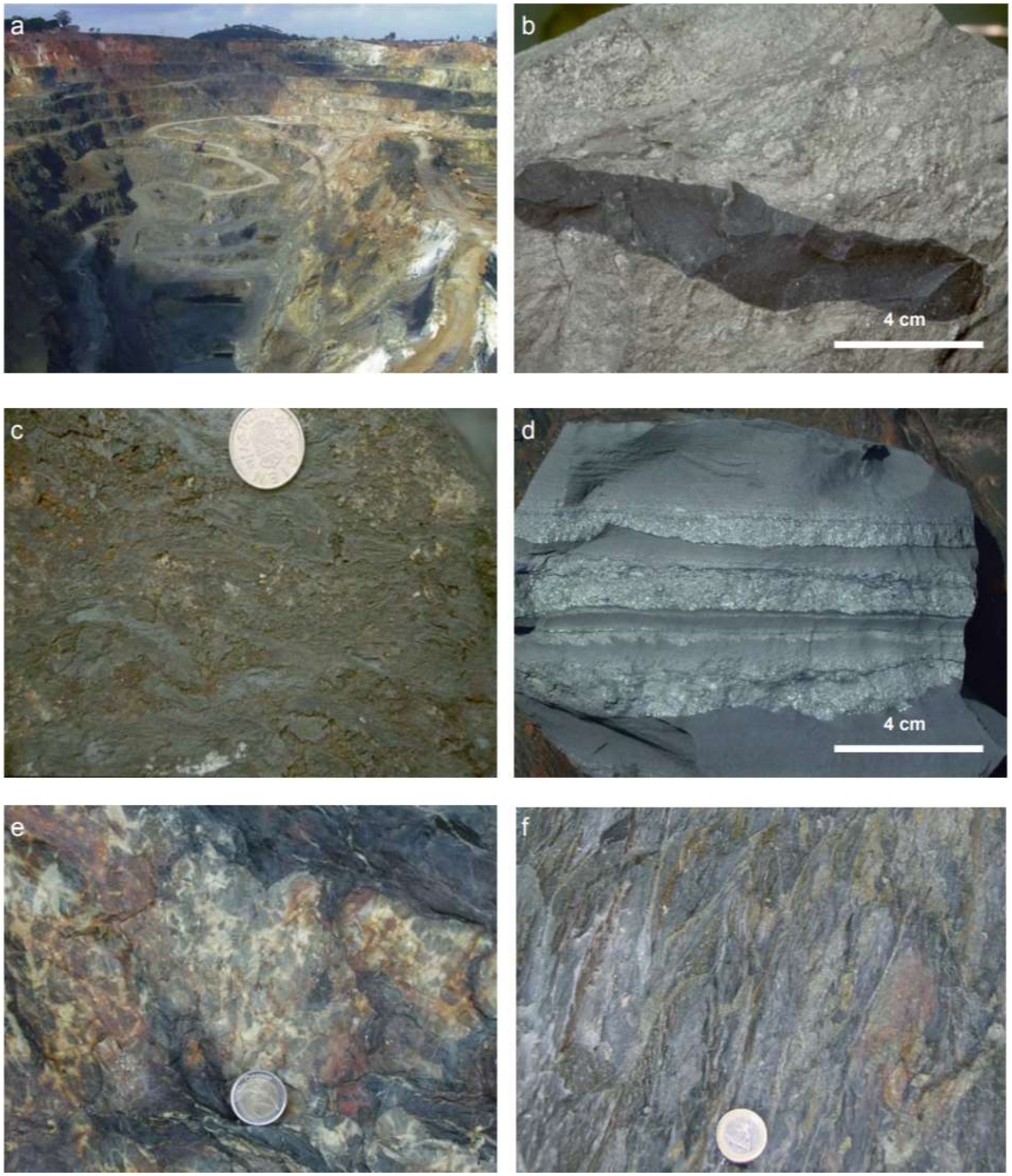

Figure 3: Representative photographs from outcrops on the Filón Norte orebody, Tharsis deposit. (a) Overview of Filón Norte open pit (Tharsis). (b) Large clast of siliceous shale supported by fine-grained pyrite in the conglomerate ore. (c) Carbonate ore showing fragments of fine alternating layers of siderite and sulphides (dominantly pyrite) cemented by coarse-grained pyrite + siderite (coin size, 2 cm). (d) Laminated ore showing layering that includes shale with local replacement by ankerite in its uppermost part, fine-grained breccia similar to the carbonate ore and finely layered pyrite with graded bedding. (e) Silicified shale in the hanging wall of the massive sulphides with lenses of chert (coin size, 2.5 cm). (f) Chloritized dark shale containing thin and irregular quartz and sulphide veins (stockwork) (coin size, 2.3 cm). Obtained from Conde et al. (2010).

Massive sulfides

Massive sulfides are found in lenses of up to 1,500 m long, 400 to 600 m wide and 130 m thick host the massive sulfides at Tharsis, although, it is not the primary thickness as there was tectonic stacking during the Variscan (Tornos et al., 1998). The composition of the massive sulfides is pyrite (anhedral to subhedral, fine- grained [50–400 µm]) ± chalcopyrite ± sphalerite ± galena ± siderite ± quartz ± chlorite (± cassiterite ± magnetite ± meneghinite ± bournonite) (Marcoux et al., 1996; Tornos et al., 1998). The most common textures are framboidal and subhedral, nevertheless botryoidal, colloform, crustiform and laminated textures could also be found. Additionally, casual centimeter sized lenses of sphalerite and galena are found in the deposit (Tornos et al., 1998).

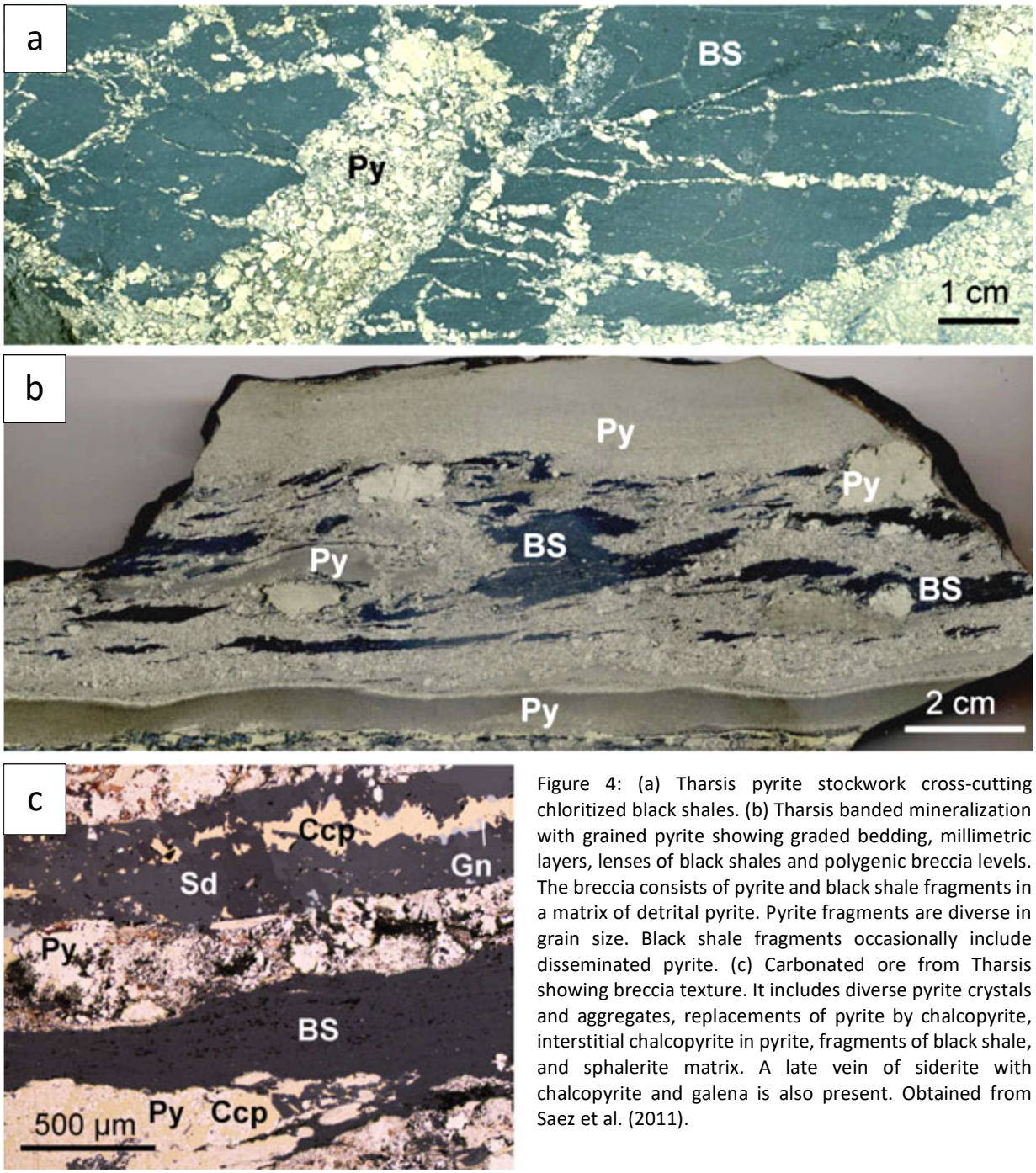

Figure 4: (a) Tharsis pyrite stockwork cross-cutting chloritized black shales. (b) Tharsis banded mineralization with grained pyrite showing graded bedding, millimetric layers, lenses of black shales and polygenic breccia levels. The breccia consists of pyrite and black shale fragments in a matrix of detrital pyrite. Pyrite fragments are diverse in grain size. Black shale fragments occasionally include disseminated pyrite. (c) Carbonated ore from Tharsis showing breccia texture. It includes diverse pyrite crystals and aggregates, replacements of pyrite by chalcopyrite, interstitial chalcopyrite in pyrite, fragments of black shale, and sphalerite matrix. A late vein of siderite with chalcopyrite and galena is also present. Obtained from Saez et al. (2011).

The footwall, the chloritized shale and massive sulfides, contact is sharp between although it has stockwork veins passing through. Furthermore, a centimeter sized layer of silicified shale (Fig. 3b) with disseminated pyrite defines this contact. The sulfides at the bottom evidence well-developed sedimentary laminations, the exhaustive alteration from magnetite, hematite and marcasite to pyrite in aggregates and pyrite in bladed textures when replacing sulfates. Moreover, in this section, brecciation from 3- to 10-cm rounded pyrite pebbles and shale in a fine-grained sulfide matrix occur in irregular lenses and biogenetic structures (worm burrows and escape structures in the interbedded shale) (Tornos and Conde, 2002). The escape structures are concentric layers of pyrite in a 2- to 3-cm-wide structure (Tornos et al. 2008).

Carbonate ores are found in mound-like structures, up to 20 m thick and 200 m long with botryoidal forms (Strauss and Beck, 1990), similar to biogenic sea-floor mounds (microbiolites) described by Russell (1996). Consists of laminated and brecciated, angular to sub-rounded, centimeter-sized clasts of sulfides and siderite in coarser grained pyrite and siderite matrix (Fig. 3c, 4c). Pyrite, bladed crystals, are pseudomorph of primary sulfate crystals in siderite-rich layers. Furthermore, the carbonate ore evidence hydrothermal conduits, 0.5 to 1 cm in diameter with concentric banding, and worm tubes (Tornos et al. 2008).

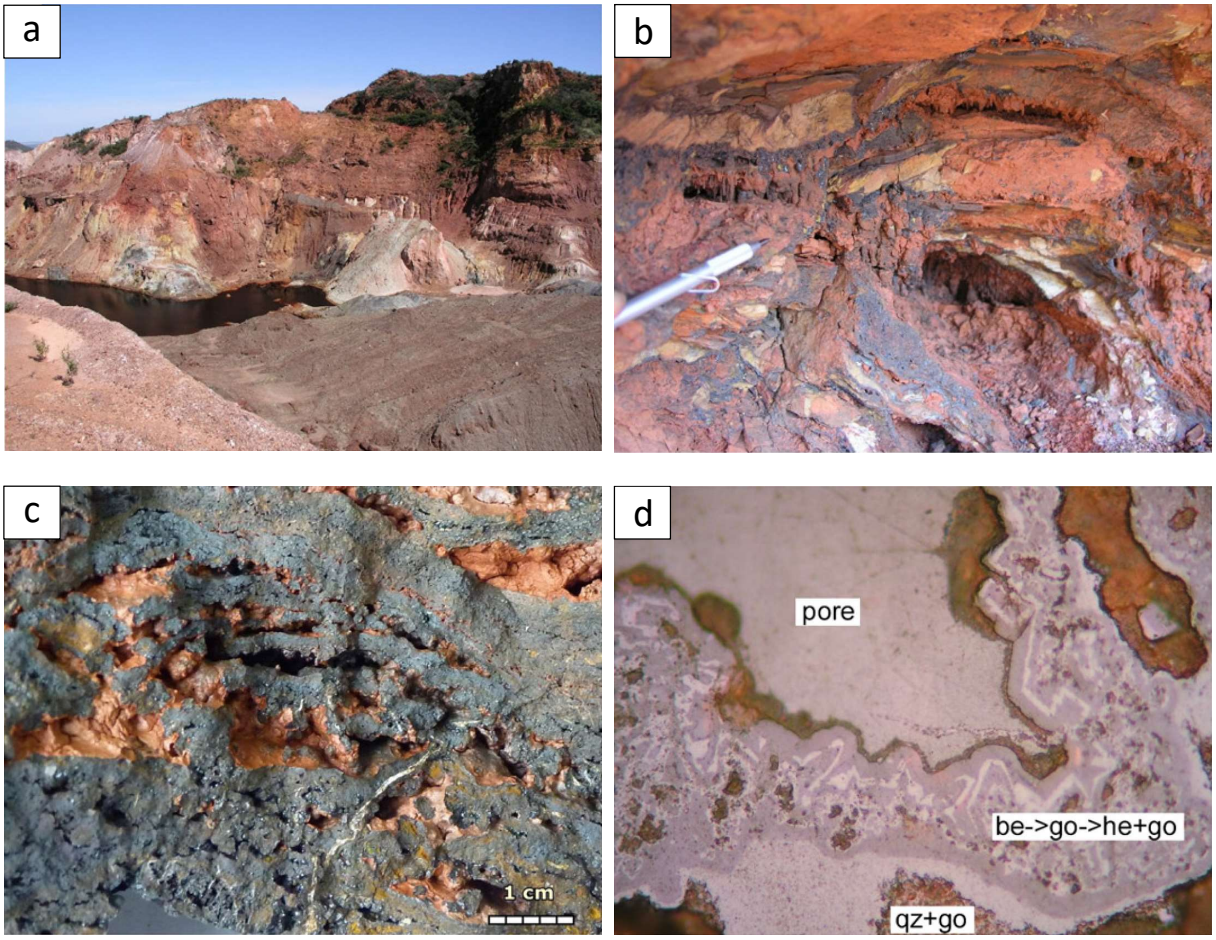

Figure 5: Field photographs showing: (a) classic goethite-rich oxidized zones (darker brown) of the gossan profiles. (b) brecciated gossan from Filón Sur. Note the planar character of the intensely gossanized rock fragments (brown light colour) and the stalactitic texture of the cementating composite (mainly goethite); (c) Typical “puff paste product” made of crusts of goethite showing a geopetal structure; voids, are carpeted by a fine film of hematite plus halloysite (Tharsis deposit); (d) micro-photograph showing a local sequence consisting of hematite and goethite displaying replica textures of subautomorphous beudantite (be), coating a mixture of quartz and goethite (Tharsis deposit). Obtained from Velasco et al. (2013).

The top of the orebody consists of 2- to 50-cm thick black shale interbedded with thin sulfide layers (banded ore) (Fig. 3d, 4a). This sequence has abundant sedimentary structures (fill and ripple marks, graded and delicate bedding, soft shale clasts, scour and synsedimentary faulting) (Tornos et al. 2008). Contrasting with the discontinuous, meter-thick, strata-bound mass-flow structures of chaotic and unsorted fragments of shale, sulfides, and chert in fine-grained sulfides matrix, found in the massive ore (Barriga and Fyfe, 1991; Fig. 3e). The mass flows occurred by proximal reworking of consolidated massive sulfide and host rocks (Tornos et al. 2008).

All the sequences have been overprinted by supergene, goethite-rich oxidized zones, alteration (Fig. 5a). This event is important as in Filón Sur, the main secondary Au enrichment occurs at intermediate levels associated with goethite (Capitan et al., 2003, 2006).

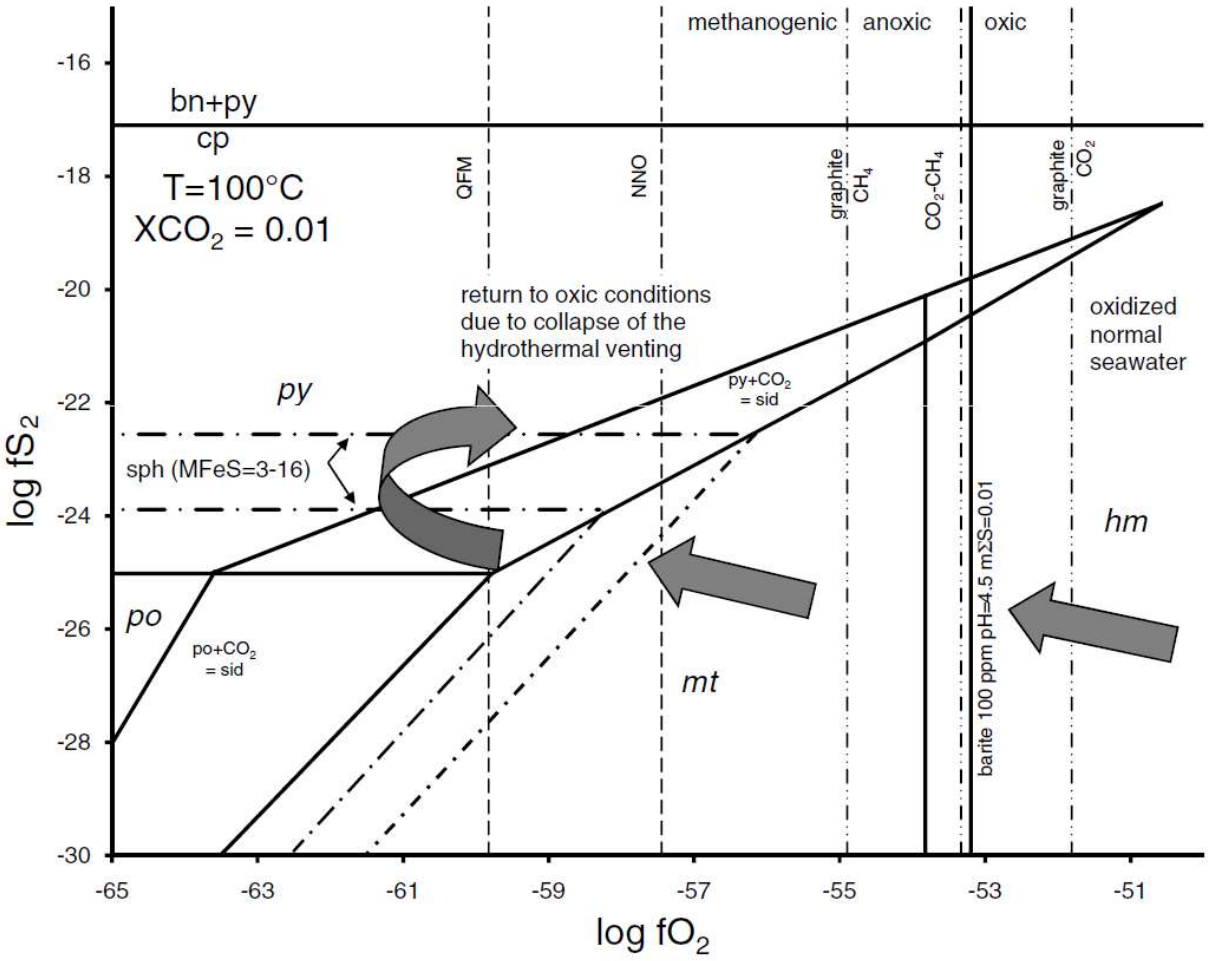

Figure 6: "Log fO2-log fS2 diagram showing a hypothetical evolution of the fO_2-log fS_2 conditions of formation of the massive sulfides in the Tharsis deposit. The evolutionary trend evolves from rather oxidizing to euxinic conditions, with precipitation of sulfates (barite?) + hematite + pyrite in the footwall followed by siderite + pyrite + sphalerite (with magnetite and cassiterite inclusions) and dominant pyrite and sphalerite, always in equilibrium with chalcopyrite and galena. Cassiterite is stable through all conditions in the diagram. The geochemistry of the shale suggests that after the formation of the orebody the ambient conditions returned to suboxic. The diagram is calculated using equilibrium constants from Patterson et al. (1981) and SUPCRT92 (Johnson et al., 1991), with the cassiterite-stannite field calculated from the free energies of formation provided by Patterson et al. (1981) and SUPCRT92. The positions of the gas buffers are from the equations of Spycher and Reed (1988), assuming a fluid phase with H2O-CO2. The boundaries between the fields of methanogenic, anoxic, and oxic waters are only approximate." Obtained from Tornos et al. (2008).

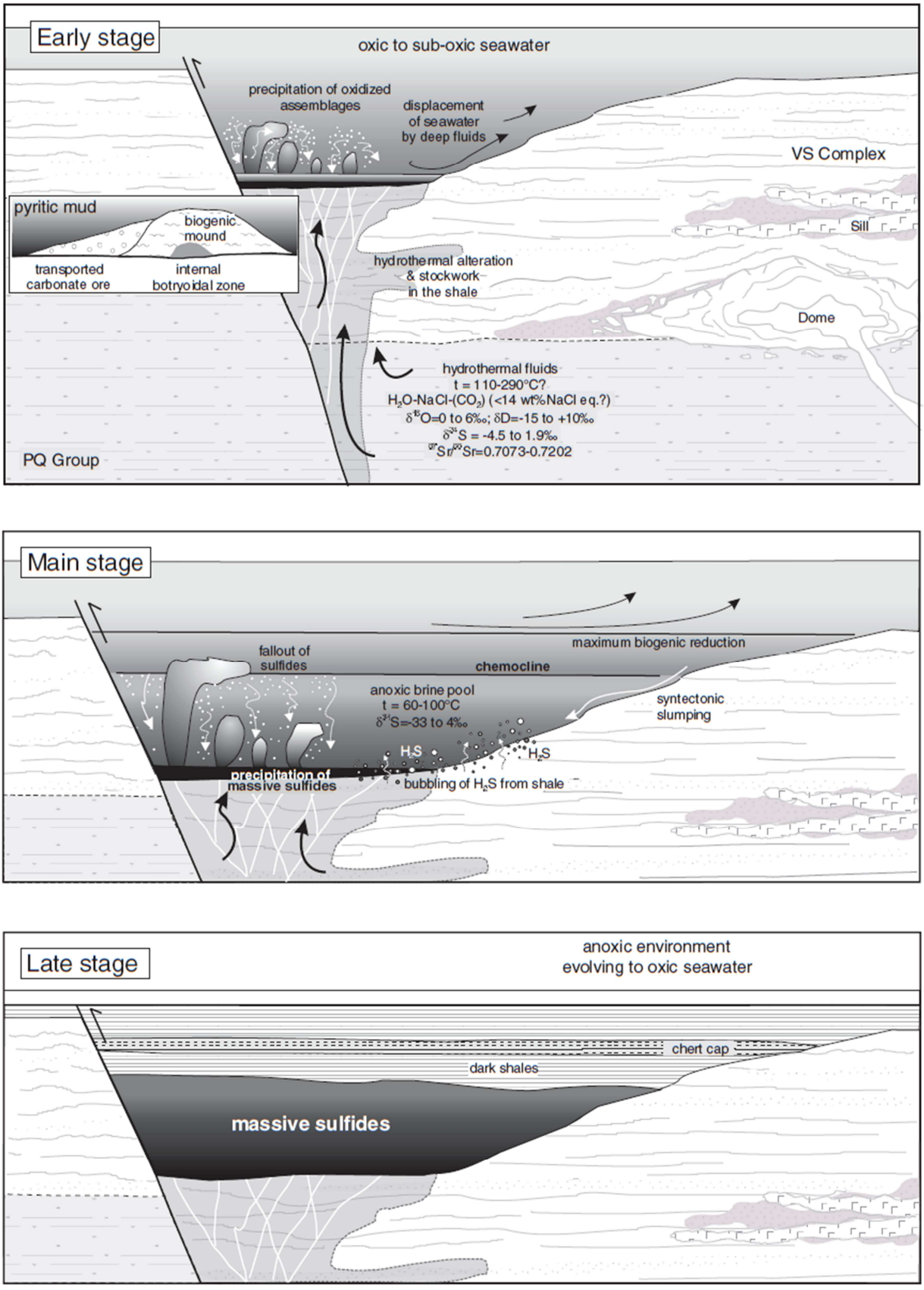

Figure 7: Genetic model for brine-pool formation and genesis of the Tharsis deposit. Obtained from Tornos et al. (2008).

References

Capitán, A, JM Nieto, R Sáez, and GR Almodóvar. 2003. 'Caracterización textural y mineralógica del gossan de Filón Sur (Tharsis, Huelva)', *Boletín de la Sociedad Española de Mineralogía*, 26: 45-58.

Capitán, MA. 2006. 'Mineralogía y geoquímica de la alteración superficial de depósitos de sulfuros masivos en la Faja Pirítica Ibérica', *Unpublished Ph. D. thesis*: 260.

Conde, C., F. Tornos, R. Large, L. V. Danyushevsky, and M. Solomon. 2010. *Laser Ablation-ICPMS Analysis of Trace Elements in Pyrite from the Tharsis Massive Sulphide Deposit* (James Cook Univ: Townsville).

Gonzalez, F., C. Moreno, R. Saez, and G. Clayton. 2002. 'Ore genesis age of the Tharsis Mining District (Iberian Pyrite Belt): a palynological approach', *Journal of the Geological Society*, 159: 229-32.

Johnson, James W, Eric H Oelkers, and Harold C Helgeson. 1992. 'SUPCRT92: A software package for calculating the standard molal thermodynamic properties of minerals, gases, aqueous species, and reactions from 1 to 5000 bar and 0 to 1000 C', *Computers & Geosciences*, 18: 899-947.

Marcoux, E., Y. Moelo, and J. M. Leistel. 1996. 'Bismuth and cobalt minerals as indicators of stringer zones to massive sulphide deposits, Iberian Pyrite Belt', *Mineralium Deposita*, 31: 1-26.

Marignac, C., B. Diagana, M. Cathelineau, M. C. Boiron, D. Banks, S. Fourcade, and J. Vallance. 2003. 'Remobilisation of base metals and gold by Variscan metamorphic fluids in the south Iberian pyrite belt: evidence from the Tharsis VMS deposit', *Chemical Geology*, 194: 143-65.

Mathur, R., J. Ruiz, and F. Tornos. 1999. 'Age and sources of the ore at Tharsis and Rio Tinto, Iberian Pyrite Belt, from Re-Os isotopes', *Mineralium Deposita*, 34: 790-93.

Nieto, JM, GR Almodóvar, E Pascual, R Sáez, and E Jagoutz. 2000. 'Evidencias isotópicas sobre el origen de los metales en los sulfuros masivos de la Faja Pirítica Ibérica'.

Oliveira, J Tomas, Zelia Pereira, Pedro Carvalho, Nelson Pacheco, and Dieter Korn. 2004. 'Stratigraphy of the tectonically imbricated lithological succession of the Neves Corvo mine area, Iberian Pyrite Belt, Portugal', *Mineralium Deposita*, 39: 422-36.

Oliviera, JT, and C Quesada. 1998. 'A comparison of stratigraphy, structure and palaeogeography of the South Portuguese Zone and South-West England, European Variscides', *PROCEEDINGS-USSHER SOCIETY*, 9: 141-50.

Patterson, DJ, H Ohmoto, and M Solomon. 1981. 'Geologic setting and genesis of cassiterite-sulfide mineralization at Renison Bell, western Tasmania', *Economic Geology*, 76: 393-438.

Pereira, Z, Reinaldo Sáez Ramos, JM Pons, JT Oliveira, and María Carmen Moreno Garrido. 1996. 'Edad devónica (Struniense) de las mineralizaciones de Aznalcóllar (Faja Pirítica Ibérica) en base a palinología'.

Saez, R., C. Moreno, F. Gonzalez, and G. R. Almodovar. 2011. 'Black shales and massive sulfide deposits: causal or casual relationships? Insights from Rammelsberg, Tharsis, and Draa Sfar', *Mineralium Deposita*, 46: 585-614.

Spycher, Nicolas F, and Mark H Reed. 1988. 'Fugacity coefficients of H2, CO2, CH4, H2O and of H2O-CO2-CH4 mixtures: A virial equation treatment for moderate pressures and temperatures applicable to calculations of hydrothermal boiling', *Geochimica Et Cosmochimica Acta*, 52: 739-49.

Tornos, F., E. G. Clavijo, and B. Spiro. 1998. 'The Filon Norte orebody (Tharsis, Iberian pyrite belt): a proximal low-temperature shale-hosted massive sulphide in a thin-skinned tectonic belt', *Mineralium Deposita*, 33: 150-69.

Tornos, F., M. Solomon, C. Conde, and B. F. Spiro. 2008. 'Formation of the Tharsis massive sulfide deposit, Iberian Pyrite Belt: Geological, lithogeochemical, and stable isotope evidence for deposition in a brine pool', *Economic Geology*, 103: 185-214.

Tornos, Fernando, and C Conde. 2002. 'La influencia biogénica en la formación de los yacimientos de sulfuros masivos de la Faja Pirítica Ibérica'.

Velasco, F., J. M. Herrero, S. Suarez, I. Yusta, A. Alvaro, and F. Tornos. 2013. 'Supergene features and evolution of gossans capping massive sulphide deposits in the Iberian Pyrite Belt', *Ore Geology Reviews*, 53: 181-203.

7. Description of the Iberian Pyrite Belt (IPB) hydrothermal fluids

Zia Steven KAHOU

Introduction

Submarine volcanism is the most important magmatic process on the planet earth. The hydrothermal circulation associated with this submarine volcanism plays a key role in the thermal and geochemical balance of the earth: internal heat dissipation and ocean recycling (Jébrak and Marcoux, 2008). Two major processes are at the origin of these fluid flows in the oceanic crust. Magmatism at the ocean ridges with hot hydrothermal fluids (>350°C) generated by forced convection and free convection as you move away from the ridge. Volcanogenic Massive Sulphides (VMS) are the result of oceanic hydrothermalism. They are the largest concentrations of massive sulphides in the world (Iberian Pyrite Belt, Ural, Canada, etc.). These deposits show a root consisting of a network of veinlets or stockwork, constituting the drain for access to hydrothermal fluids and a lenticular, stratiform mineralized body, generally deposited at the base of the basin or in the underlying sediments. The sulphide ore has a zonation of Pyrite, Chalcopyrite and Pyrrhotite at the base and galena, sphalerite and/or gold at the top. These deposits have been and remain an important source of Copper (5% of world production), Zinc (50% of world production), Lead, Tungsten and Tin. They have also been an important source of sulphur for many years.

Geological setting

The Iberian Pyrite Belt (IPB) is the largest concentration of volcanogenic massive sulphides in the world (Sáez et al., 1996). It forms a belt 230 km long and 40 km wide at the SW of the Iberian plate (Fig. 1). The deposit was formed during the early Carboniferous in a transtensional environment in several E-W trending throughs (Marignac et al., 2003). These volcanogenic massive sulphides underwent both ductile deformation and thermal signature under metamorphic conditions on the Prehnite-Pumpellyite facies (Tornos, 2006). According to Jébrak and Marcoux (2008), three deposit environments are generally mentioned for the establishment of these deposit: (1) volcanic domain in the North with felsic domes, sills and volcanoclastic sediments; (2) intermediate domain with felsic volcanism associated with hydrothermal exhalations on the sea floor; and (3) highly sedimentary southern domain where metallic sulphides are associated with black shale deposits.

Hydrothermal alteration on the Iberian Pyrite Belt

Alteration types

According to Sánchez-España (2000), the hydrothermal alteration in the IPB can be divided into 4 major episodes from the Late Carboniferous to the present.

1) regional alteration in relation to the late Devonian volcanism so called "hydrothermal metamorphism" resulting from the interaction between sea waters and volcanic rocks of the ocean floor.
2) localized hydrothermal alteration related to the stockwork installed during the sulphide deposition. Concomitantly with this hydrothermal alteration, intense metasomatism developed, responsible for the main textural and chemical transformations of minerals.
3) low-grade metamorphism set up during the Hercynian period. Episode that does not seem to have affected the chemistry and mineralogy of rocks, except for minor recrystallizations.
4) supergene alteration with mineralization affected by intense weathering alteration due to meteoric waters: oxidation of primary Fe and Cu-sulphides, and precipitation of Cu-sulphates and iron oxides such as brochantite, hematite and goethite.

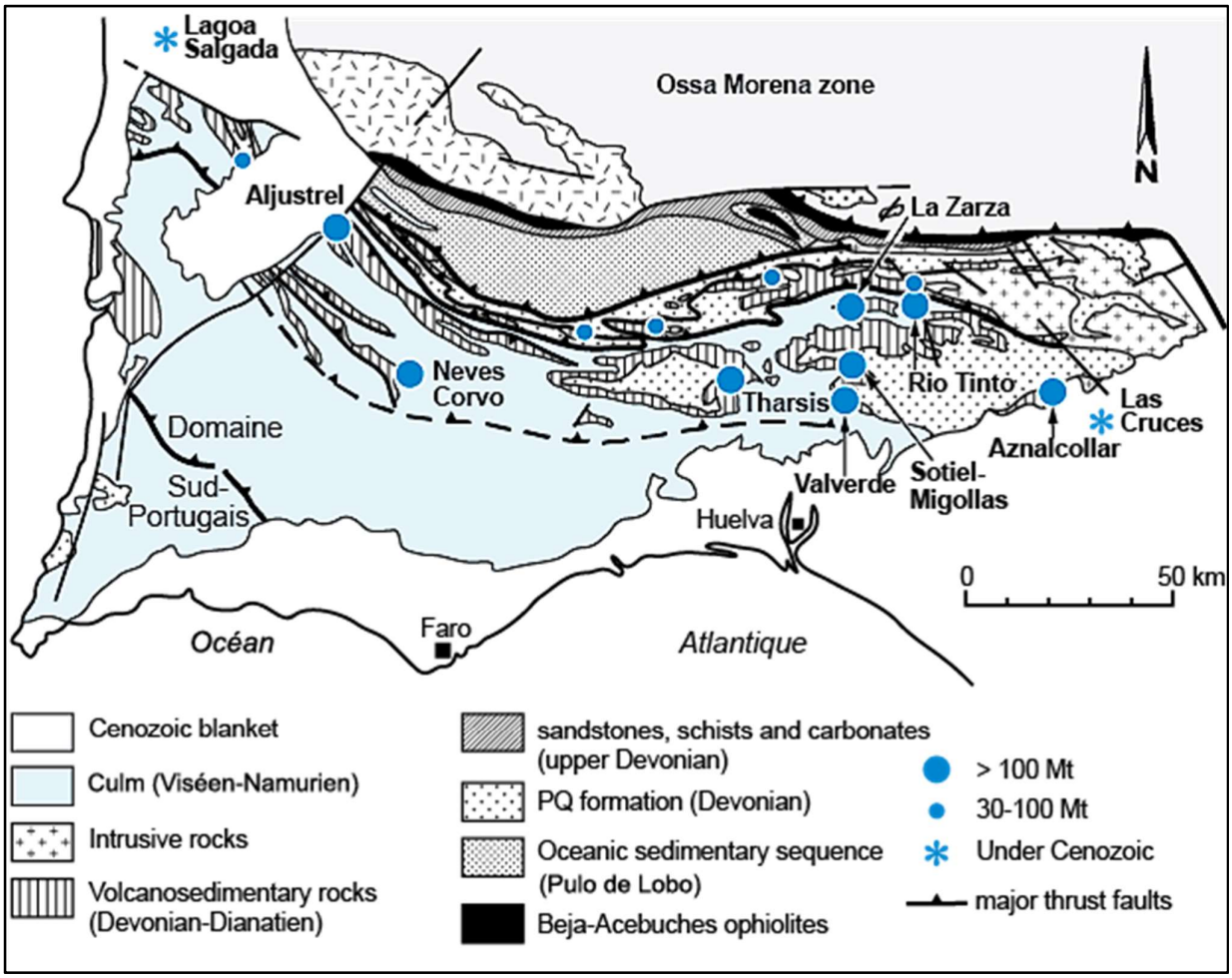

Figure 1: Simplified geological map of the South Iberian pyrite belt (Spain and Portugal) with position of the most important deposits. The clusters are all associated with the rhyolites of the devono-dinantian volcanosedimentary group. Modified from Jébrak and Marcoux (2008).

Sánchez-España (2000), Relvas et al. (2001) and Jébrak and Marcoux (2008) have proposed the model below to explain the hydrothermal and mineralizing history of Iberian Pyrite Belt:

1) Primary stage, with fluids at moderate temperatures and pH (150°C-250°C; pH ~ 4-5) carrying the mineralization that will react with porous volcanic tuffs. In this stage, feldspar and albite will be destabilized and chlorite, pyrite and sphalerite will crystallize;
2) Second, evolved, stage with warmer (300°C-350°C) and acidic (pH < 4) fluids will generate intense alteration of primary minerals. Pyrite and Chalcopyrite will precipitate abundantly during this stage. Chemically, there will be addition of Fe, Mg, Zn, Cu and Sn and depletion in K and Na;
3) Latest hydrothermal stage with the disappearance of the original rock to chloritic rocks. Moreover, an increase in the amount of CO_2 is responsible for the local precipitation of Fe-rich carbonates. In addition to these studies mentioned above, Sánchez-España et al. (2003) have shown via a fluid-inclusion study, in the northern IPB, that the homogenization temperatures mostly range from 120°C to 280°C with a salinity of 2 to 14 wt.% NaCl eq., a result which show an evidence of *(a)* long periods of heated seawater convection, *(b)* boiling of hydrothermal fluids accompanied by adiabatic cooling and *(c)* interaction of heated seawater with volcanic and sedimentary rocks.

Isotopes studies to constrain the source of fluids and metals

Many studies have used, in the recent years, the isotopes to point out the origin of ore-forming metals. In the IPB, many authors (e.g. Mathur et al., 1999; Sánchez-España, 2000 and Relvas et al., 2001) used stable and radiogenic isotopes to address the source and evolution of mineralizing fluids. In the Tharsis and Rio Tinto VMS deposit, Re-Os isotope has shown that the source of metals was crustal. Furthermore, some previous studies on O, H and S isotopes have shown that the metals were mainly transported by seawater brines that leached Cu, Zn, Pb, Sn and W from the continental crust. In the Neves Corvo ore genesis, Sr, Nd and Pb isotopes studies initiated by Relvas et al. (2001) have shown that sulphides and tin ores have different sources. If the sulfides ores are consistent with volcanic-seawater hydrothermal fluids, the tin ores have shown an external source, a magmatic source from a deeper Palaeozoic basement or a metamorphic fluid deeply circulated through older basement rocks.

The stable isotope results ($\Delta^{13}C$, $\Delta^{18}O$ and ΔD) have shown that the ore-forming fluids were most likely dominated by seawater, with later infiltration into the upper crust, interaction with the volcanic and sedimentary rocks, agreeing with the VMS hydrothermal model. Although, Sánchez-España et al. (2003) suggest that magmatic fluids have played a subsequent role as a direct contributor of metals. Then, two main fluids sources can be invoked: (1) seawater; and (2) a primary magmatic fluid. Starting from all mentioned above, we can therefore propose this model (Fig. 2) of Jébrak and Marcoux (2008) to explain the hydrothermal system allowing the genesis of a VMS ore-deposit.

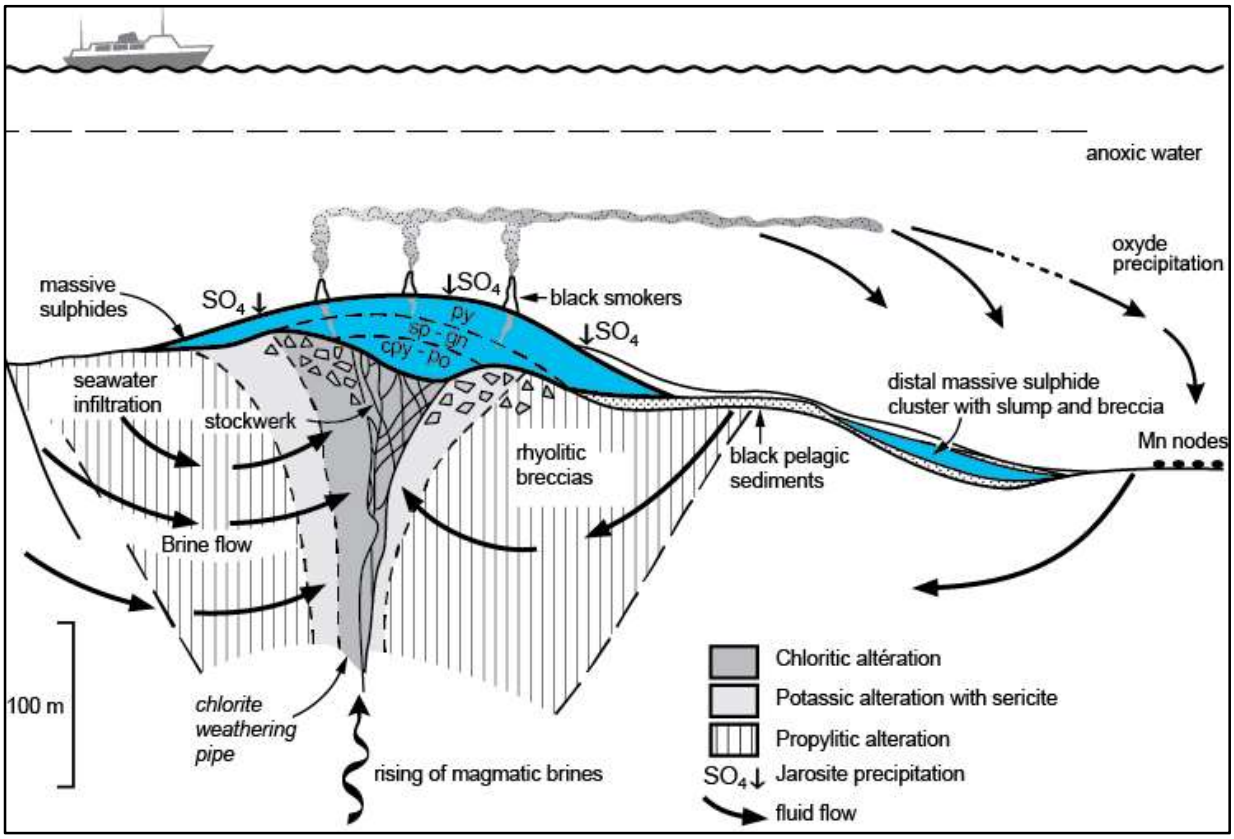

Figure 2: Idealized pattern of a VMS sulphide cluster and its feed stockwork which show the zonation of the hydrothermal alteration around the stockwork and the mineral zonation within the cluster. Modified from Jébrak and Marcoux (2008).

Conclusion

The VMS of Iberian Pyrite Belt were formed by the convection of seawater mixed with magmatic and/or metamorphic fluids in agreement with current hydrothermal systems. Although most of the fluid is heated seawater, the presence of magmatic fluids is essential to provide metallic sulphides. The system progressively evolves from a fluid with a moderate pH and temperature to hot, acidic and saline fluids, responsible for intense weathering and abundant precipitation of metal sulphides such as pyrite, chalcopyrite, galena, cassiterite and sphalerite. VMS deposits have a characteristic zonations from the fluid-rock interaction (Fig. 3).

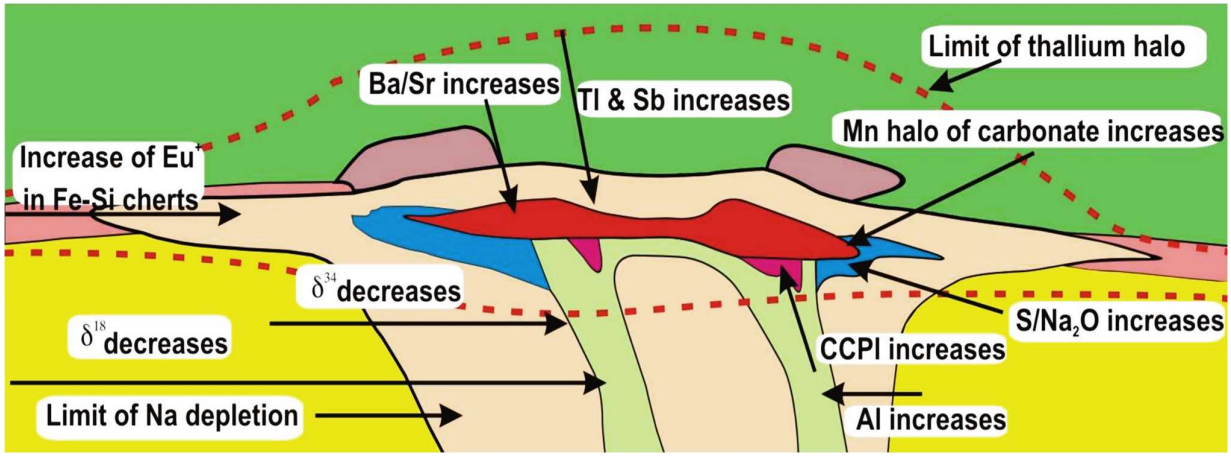

Figure 3 : geochemical and isotopic characteristics of footwall and hanging wall alteration zones with distance from massive sulphide. Obtained from Gibson et al. (2007).

References

Gibson, H. L., Allen, R. L., Riverin, G., & Lane, T. E. (2007). The VMS model: Advances and application to exploration targeting. In Proceedings of Exploration (Vol. 7, pp. 713-730).

Jébrak M, Marcoux E (2008) Géologie des ressources minérales, Ministère des ressources naturelles et de la faune. Québec

Marignac C, Diagana B, Cathelineau M, et al (2003) Remobilisation of base metals and gold by Variscan metamorphic fluids in the south Iberian pyrite belt: evidence from the Tharsis VMS deposit. Chemical Geology 194:143–165. doi: 10.1016/S0009-2541(02)00275-9

Mathur R, Ruiz J, Tornos F (1999) Age and sources of the ore at Tharsis and Rio Tinto, Iberian Pyrite Belt, from Re-Os isotopes. Mineralium Deposita 34:790–793. doi: 10.1007/s001260050239

Relvas JM, Tassinari CC, Munhá J, Barriga FJ (2001) Multiple sources for ore-forming fluids in the Neves Corvo VHMS Deposit of the Iberian Pyrite Belt (Portugal): strontium, neodymium and lead isotope evidence. Mineralium Deposita 36:416–427. doi: 10.1007/s001260100168

Sáez R, Almodóvar GR, Pascual E (1996) Geological constraints on massive sulphide genesis in the Iberian Pyrite Belt. Ore Geology Reviews 11:429–451. doi: 10.1016/S0169-1368(96)00012-1

Sánchez-España J (2000) Mineralogía y geoquímica de yacimientos de sulfuros masivos en el área nor-oriental de la faja pirítica ibérica (norte de huelva, españa). Http://purl.org/dc/dcmitype/Text, Universidad del País Vasco - Euskal Herriko Unibertsitatea

Sánchez-España J, Velasco F, Boyce AJ, Fallick AE (2003) Source and evolution of ore-forming hydrothermal fluids in the northern Iberian Pyrite Belt massive sulphide deposits (SW Spain): evidence from fluid inclusions and stable isotopes. Mineralium Deposita 38:519–537. doi: 10.1007/s00126-002-0326-z

Tornos F (2006) Environment of formation and styles of volcanogenic massive sulfides: The Iberian Pyrite Belt. Ore Geology Reviews 28:259–307. doi: 10.1016/j.oregeorev.2004.12.005

8. Las Cruces VMS deposits: Supergene alteration

Julian Mauricio Reyes Alvarez

Introduction

Las Cruces deposit is located in the eastern section of the IPB. The mine is operating, mainly, the supergene Cu-enriched zone with at least 17.6 Mt of ore grading 6.2 wt% Cu. Furthermore, an upper section of the gossan is Au-Ag-Pb–rich with 3.6 Mt of ore grading 3.3% Pb, 2.5 g/t Au, and 56.3 g/t Ag (Fig. 1). Gold concentration ranges from 0.01 to >100 ppm in three different settings: (1) related to Fe-oxides lithofacies in the upper section of the gossan; (2) associated to leached black shales in the lower section of the gossan; (3) linked to cementation zones proximal to subvertical faults (Yesares et al. 2017).

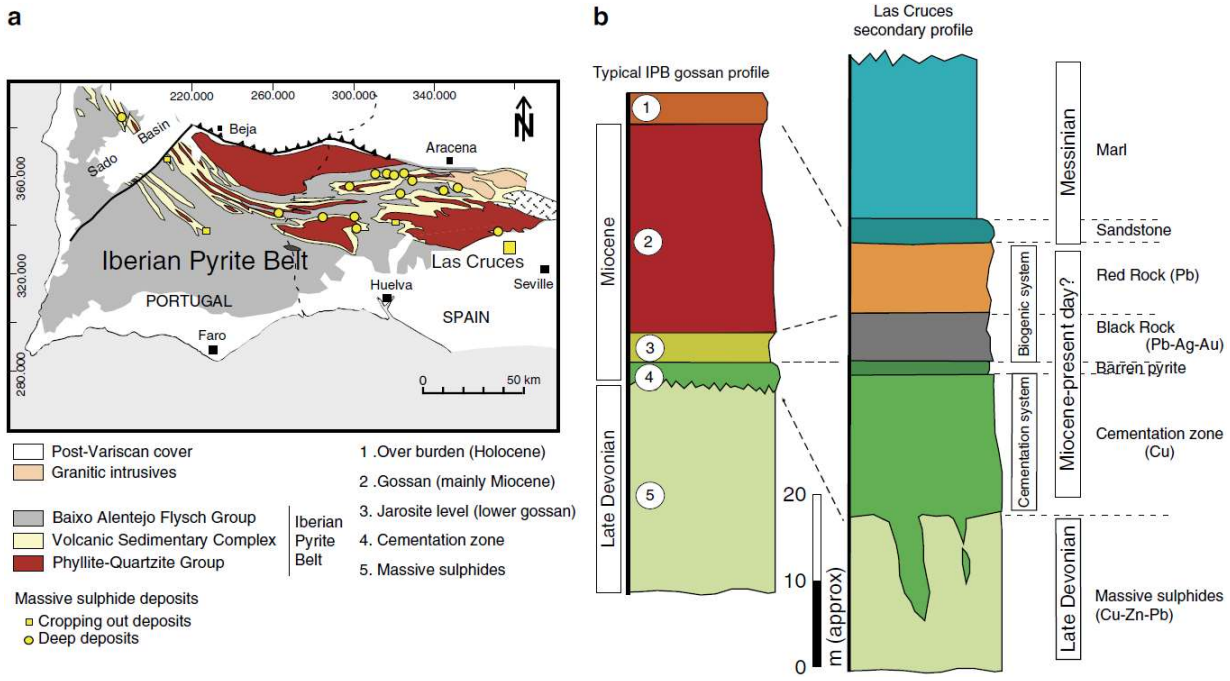

Figure 1: Geologic setting of the Las Cruces mine. (a) Regional geological map with the deposit location; (b) sections of the typical gossan of the Iberian Pyrite Belt and secondary mineralized zone at Las Cruces (graphical scale, ca. 20 m). Outcropping ore deposits of the Iberian Pyrite Belt have well-formed gossans. Las Cruces is an exception, with a secondary zone covered by Cenozoic sediments. The quoted ages are depositional ages for the primary massive sulfides and the sediments but are formational ages of the gossan and secondary mineralization. Taken from Tornos et al. (2014).

Geological Setting

The Las Cruces deposit is under a thick sequence (140–150 m) of carbonate-rich of post-Alpine (Neogene-Quaternary) origin, the Guadalquivir basin (Fig. 1). The orebody is within a sequence of black shales, interbedded with felsic volcanic and volcaniclastic rocks. The ore is found as massive sulfides and, below, as stockwork. The orebody is 60-100 m thick and 1 km long, dipping 35° to the north. A gossan cap and a copper-rich cementation zone overprints the upper section of the massive sulfides (Yesares, Saez, et al. 2015).

Three structural events have been recorded in the Las Cruces deposit (Fig. 2):

1) low-angle faults related to early-Variscan deformation. This event stacked the massive sulfides by shearing the deposits, especially black shales that served as detachment horizons;
2) subvertical faults associated to late-Variscan deformation;
3) NNW-SSE trending high angle faults and younger east-west faults, both late-Variscan, were reactivated during Alpine deformation. This event is related to secondary enrichment processes.

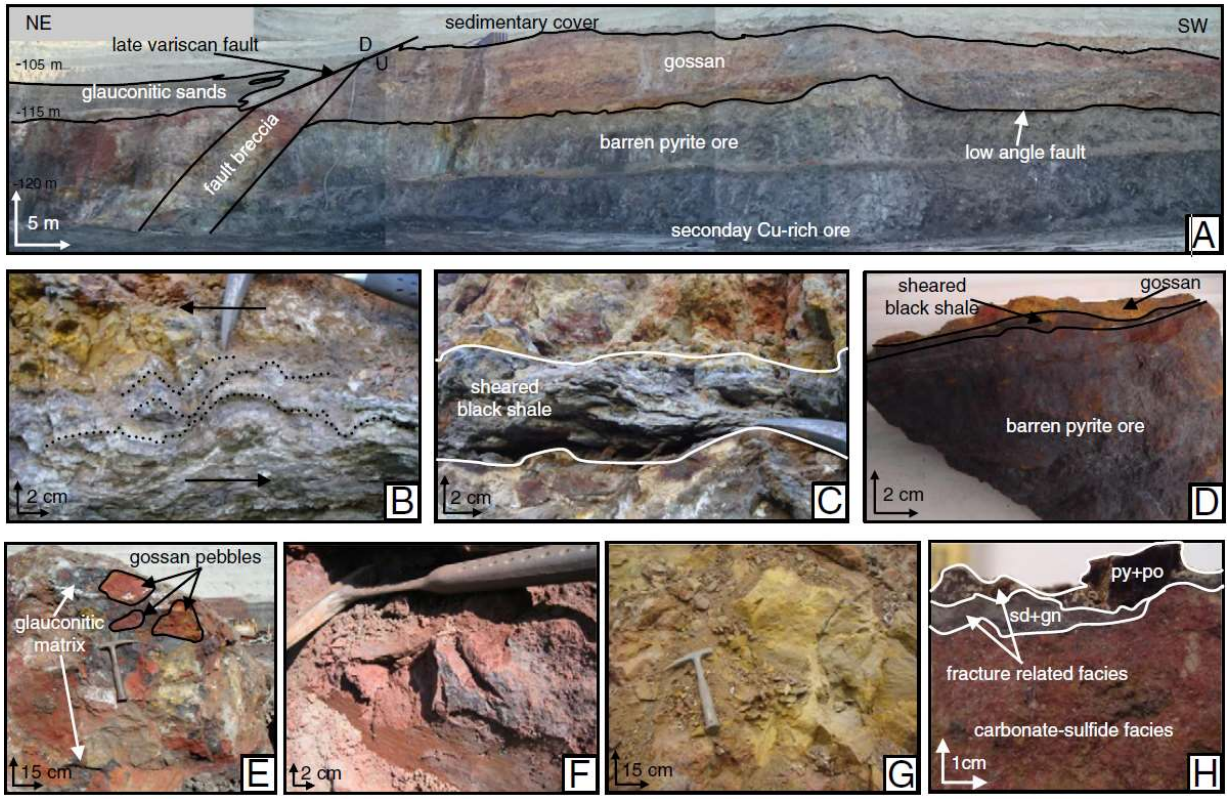

Figure 2. Las Cruces outcrops overview. (A) NE–SW section of the open pit showing the contact of the gossan with the primary ore (below) and the sedimentary cover on top; (B) and (C): sheared black shale level. Drag folds indicating the direction of movement can be observed (D); (E) basal conglomerate: gossan pebbles in a glauconitic sand matrix; gossan facies: (F) Fe-oxide facies; (G) carbonate-sulfide facies; and (H) fracture-related facies. Taken from Yesares et al. (2014).

Las Cruces deposit

Las cruces deposit is divided in to major environments: (1) primary mineralization, massive sulfides, formed by pyrite ± chalcopyrite ± sphalerite ± galena (± Tennantite – tetrahedrite ± arsenopyrite ± Bi and Pb-sulfosalts); and (2) supergene profile that could be dived in further two sections: (a) 50 m thick cementation zone, better developed at late-Variscan subvertical faults (Yesares et al., 2014, 2015); (b) up to 20 m thick gossan, with a sharp contact at the base with the massive sulfides, and the erosive discordance of the Guadalquivir basin on top.

Cementation zone

Four different facies have been identified in the cementation zone (Yesares, Saez, et al. 2015):

1) Pyritic sands, up to 5 m thick bed of sand-like (crumbled and leached) barren pyrite at the top of the cementation zone;
2) Chalcocite-rich secondary ore, is the main Cu supergene enrichment from the massive sulfides and stockwork mineralization. This zone is below the pyritic sands with a mineralogy of chalcocite + digenite + djurleite ± covellite ± bornite ± enargite;
3) Covellite-rich secondary ore, 12 m thick at the bottom of the cementation zone, form around a deep subhorizontal fault. The mineralogy is covellite ± chalcocite ± digenite ± enargite ± bornite.
4) Fault breccia-related Au-Ag–rich secondary ore, subvertical breccia-fault zone cross cutting the cementation zone, up to 5 m wide. Composed of fault gouge (mainly formed by pyrite clasts) and newly formed grains of proustite, pyrargyrite, cinnabar, and native Au. The most common textures are cinnabar filling fractures and voids and coarse-grained aggregates of Ag-sulfosalts. Au appears as disseminated free grains.

Gossan

The main mineralogy at the gossan is siderite + Fe-sulfides + galena + calcite ± goethite ± hematite. The alteration can be subdivided in four facies (Yesares, Saez, et al. 2015):

1) Carbonate-sulfides, controlled by subvertical faults heterogeneously distributed. Are the most abundant facies, its mineralogy is siderite + calcite + galena + Fe-sulfides ± hematite ± goethite (± Ag-sulfides ± Au-Ag-Hg amalgams) (Fig. 3);
2) Fe-oxides, close to faults with the siderite + Fe-sulfides + galena ± goethite ± hematite mineral assemblage. The most common texture is sub-rounded goethite and hematite bordered by microcrystalline siderite, covered by alternating microbands of goethite and siderite (Yesares et al., 2015). Disseminated Au particles are related to these textures;
3) Fracture-related, filling late fractures cross cutting the gossan, precipitating siderite + calcite + galena + Fe-sulfides;
4) Leached black shales, is a redox front during weathering related to a low-angle Variscan fault detachment (Yesares et al., 2014). The zone is located at the bottom of the gossan with a thickness between 5 - 15 cm. Formed by residual minerals as quartz + barite + monazite + Ti-oxides and alteration phyllosilicates (smectite + kaolinite groups) + galena + Ag-sulfides + cinnabar + Au-Ag-Hg amalgams (Fig. 6). Au-Ag-Hg amalgams evidence supergene deposition in their textures (Yesares et al, 2014).

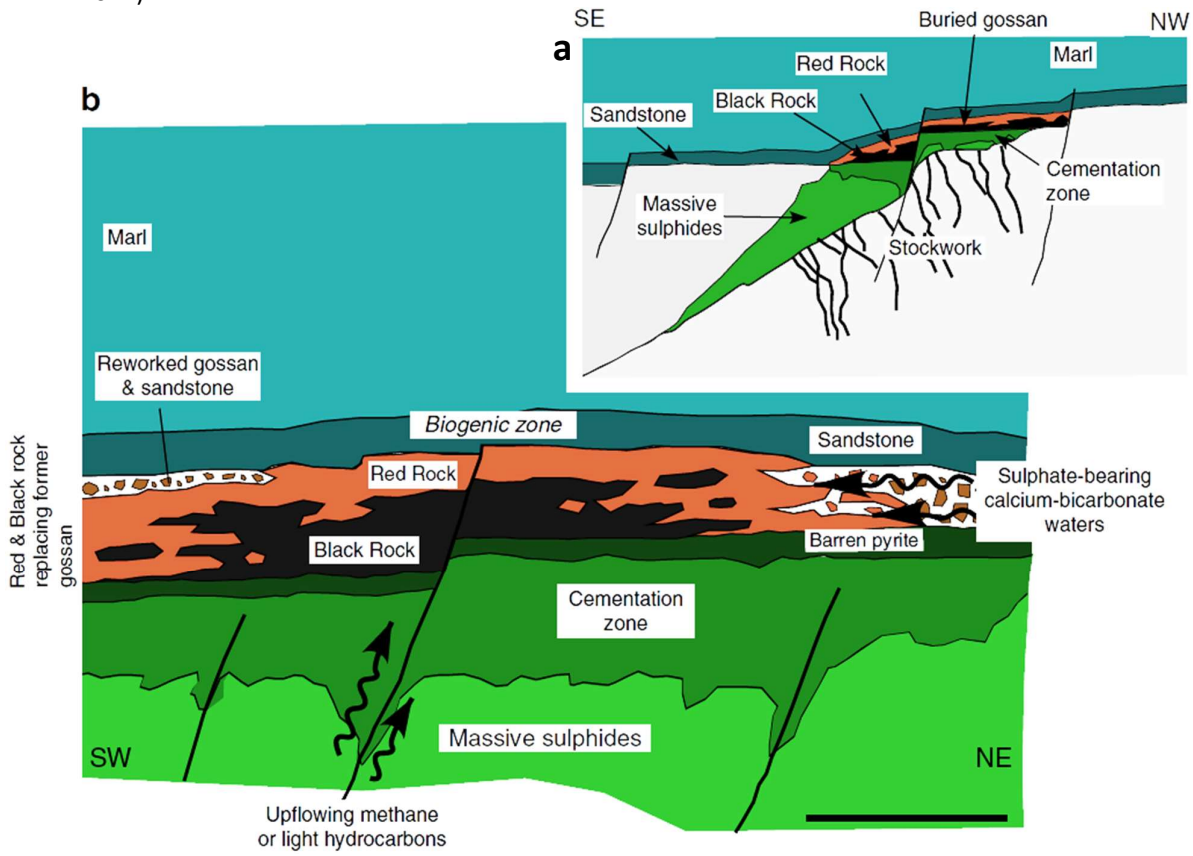

Figure 3: Model for the genesis of the biogenic carbonate–sulfide rocks. (a) Idealized cross section of the deposit. The SE–NW distance is 300 m. (b) proposed genetic model for the deposit. Carbonate–sulfide rocks (Red and Black rocks) formed in the supergene alteration zone (gossan) capping an older massive sulfide deposit. The porous gossan accumulated methane or light hydrocarbons that acted as electron donors for microbial reduction of aqueous sulphate transported by groundwater. This process destabilized goethite/hematite and oxidized minerals (beudantite, cerussite), leading to the formation of siderite, calcite, galena and silver-bearing sulfides, together with coarse-grained gold that has almost completely replaced the former gossan. Scale bar, 50 m. Taken from Tornos et al. (2014).

Gold distribution

The massive sulfides have gold concentration of 0.7 ppm, while by supergene alteration is enriched in the gossan to 5.88 ppm (Yesares et al., 2014, 2015). Minor amounts of gold can be found in the carbonate-sulfide facies, as Au is related to Fe-oxide and leached black shales facies. The highest concentrations are reached at the bottom of the gossan related to Au-Ag-Hg amalgams, heterogeneously distributed, in reductant lithologies (Yesares et al., 2014). At the supergene Cu-rich mineralization gold concentration is very low (0.03 – 0.77 ppm), however, 100 ppm concentrations could be registered at subvertical faults that controlled secondary mineralization.

Three types of gold can be found, each differentiated by the geochemistry, depositional context, supergene traps, mineral associations, texture (crystal morphology and grain size) and fineness (Yesares et al. 2014):

1) Coarse grains, high-fineness, Fe-oxide associated, at the top of the gossan. The association of Nadorite ($PbSbO_2Cl$) with fine Au particles in this facie reflects saline seawater involvement. Gold related to skeletal galena has elongated shapes;
2) Coarse Au-Ag-Hg amalgams, related to leached black shales in the bottom of the gossan;
3) Medium-sized particles, medium fineness, related to newly formed proustite and cinnabar in the fault breccia-related Au-Ag–rich secondary ore gouge within the cementation zone.

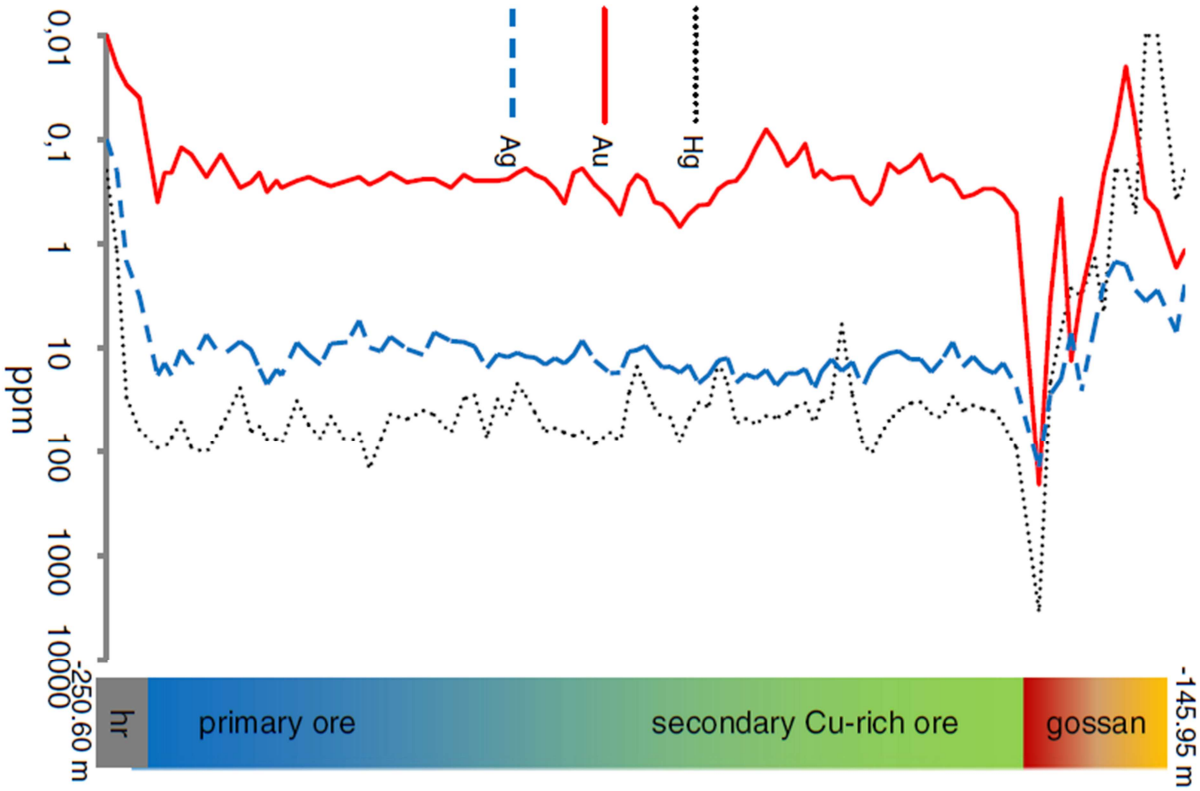

Figure 4: Au, Ag, and Hg vertical distribution of Las Cruces deposits based on analysis from a representative drill hole crosscutting the gossan, secondary Cu-rich ore and primary sulfides. Taken from Yesares et al. (2014).

The different textures suggest different mobilization and precipitation mechanisms of gold during weathering of the massive sulfides and later evolution during sedimentation. The field relationships in the supergene profile indicate multiple fluid pathways. Moreover, the association of Au to different supergene facies and lithologic traps indicate different precipitation mechanisms.

Gossan evolution stages	Environmental conditions and Au, Ag and Hg behavior	Neo-formed minerals	Au, Ag and Hg behavior and mineral equilibria	References
Stage I (Upper Oligocene–Lower Miocene) Tectonic uplifting, deposit exhumation and gossan formation	Oxygenated, acid-sulfate and chloride-rich conditions pH < 5.5; Eh > 0.9 V Precious metals are released from primary sulfides and enriched in the gossan	Fe-oxyhydroxides, Fe-sulfates, native Au, Ag-halides, Hg-sulfates	Suggested mobilization mechanism $4Au + 16Cl^- + 3O_2 + 12H^+ = 4AuCl_4^- + 6H_2O$ $4Ag + 4Cl^- + O_2 + 4H + = 4AgCl^0 + 2H_2O$ $Hg^{2+} + 2Cl^- + 3O_2 + 12H^+ = HgCl_2^0 + 6H_2O$ Suggested precipitation mechanism $4AuCl_4^- + 3Fe^{2+} + 6H_2O = Au^0 + 3Fe^{3+}OOH + 4Cl^- + 9H^+$ $AgCl^0 = AgCl$ $2HgCl_2^0 + 2Cl^- = Hg_2Cl_2 + Cl_2$ $HgCl_2^0 + H_2O = HgO + 2Cl^- + 2H^+$ $0.5Hg^{2+} + 3Fe^{3+} + 2SO_4^{2-} + 6H_2O =$ $Hg_{0.5}Fe_3(SO_4)_2(OH)_6 + 6H^+$	Mann (1984) Mann (1984) Saunders (1993) Dutrizac and Eno (1981)
Stage II (Upper Miocene Lower Pliocene) Ore burial under carbonate-rich sedimentary cover	Neutral and reduced conditions pH ~ 6–7; Eh < 0 V In the upper gossan: Buffered solutions and precious metal remobilization In the lower gossan: Migrating solutions interact with high reductant lithologies including organic matter-rich rocks	Siderite, calcite, Fe-sulfides, Pb-sulfides, Fe-oxyhydroxides, native Au, Hg, Ag-sulfates Fe-sulfides, Pb-sulfides, Ag-sulfides, cinnabar, amalgams	Suggested mobilization mechanism $2Au^0 + 4S_2O_3^{2-} + 2H^+ + 0.5O_2 = 2Au(SO_3)_2^{3-} + H_2O$ $2Ag^0 + 4S_2O_3^{2-} + 2H^+ + 0.5O_2 = 2Ag(SO_3)_2^{3-} + H_2O$ $Ag(SO_3)_2^{3-} + O_2 = Ag_2SO_4$ $Hg^{2+} + 0.5O_2 + H_2O = Hg(OH)_2^0$ $HgCl_2 + 2H_2O = Hg(OH)_2^0 + 2H^+ + Cl^-$ Suggested precipitation mechanism $Au(SO_3)_2^{3-} + O_2 = Au_2SO_4; Au_2SO_4 = 2Au^+ + SO_4^{2-}$ $Au^+ + Fe^{2+} + 2H_2O = Au^0 + FeO(OH) + 3H^+$ $Ag_2SO_4 + Fe^{3+} + H_2O = AgFe_3(SO_4)_2(OH)_6$ $Hg(OH)_2^0$ sorbed in oxides $Hg(OH)_2 + Fe^{2+} = Fe(OH)_3 + Hg^0$	Freyssinet et al. (2005) Hepler and Olofsson (1975) Stroffregen (1986) Charlet et al. (2002)

Table 1
Summary of the main Au-Ag-Hg mineralization reactions used in the proposed genetic model for the Las Cruces deposits. Taken from Yesares et al. (2014).

Model

Three mechanism cause gold enrichment in Las Cruces deposit (Yesares, Aiglsperger, et al. 2015):

1) gold dissolution from primary sulfides as chloride complexes during supergene alteration in oxidizing, Fe-rich, acidic, saline, subaerial, conditions. Au is transported downward through the gossan profile;
2) reducing the solubility of gold by changing the redox state of the fluid as a result of the precipitation of Fe-oxyhydroxides. Results in secondary Au enrichment in the upper gossan, as coarse-grained, high-fineness gold particles;
3) under the sediment cover, remobilization of Au as hydroxidehalide, hydroxide, thiosulfate and bisulfide complexes in the gossan bottom and cementation zone. Fluid move through Alpine reactivated faults to the cementation zone. Precipitation is related to reducing environments, black shales and primary sulfides.

Supergene Au could also complex with organic, halide, hydroxide, halide-hydroxide and sulfur ligands, depending on the weathering conditions. Additionally, near the surface, biological activity contributes to gold dissolution-precipitation processes during weathering. The source of all gold types in the supergene profile are the primary mineralization, that were constantly leached.

In the Miocene-Pliocene the deposition of the Guadalquivir basin carbonate-rich sediments buried the deposit changing the system conditions (i.e., Eh, pH, T) enhancing the precipitation of medium-fineness Au located in the gossan base and in fault breccias in the cementation zone (Yesares et al., 2017). The environment conditions at the gossan changed from oxidizing and acidic to near-neutral and reducing during the burial stage, thanks to the rise of the redox front and a more alkaline fluid from the interaction with the carbonate-rich sediments. At this stage fluid flowed through late subvertical faults cross cutting the sedimentary cover, gossan and cementation zone.

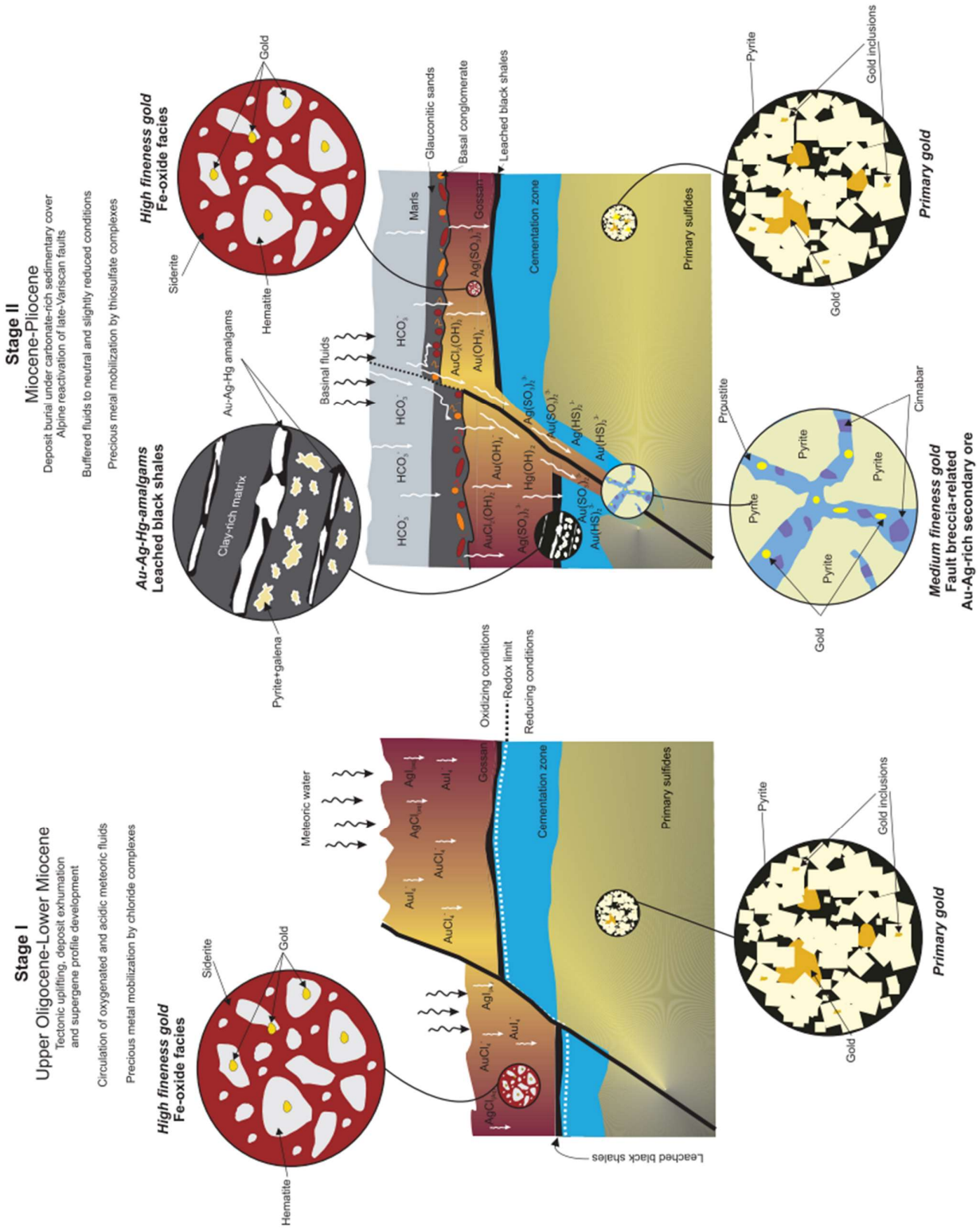

Figure 5: Two-stage genetic model for the Las Cruces Au mineralization. Stage 1. Precious metals mobilization and fixation during gossanization of the massive sulfide deposit. Stage 2. Later supergene profile evolution beneath the carbonate-rich sedimentary cover. Taken from Yesares, Aiglsperger, et al. (2015).

In the IPB gossans there is marine aerosol involvement, crucial for Au-halide and Au-hydroxidehalide complexes, evidenced in Ag-bearing minerals precipitation, iodargyrite and chlorargyrite in other deposits (Capitán, 2006; Velasco et al., 2013). This feature is better seen in deposits which were closer to the sea during the Miocene marine transgression. Weathering profiles of a VMS deposits show Au enrichment at the bottom of the gossan, uneven Au distribution and systematically association to Fe-oxyhydroxide (Yesares et al. 2017).

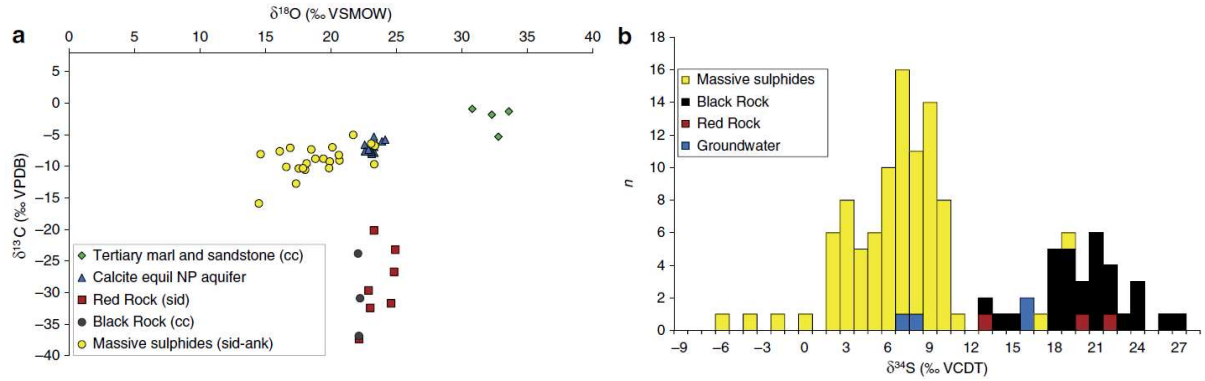

Figure 6: isotope geochemistry: (a) Carbon–oxygen isotope composition of carbonates (sid, siderite; cc, calcite; ank, ankerite), overlying Tertiary sandstone and marl, and calculated $d^{18}O$-$d^{13}C$ isotope composition of calcite in equilibrium with the local groundwaters (25 °C). Calculated from the tabulated $d^{18}O$- $d^{13}C$ values and fractionation factors of Kim and O'Neil (1997) for O and those of Romanek, Grossman, and Morse (1992) for C. For comparison, data are shown for the Variscan (primary-ore related) hydrothermal siderite–ankerite assemblage occurring in VMS deposits of the Iberian Pyrite Belt. (b) Sulphur isotope composition compared with the $d^{34}S_{sulphate}$ values of the local groundwater and $d^{34}S$ values of the primary sulfides at Las Cruces (Velasco et al. 1998). Taken from Tornos et al. (2014).

References

Capitán, MA. 2006. 'Mineralogía y geoquímica de la alteración superficial de depósitos de sulfuros masivos en la Faja Pirítica Ibérica', *Unpublished Ph. D. thesis*: 260.

Kim, Sang-Tae, and James R O'Neil. 1997. 'Equilibrium and nonequilibrium oxygen isotope effects in synthetic carbonates', *Geochimica Et Cosmochimica Acta*, 61: 3461-75.

Romanek, Christopher S, Ethan L Grossman, and John W Morse. 1992. 'Carbon isotopic fractionation in synthetic aragonite and calcite: effects of temperature and precipitation rate', *Geochimica Et Cosmochimica Acta*, 56: 419-30.

Tornos, F., F. Velasco, C. Menor-Salvan, A. Delgado, J. F. Slack, and J. M. Escobar. 2014. 'Formation of recent Pb-Ag-Au mineralization by potential sub-surface microbial activity', *Nature Communications*, 5: 8.

Velasco, F, J Sánchez-España, AJ Boyce, AE Fallick, R Sáez, and GR Almodóvar. 1998. 'A new sulphur isotopic study of some Iberian Pyrite Belt deposits: evidence of a textural control on sulphur isotope composition', *Mineralium Deposita*, 34: 4-18.

Velasco, F., J. M. Herrero, S. Suarez, I. Yusta, A. Alvaro, and F. Tornos. 2013. 'Supergene features and evolution of gossans capping massive sulphide deposits in the Iberian Pyrite Belt', *Ore Geology Reviews*, 53: 181-203.

Yesares, L., T. Aiglsperger, R. Saez, G. R. Almodovar, J. M. Nieto, J. A. Proenza, C. Gomez, and J. M. Escobar. 2015. 'Gold Behavior in Supergene Profiles Under Changing Redox Conditions: The Example of the Las Cruces Deposit, Iberian Pyrite Belt', *Economic Geology*, 110: 2109-26.

Yesares, L., R. Saez, G. R. De Almodovar, J. M. Nieto, C. Gomez, and G. Ovejero. 2017. 'Mineralogical evolution of the Las Cruces gossan cap (Iberian Pyrite Belt): From subaerial to underground conditions', *Ore Geology Reviews*, 80: 377-405.

Yesares, L., R. Saez, J. M. Nieto, G. R. de Almodovar, and S. Cooper. 2014. 'Supergene enrichment of precious metals by natural amalgamation in the Las Cruces weathering profile (Iberian Pyrite Belt, SW Spain)', *Ore Geology Reviews*, 58: 14-26.

Yesares, L., R. Saez, J. M. Nieto, G. R. De Almodovar, C. Gomez, and J. M. Escobar. 2015. 'The Las Cruces deposit, Iberian Pyrite Belt, Spain', *Ore Geology Reviews*, 66: 25-46.

9. Rio Tinto: The Mars-like VMS deposit

Mauro Bongiovanni

Introduction

The Rio Tinto complex is located in the South Portuguese Zone, in the eastern part of the Iberian Pyrite Belt (Fig. 2). In this belt, several VMS deposits developed around 360 Ma, with the largest ones probably controlled by the larger, most active and well-connected faults and fractures that developed over an area heated by a mantle plume. They have been subsequently folded and metamorphosed during the Variscan orogeny between 330 and 300 Ma (Díez-Montes et al. 2015; Martin-Izard et al. 2015). In Rio Tinto, mining for Cu, Au, Ag and pyrite has been carried out, using both open pit and underground mining methods, from approximately 2500 BC to present day (Hudson-Edwards et al. 1999). It is a worldwide known deposit not only for the ore itself, but also because of the bright colored minerals that covered the riverbed of the draining stream, due to acidic fluids generated by sulphides alteration. This phenomenon is very difficult to control and to remediate, but can have a severe impact on the environment because of heavy metals. In addition it has been recently recognized as an analog for Fe-rich outcrops observe on Mars.

Local geology (Adamides 2013)

The main lithological sequence includes a sequence of porphyritic felsic volcanic rocks underlain by mafic volcanics and meta-sedimentary rocks (Fig. 1). The felsic volcanics are cream- to grey-colored and contain phenocrysts of quartz and minor feldspar in a fine-grained felsic matrix. They are mostly rhyolitic, but several lithologies have been included in this unit (dacites, tuffs, hydrothermal breccias…). Different textures can be observed within this unit, some of them are still visible despite the hydrothermal alteration and weak metamorphism; the rocks are locally sheared and developed a strong slaty cleavage with quartz phenocrysts.

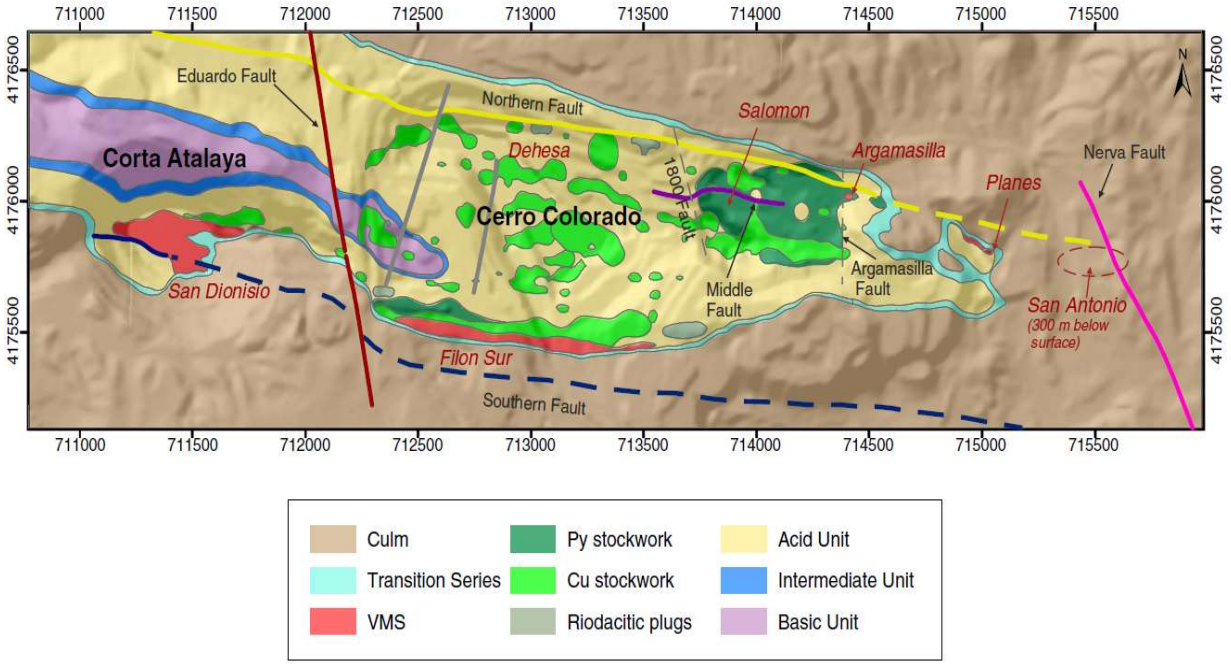

Figure 1: Local geological map of the Rio Tinto deposit. Obtained from Martin-Izard et al. (2015).

As mafic volcanics are andesitic, there is an obviouos bimodal nature in the genesis of these units. The Culm group is made of a monotonous sequence of cleaved blue-grey slate with intercalations of sandy and silty layers. They are interpreted to represent a turbidite infilling a subsiding basin. Finally, a ferruginous conglomerate (gossan or “iron hat”) outcrops south of Filon Sur and contains clasts of different lithologies cemented with Fe-rich materials, mainly goethite and hematite. It is interpreted to have formed by weathering of the surrounding rocks and fluids percolation.

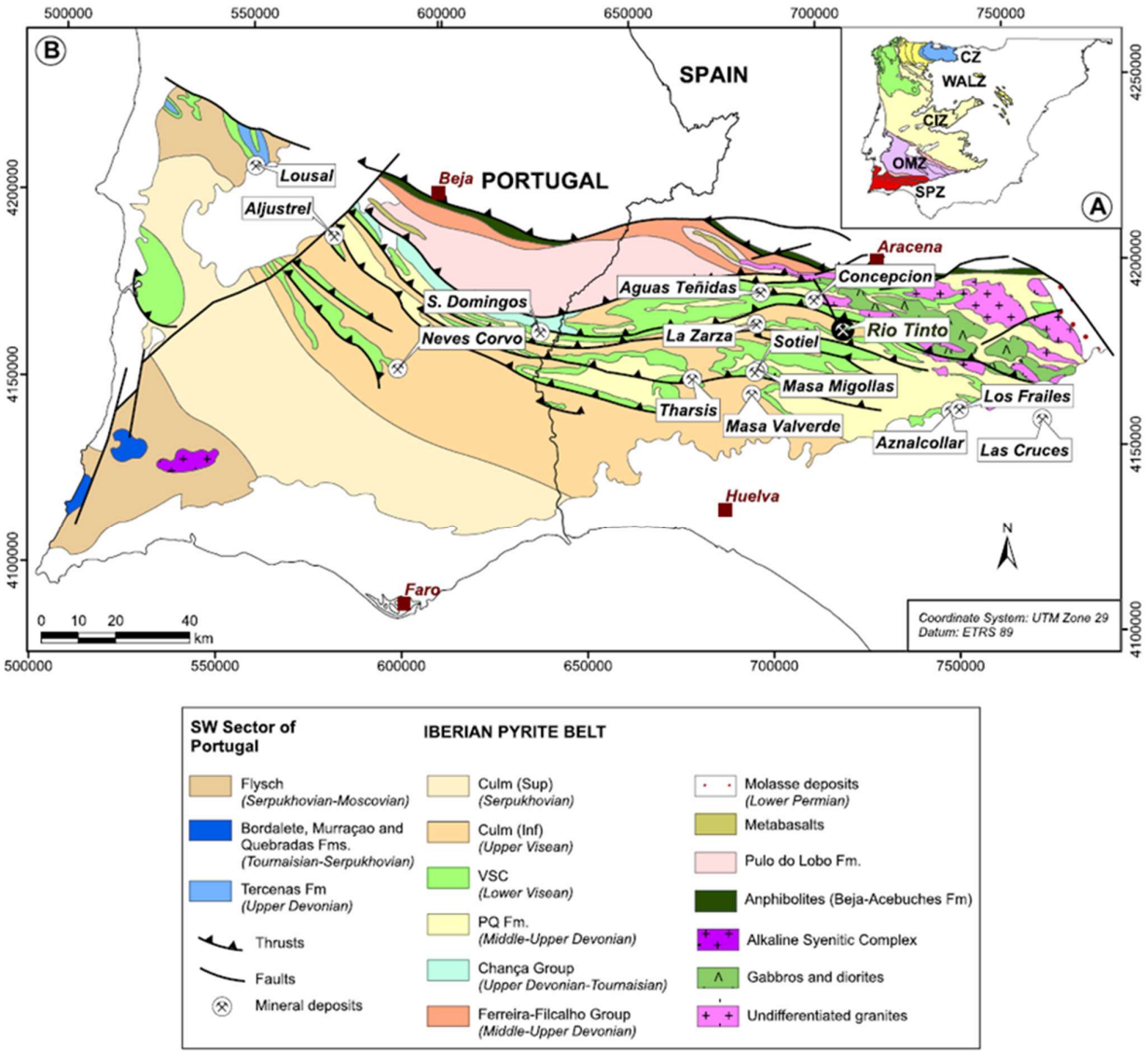

Figure 2: Geological map of the Iberian Pyrite Belt and location of Rio Tinto mine. Obtained from Díez-Montes et al. (2015).

Tectonics and ore genesis (Martin-Izard et al. 2015)

Rio Tinto area is characterized by two E-W trending normal faults (Northern and Southern fault) that formed when the subsiding area evolved into a transtensional graben, forming a rollover anticline (Fig. 3A). These faults bounding the sub-basins are related to a pull-apart structure, are favorable for the intrusion of igneous rocks and played a critical role for the genesis, location and structure of the VMS and cupriferous stockworks of Rio Tinto (Fig. 3B). Finally, during the transpressional phase, shortening generated folding of the volcano-

sedimentary sequence, the VMS mineralization and the cupriferous stockworks which are in part dismembered from the original conduits (Fig 3C).

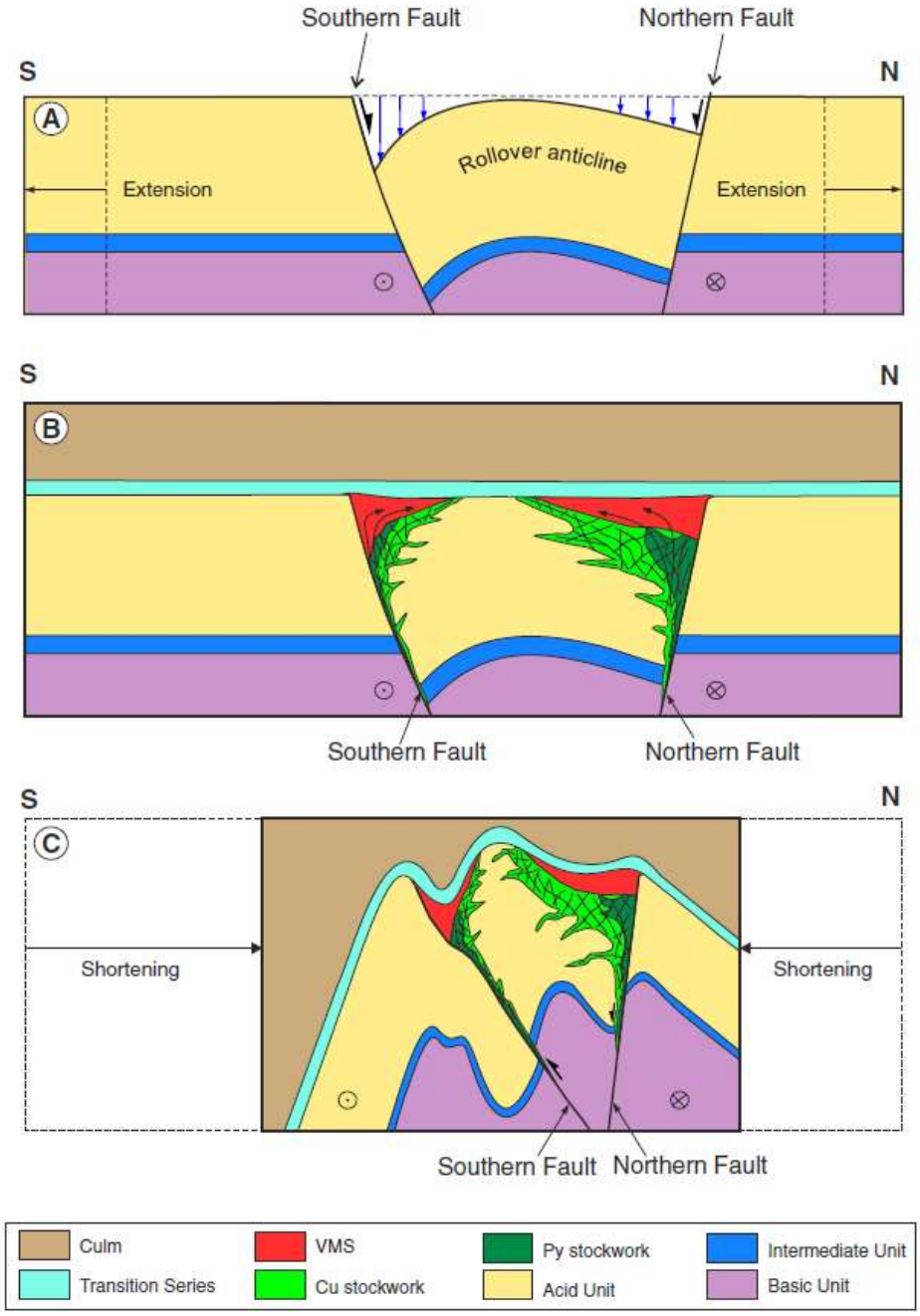

Figure 6: Model of the genesis of Rio Tinto VMS deposit. See text for details. Obtained from Martin-Izard et al. (2015)

Mineralization (Adamides 2013)

Two mayor open pits, San Dionisio-Atalaya and Cerro Colorado, expose the underlying lithology (Fig. 4). The geometry of ore bodies has been discussed in the past, but recently most authors agree on the current model, with similarities between different mineralizations in the whole Rio Tinto district. The sulphide mineralogy of the deposits is dominantly pyrite with minor chalcopyrite, sphalerite and galena in proportions which vary with location in individual deposits as well as between deposits.

Cerro Colorado is dominated by chalcopyrite, in contrast to San Antonio and San Dionisio, where Pb and Zn become important components of the assemblage. Sulfosalts containing Bi, As, Pb and Sb have been also identified as relevantly abundant. Pyrite is usually euhedral, while chalcopyrite fills interstitial spaces (as all of the other main sulphides, that are therefore contemporaneous) and partly replace pyrite (Fig. 5). Silicification has occurred intensely causing the destruction of the original textures, and the attainment in some cases of a completely glassy aspect, confirming the introduction of silica from hydrothermal fluids.

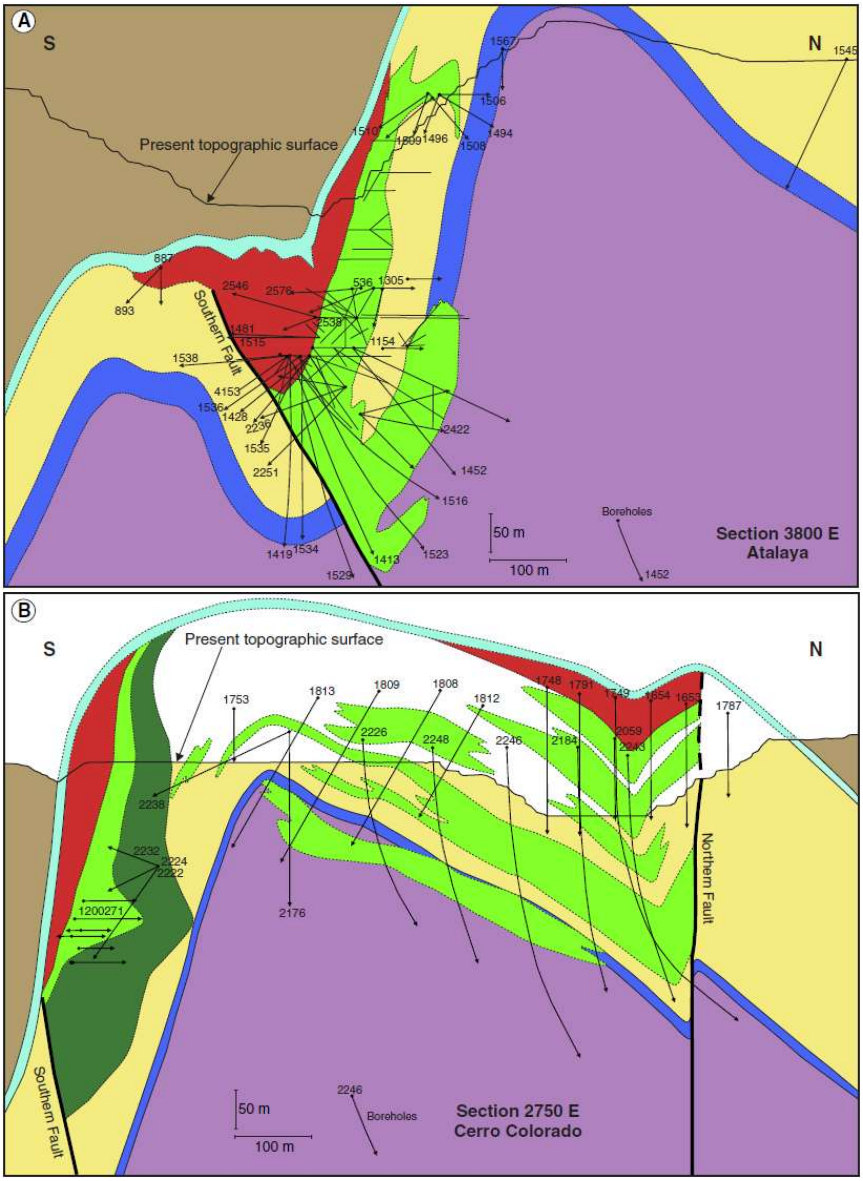

Figure 4: Model of the ore geometry in the two main open pits: A) San Dionisio-Atalaya; B) Cerro Colorado. See figure 3 for units legend. Obtained from Martin-Izard et al. (2015).

Sericitic alteration, typical of the outer part of VMS deposits, is particularly evident in felsic rocks that are colored in light yellow-green to light grey. Chloritic alteration, instead, gave the host rock a dark green/black color and it is intimately associated with the pyritic mineralization. In a few cases, typical assemblages characteristic of advanced argillic alteration have also been observed. Finally, ferruginisation is often associated with carbonate alteration and can be either pervasive or forming fine networks of hematite or limonite.

The close spatial relationships between black shale and massive sulphide suggest deposition of the Filon Sur and San Dionisio deposits partly by sub-sea floor replacement of pelitic units (similar to the shale-hosted deposit type). This is considered the most efficient mechanism of ore deposition, in contrast to the exhalative deposits where most of the metal load may be lost into the ambient seawater.

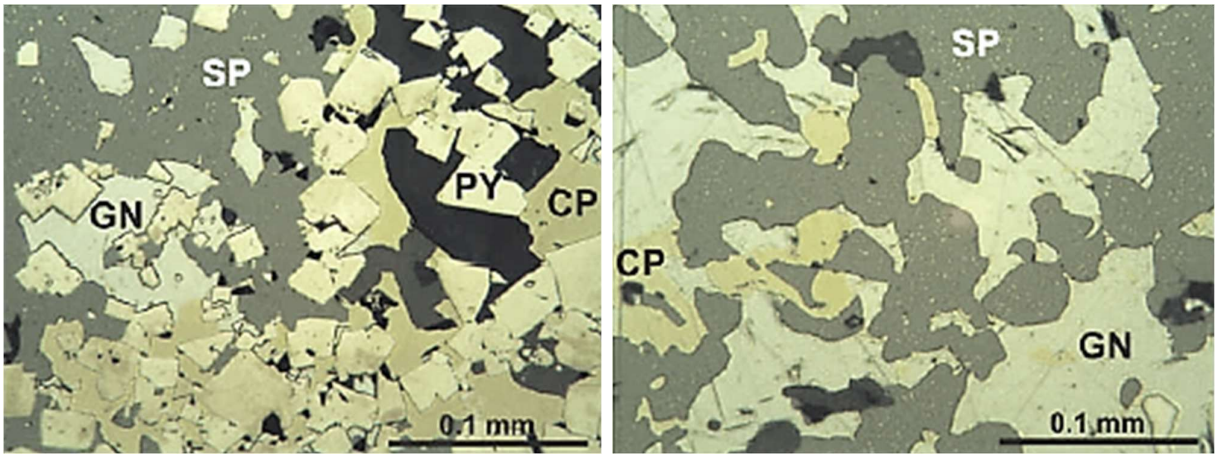

Figure 5: Reflected light images of the main sulphides: Pyrite (PY) forms euhedral crystals while Chalcopyrite (CP), Galena (GN) and Sphalerite (SP) are all interstitial with coeval relationships between them. Obtained from Adamides (2013).

Acid Mine Drainage (Hudson-Edwards et al. 1999)

Mining activities have affected water and sediments quality, especially since 1873 when the mines were acquired by a British syndicate. Cu, As, Pb, Ag and Zn are dissolved from the ore minerals during their erosion and alteration (mostly oxidative) and flushed by meteoric water. Several minerals precipitate in the alluvium deposit and trap heavy metals: these are sulphides, Fe±As oxides, Fe (oxy)(hydr)oxides and Fe oxyhydroxy-sulphates. They are divided into primary (remnants of mine-waste and tailings) and secondary (products of oxidation, precipitation and dissolution reactions) and they have a complex mineralogy. Most of the analyses done in Rio Tinto area used XRD to distinguish between mineral phases and relatively complicated models schematizing their genesis and relationships have been proposed.

The pH in the mine area is very low (around 1.5) and as soon as the outflowing streams flow into non-polluted river it gets progressively neutralized, causing precipitation of the Fe-rich phases mentioned above, that give bright colors (red/yellow/purple) to the riverine sediments (Fig. 6). Those Fe-rich minerals are often in colloidal form, therefore with high sorption capacity and specific area. The fate of the heavy metals becomes dependent on the sorbing minerals evolution: the latter have various stability environments and solubilities, therefore it is difficult to predict and model the fate of contaminants along the river.

Bacteria have an important role in this environment as they influence the mineralogical composition of Rio Tinto sediments by controlling redox reactions rates. In some cases they even produce sedimentary structures at decimetric scale (Fernandez-Remolar et al., 2005). Seasonal variations strongly influence the fate of secondary minerals and effluorescences (together with the sorbed heavy metals) that can partly or totally dissolve, re-precipitate or being substituted. Many cases of newly formed minerals have been reported to happen after rainy periods. As different phases have different solubilities and stability over time, the contamination is triggered at various time scales. Remediation strategies are currently being considered by the authorities, but actions like forcing the pH to rise may have effects that are difficult to predict. A more alkaline pH would induce precipitation of the Fe-rich phases, sorbing heavy metals, reducing their concentration in the water but polluting the sediments.

Figure 6: Photographs of the Rio Tinto river downstream. Obtained from Andaluciadiary.com

Mars Analog (Fernandez-Remolar et al., 2005)

The NASA rover *Opportunity* has observed the presence of sulphate- and hematite-rich sedimentary rocks exposed in craters and other surface features of Meridiani Planum, on Mars. The Rio Tinto basin provides a good (but still partial) environmental analog to Meridiani Planum rocks for two main reasons. First, both iron oxides and ferric sulphates, including jarosite, form at Rio Tinto under well characterized physicochemical (and biological) conditions. Second, the modern drainage, where depositional processes can be observed in action, is complemented by a historical record of deposition preserved is diagenetically stabilized sedimentary rocks in terraces at three levels above the river.

Meridiani rocks accumulated via eolian and aqueous processes in an arid environment characterized by dunes and interdune depressions, while Rio Tinto sediments formed in seasonally arid stream beds. Despite this fact, the mineral assemblage identified in Rio Tinto rocks and sediments is quite similar to that observed and/or inferred for Meridiani outcrops. Meridiani outcrops have remained sulphate-rich, including ferric sulphates that do not persist into the rock record at Rio Tinto. This suggests that mineral formation and diagenesis occurred under conditions of strong water limitation.

References

Adamides N (2013): Rio Tinto (Iberian Pyrite Belt): a world-class mineral field reopens. *Applied Earth Science vol: 122 (1) pp: 2-15*

Díez-Montes A, García-Crespo J, Ayala C, García-Lobón JL, Sánchez-García T, Rey-Moral C, Bellido F, Rubio F, Mediato JF, Tornos F (2015): Modelling of the Río Tinto Area. *In "3D, 4D and Predictive Modelling of Major Mineral Belts in Europe" Mineral Resources Review, Springer.*

Fernández-Remolar D, Morris R, Gruener J, Amils R, Knoll A (2005): The Río Tinto Basin, Spain: Mineralogy, sedimentary geobiology, and implications for interpretation of outcrop rocks at Meridiani Planum, Mars. *Earth and Planetary Science Letters vol: 240 (1) pp: 149-167*

Hudson-Edwards K, Schell C, Macklin M (1999): Mineralogy and geochemistry of alluvium contaminated by metal mining in the Rio Tinto area, southwest Spain. *Applied Geochemistry vol: 14 (8) pp: 1015-1030*

Martin-Izard A, Arias D, Arias M, Gumiel P, Sanderson D, Castañon C, Lavandeira A, Sanchez J (2015): A new 3D geological model and interpretation of structural evolution of the world-class Rio Tinto VMS deposit, Iberian Pyrite Belt (Spain). *Ore Geology Reviews vol: 71 pp: 457-476*

Andalucia Diary (http://andaluciadiary.com/rio-tinto-river-huelva) visited on 13/04/2019

10. The Aguablanca Ni-Cu-PGE ore deposit

Thomas de Selva-Dewint

Geological background

The Aguablanca Cu-Ni ore deposit is an othomagmatic sulfide deposit (Casquet et al., 2001), which was discovered in 1993 after a regional geochemical stream-sediment survey that identified significant Cu anomalies which were related to a poorly exposed gossan with minor old workings (Tornos et al., 2001). The ore deposit contains 15.7 million tons (Mt) of ore, with a grade of 0.66 wt% Ni, 0.46 wt% Cu, 0.47 g/t PGE.

The ore deposit is hosted in mafic in ultramafic rocks of the Aguablanca stock. The Aguablanca stock is itself part of a larger high-K calc-alkaline plutonic complex, called Santa Olalla, which has an age of about 338 Ma (Casquet et al., 2001). The complex is located in the SW of the Ossa-Morena Zone (OMZ) of the Iberian Variscan Belt, and can therefore also be referred to as one of the Variscan massifs (Fig. 1). The Santa Olalla plutonic complex consists of two plutons: the Santa Olalla main pluton and the Aguablanca stock (Tornos et al., 2001). The Santa Olalla main pluton shows normal zoning from granodiorites/monzogranites in the middle of the intrusion, to tonalities/quartzdiorites in the rim of the intrusion (Tornos et al., 2001). The magmatic foliation of these rocks is subhorizontal. The Aguablanca stock on the other hand is of more mafic nature. It mainly consists of coarse-grained amphibole-biotite (quartz) diorites, with a steep magmatic foliation. At the northern edge of the Aguablanca stock there is a 10 to 400-m package of coarse-grained pyroxenitic gabbros, gabbronorites and norites, which are magmatic cumulates (Tornos et al., 2001), which is also where the orebody can be found (Fig. 2).

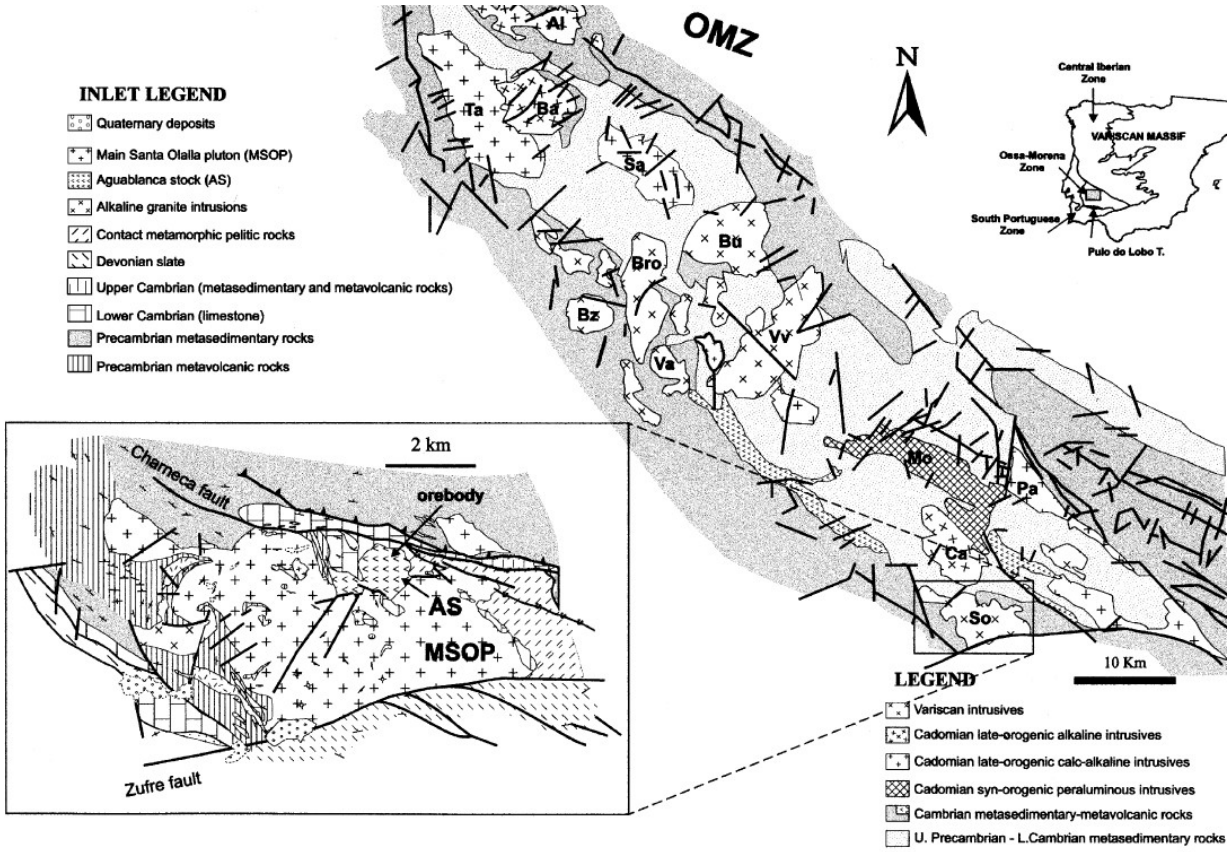

Figure 1. Geological map of the Santa Olalla plutonic complex (Casquet et al., 2001).

During Cadomian times (620-480 Ma), the Ossa-Morena Zone was accreted to the autochthonous Iberian terrane (Tornos et al, 2001). During the later Variscan orogeny, it acted as the overriding plate above the underriding South Portuguese Zone undergoing an oblique northwards subduction (Tornos et al. 2001). The Santa Olalla plutonic complex is located right at border with the South Portuguese Zone (with the Zufre fault separating both). To the north it is bounded by a narrow, high angled strike-slip fault called the Cherneca fault (Fig. 1).

The plutons intruded a package of carbonate and calc-silicate rocks, metavolcanics and slates from the Late-Proterozoic to Early Cambrian. This package lies on top of what is known as the *Serie Negre*, which is a sequence of Late-Proterozoic pyrite-bearing black slates and quartzites (the two alternate) with some minor amphibolites (Casquet et al., 2001). Around the plutons, the regional cleavage and bedding are wrapped around the massive (Casquet et al. 2001). The regional metamorphism caused by the earlier Varisan orogeny is of greenschist facies (Tornos et al., 2001). The emplacement of the Santa Olalla plutonic complex also caused contact metamorphosis, causing there to be a contact aureole all around the mafic complex (Casquet et al., 2001). This contact metamorphism achieved local migmatisation of the rocks were temperature conditions were the highest (around 700-750°C) (Tornos et al., 2001). The contact metamorphosis of limestones and more Ca-rich rocks also explains the presence of many skarns and marbles around the intrusion.

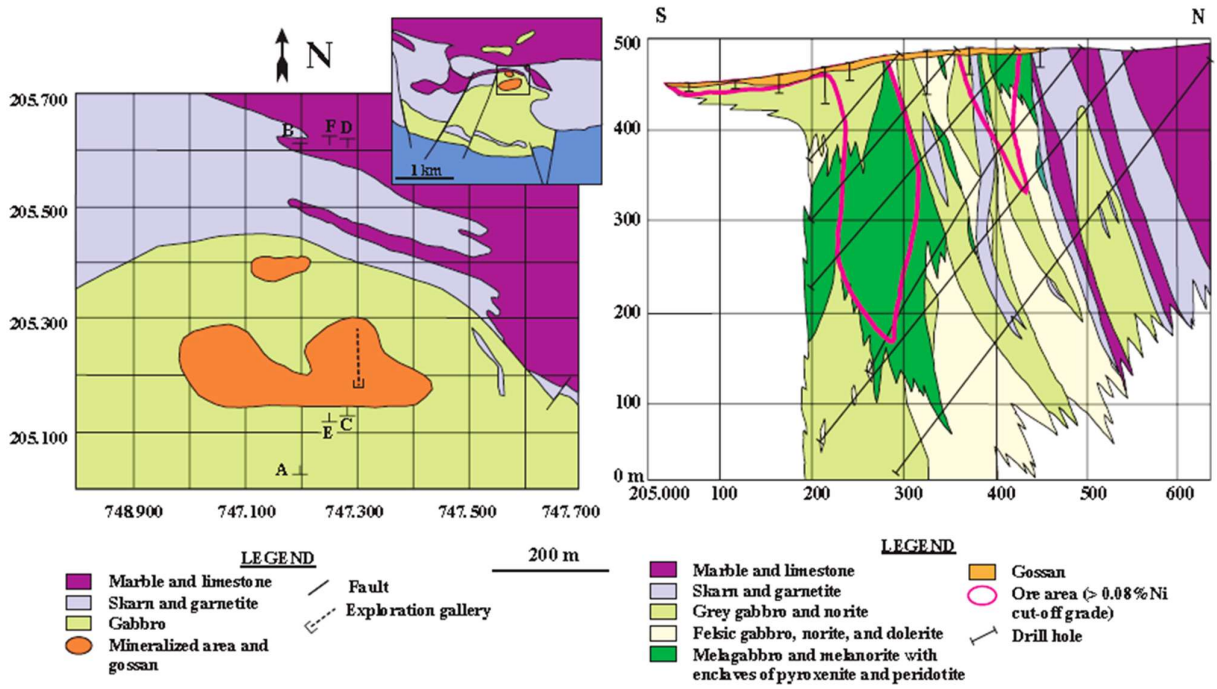

Figure 2. Close up of the location of the Aguablanca ore deposit, with its corresponding N-S cross-section (Ortega et al., 2004).

Mineralization

In the NE of the Aguablanca stock the ore deposit can be found under the form of a pipe-like breccia body, which reached at least up to 700m under the surface (Tornos et al., 2001). As visible in Fig. 3, it occurs under the form of a lens-shaped breccia inside the Aguablanca stock. It is about 500 m long, 60-100 m wide and more than 700 m deep. It dips towards the south with an angle of 70° (Casquet et al., 2001). The breccia itself consists of many clasts of different sizes and different origin, including orthopyroxenites, websterites, clinopyroxentites, gabbros and gabbronorites. The texture of the clasts all point to a cumulate origin. There are also some skarn, hornfels and marble clasts present (coming from the country rock). The main minerals found inside of the cumulate clasts are ortho-, clinopyroxene and plagioclase.

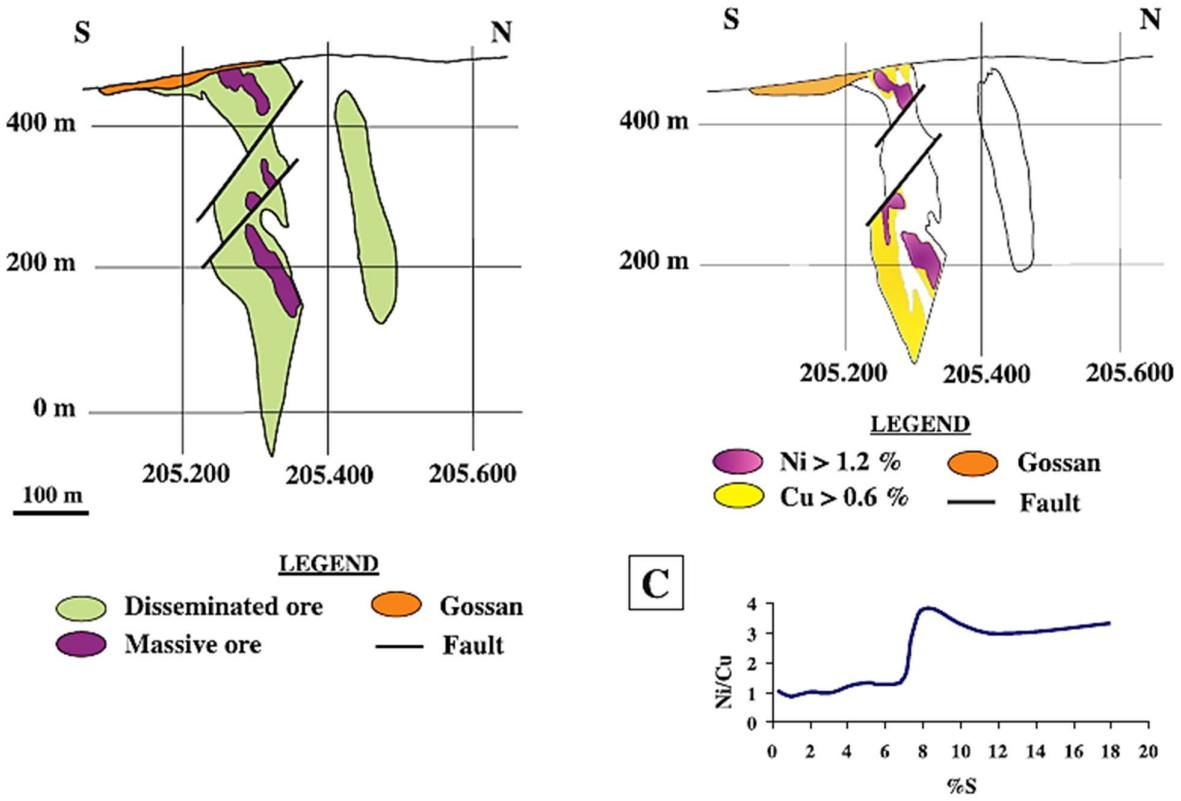

Figure 3: Section of the ore body from Ortega et al. (2004), showing its shape and the ore distribution. The curve in C was made using 235 samples.

The breccia pipe is ore rich in some places, but also more ore-barren in other places (with only 1-5 vol% disseminated sulfides). Understanding the geometry of where the ore occurs is thus of great importance. When ore mineralization occurs, it mainly consists of pyrrhotite, pentlandite and chalcopyrite (Casquet et al., 2001). In ore-rich zones, the breccia can be recognized as follows (Tornos et al., 2001, Fig. 4, Fig. 5):

1. Matrix: undeformed and sulfide rich.
2. Clasts: as in the entire breccia, mostly pyroxenites
3. Enclosed inside the breccia are irregular, m-sized, ellipsoidal *bodies of massive sulfides* (Fig. 5, D). Present in these bodies are: (a) Randomly oriented crystals of bronzite and diopsite-augite. These two crystal types *coalesce* to form aggregates of coarse-grained pyroxenites; (b) The entire intercumulis is made of sulfides. The contact between the aggregates and the intercumulus is always sharp (no reaction rims etc.).

The sulfide mineralization itself in the breccia occurs in the form of three ore types (Piña et al., 2012, Fig. 4, Fig. 5):

1) Semi-massive ore: this represents the crystallization of monosulfide solid solution cumulates (i.e. cumulates, all bonded with a single sulfur, along the same solid solution).
2) Disseminated ore: representing in-situ crystallization of an original sulfide melt.
3) Chalcopyrite-veined ore: formed by the crystallization of Cu-rich residual sulfide liquid (Fig. 5, F).

These three mineralization types occur concentrically in the breccia, with an inner core of semi-massive sulfide-bearing rocks in the middle, and disseminated sulfide-bearing gabbronorites (lower grade) surrounding it until the rocks become entirely sulfide free. The chalcopyrite veinlets crosscut both the semi-massive ore and the disseminated ore throughout the deposit. The highest ore grades can be found in the centre of the breccia pipe, with grades of 2.4% Cu and 5.4% Ni (Tornos et al., 2001).

Subsolidus hydrothermal alteration affection all of the rocks in the Aguablanca stock, with mafic rocks being more altered than ultramafic rocks in general (Tornos et al. 2001). A first stage of hydrothermal activity caused mafic minerals (olivine and mostly pyroxenes) to be replaced by clinoamphiboles (e.g. actinolite), biotite-phlogopite and some clino-zoisite. Plagioclase got altered to sericite. In a second stage then talc, clino-chlorite-ripidolite, calcite, illite and clay minerals got introduced. The hydrothermal alteration is thought to have happened between 325 and 307 Ma, and was therefore clearly after the subduction-related magmatic activity (Tornos et al., 2001).

Based on LA-ICP-MS data, it can be said that the PGE and other chalcophile elements were carried by the BMS (base metal sulfides) (Piña et al., 2012). In practice these BMS are pyrrhotite and pentlandite, which contain most of the Pe, Os, Ir, Pu, and Rh and are mostly present in the semi-massive ore. However, the Pd and Pt occurs in mostly PGM (platinum group minerals) like Pd-Pt bismuthotellurides and Pt-arsenides, but some Pt can also be found in the pentlandite and chalcopyrite. A lot of Co is also present in the pentlandite and the chalcopyrite also hosts major amounts of Ag and Cd. Au however is not found in association with the BMS (Piña et al., 2012).

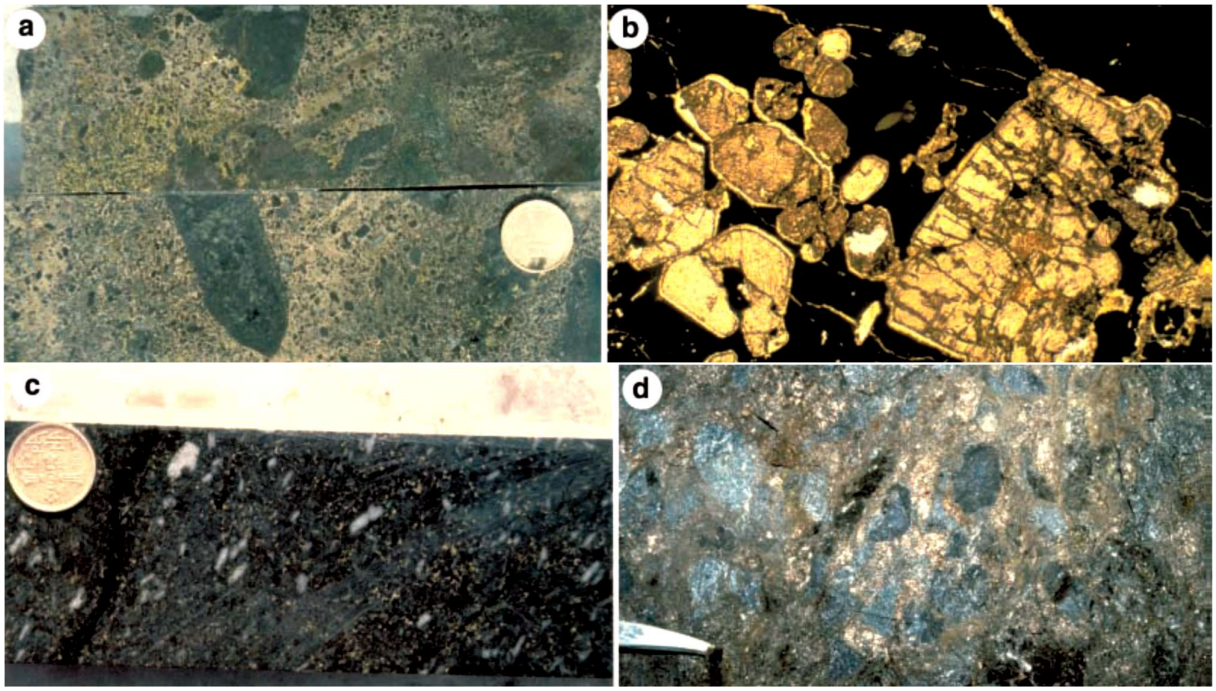

Figure 4. Mineralized samples from Tornos et al., 2001. (a) Large pyroxenite clasts in a semi-massive matrix of the ore breccia. b) Microscope image (2.5mm field of view) of ortho- and clinopyroxene crystals with sulfide intercumulus. Biotite-phlogipite are present at the rims o the clinopyroxene due retrograde reactions. c) Gabbronorite (of the unit around the breccia pipe), with disseminated sulfides. d) massive sulfide ore matrix supporting clasts of barren pyroxenite.

Geological model

Overall the shape and orientation of both plutons points to a formation along subvertical extensional zones associated with left-lateral shearing (Tornos et al., 2001). This extensional behavior is probably what allowed the magma to intrude up to such shallow depths. During the Variscan orogeny, the entire Ossa Morena Zone experienced episodic left-lateral displacement in NWN-ESE direction. This movement was the strongest in the Badajoz Cordoba Shear Zone, but other smaller-scale shear zone with the same orientation probably also helped to accommodate some of the displacement. The Cherneca fault north of the Santa Olalla plutonic complex would be an example of such a shear zone with the right orientation (Tornos et al., 2001). The extension thus was concomitant with the Variscan orogeny, and therefore so was the uprising of the

intrusions. This transpression caused by the subduction of the SPZ under the OMZ was accompanied high-K calc-alkaline magmatism along the margin of the OMZ. Because of this, the Aguablanca Cu-Ni ore deposits have to be classified as synorogenic (which is unusual for Ni-Cu deposits) (Casquet et al., 2001).

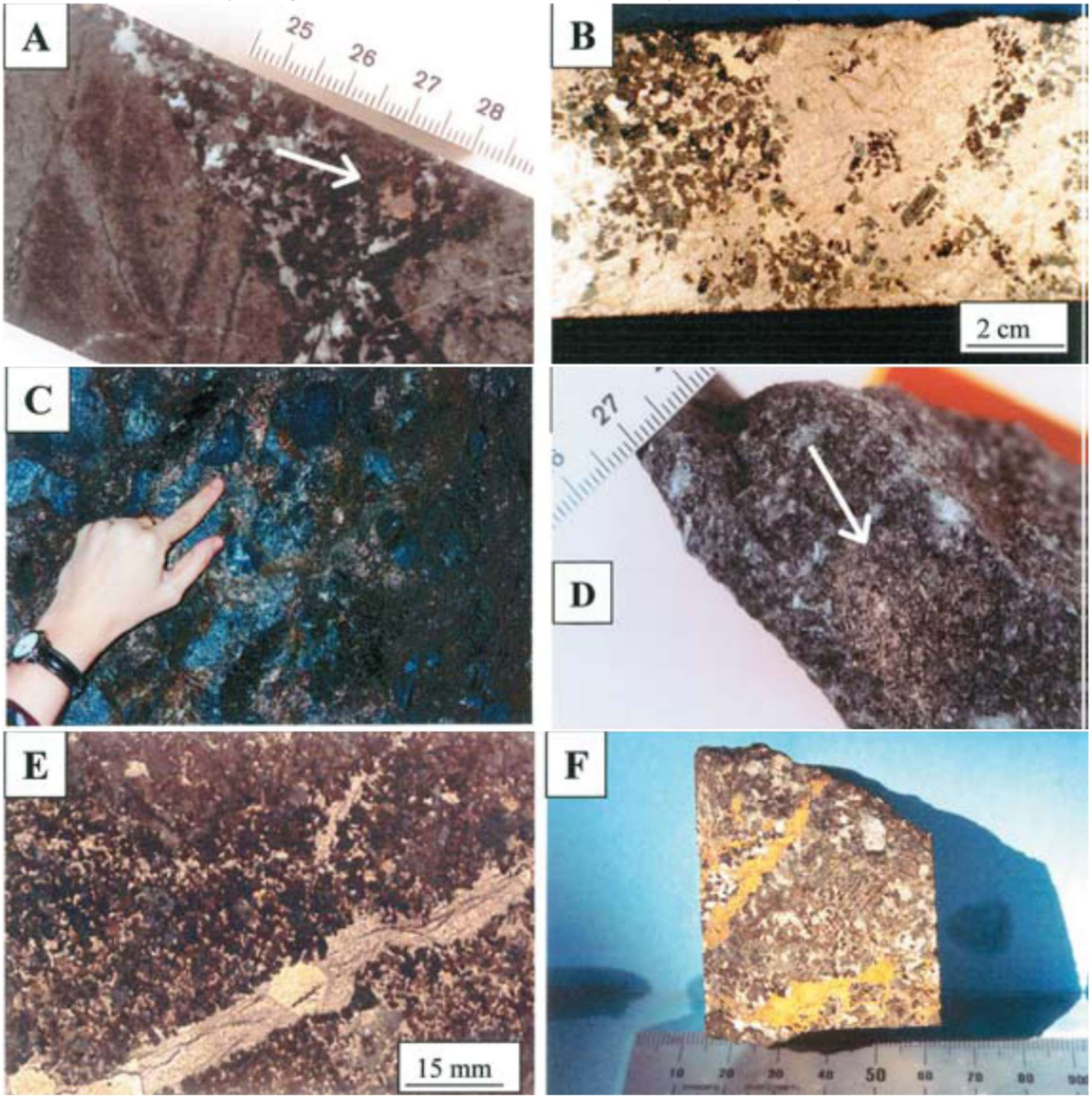

Figure 5: Mineralized samples from Ortega et al. (2004). A) Leucogabbro host, with breccia crosscutting it. The clasts in the breccia are ultramafic and barren. Sulfides are found under the form of droplets, disseminated in the matrix. B) Pure massive sulfide matrix, with some ultramafic clasts. C) Massive sulfide ore breccia. D) Sufide nodules/blobs found inside of the breccia. E) Disseminated breccia ore, with veins of pyrite and pyrrhotite running through. F) Leucograbbro with disseminated sulfides and chalcopyrite veinlets running through it.

The Santa Olalla Main Pluton and Aguablanca stock do show geochemical continuity, and therefore it is likely that their magma source was the same magma chamber at depth (Tornos et al., 2001). The reason for the presence of the breccia pipe is not quite clear. It could be that is was the feeder conduit of a pluton that is now eroded away. But the presence of so many cumulate fragments points to the possibility of the presence of a large magmatic stratiform complex / magma chamber more at depth, where pyroxenite, gabbro, norite and massive sulfides would be interbedded with each other in a stratiform manner (Tornos et al., 2001). Somehow something would have caused some overpressure inside this crystallized stratiform complex, causing the sulfide magma to shoot out from below (magmas are present more at depth). Supporting this theory is the fact that the clasts in the breccia show evidence of subsolidus deformation, meaning that they

would already have been crystallized before they got broken up and transported away, whereas the sulfides do not show any such evidence, meaning that they must have still been in the plastic state during brecciation (as blebs for example) (Tornos et al., 2001).

The mafic rocks of the Aguablanca stock shows quite high $^{87}Sr/^{86}Sr_i$ and low $^{143}Nd/^{144}Nd_i$ values, compared to other Variscan intrusions in the Ossa Morena Zone (Tornos et al., 2001). The values however, plot somewhere in between the values of unmineralized Variscan plutons and the host metasedimentary rocks in the region, pointing clearly to contamination. The Aguablanca stock must therefore indeed have undergone both fractional crystallization and contamination processes to come to its present composition. Additional evidence for the contamination of the host rocks to have happened includes the high orthopyroxene-olivine ratio in the igneous rocks, the presence of enclaves of sedimentary rock in the stock and the abundance of spinal in the gabbros.

This contamination also forms the basis behind the theory explaining the presence of sulfur in this particular intrusion. The sulfur is thought to have been incorporated from the host rocks via magmatic assimilation or metamorphic sulfur devolatization. Extensive interaction with the underlying black shales of the *Serie Negre* was probably critical. An immiscible sulfide liquid would have been formed, leaving behind a silica-rich element-depleted magma which crystallized to form pyroxenites and the bottom of the magma chamber and feeder zones. In general it seems to be a common trend for Cu-Ni mineralizations to be related to crustal contamination (Tornos et al., 2001). Once the chalcophile elements got inside of the immiscible sulfide liquid, they each had a different behavior throughout the fractionation process according to their partition coefficients. Some elements got partitioned into the monsulfide solid solution (mms) part of the sulfide liquid, and other more incompatible elements partitioned into the more Cu-rich sulfide fluid. The mms crystallized into pentlandite and pyrrhotite, whereas Cu-rich sulfide liquid crystallized into chalcopyrite (Piña et al., 2012).

The presence of the three different ore types discussed in the previous section, is also the result of the fractionation and crystallization of an immiscible sulfide liquid which was segregated from the mafic silicate melt (Piña et al., 2012). As already explained, PGE distribution is mainly governed by base metal sulfide (BMS) distribution. The PGE were also collected by the immiscible sulfide melt due to their high partition coefficients between the sulfide and silicate liquid. Later, during the sulfide fractionation, they were partitioned into the three different ore types (Piña et al., 2012).

Based on all this evidence, Tornos et al. (2001), propose a two-stage model explaining the evolution of the Aguablanca stock and the presence of the ore deposit (Fig. 6):

1) In the first stage is related to the extensional zones being created due to the transpressional tectonics during the Variscan orogeny. Extensive assimilation of the pyritic black slates happened in a conduit system (formed due to the extension) with a magma chamber in the middle crust. This contamination resulted in an immiscible sulfide magma being segregated from the remnant magma. The contamination also prevented the crystallization of olivine at that point, explaining the lack of thereof in the rocks. These two magma then rose further and formed another, shallower magma chamber. In this shallower magma chamber, fractional crystallization happened, forming a stratiform magmatic complex consisting of mafic and ultramafic cumulates interlayered with massive sulfides (very much like the textbook example of a magmatic Ni-Cu ore deposit).
2) This magma chamber was thus partly already crystallized into a stratiform magmatic complex, and party still had some residual magma inside it, when a second tectonic event took place. This event caused overpressure inside the magma chamber, triggering the residual melts to burst up, breaking up and entraining parts of the already consolidated cumulated with it. This is why in the present day breccia pipe sulfides occur both in de matrix (this was the residual magma), and in as sulfide blebs (which were already consolidated and interbedded in between the stratiform cumuli). The upward brecciation of the sequence happened due to the opening of tensional fractures related to the Chernaca ductile shear zone, triggering multiple melt injections (Piña et al., 2012).

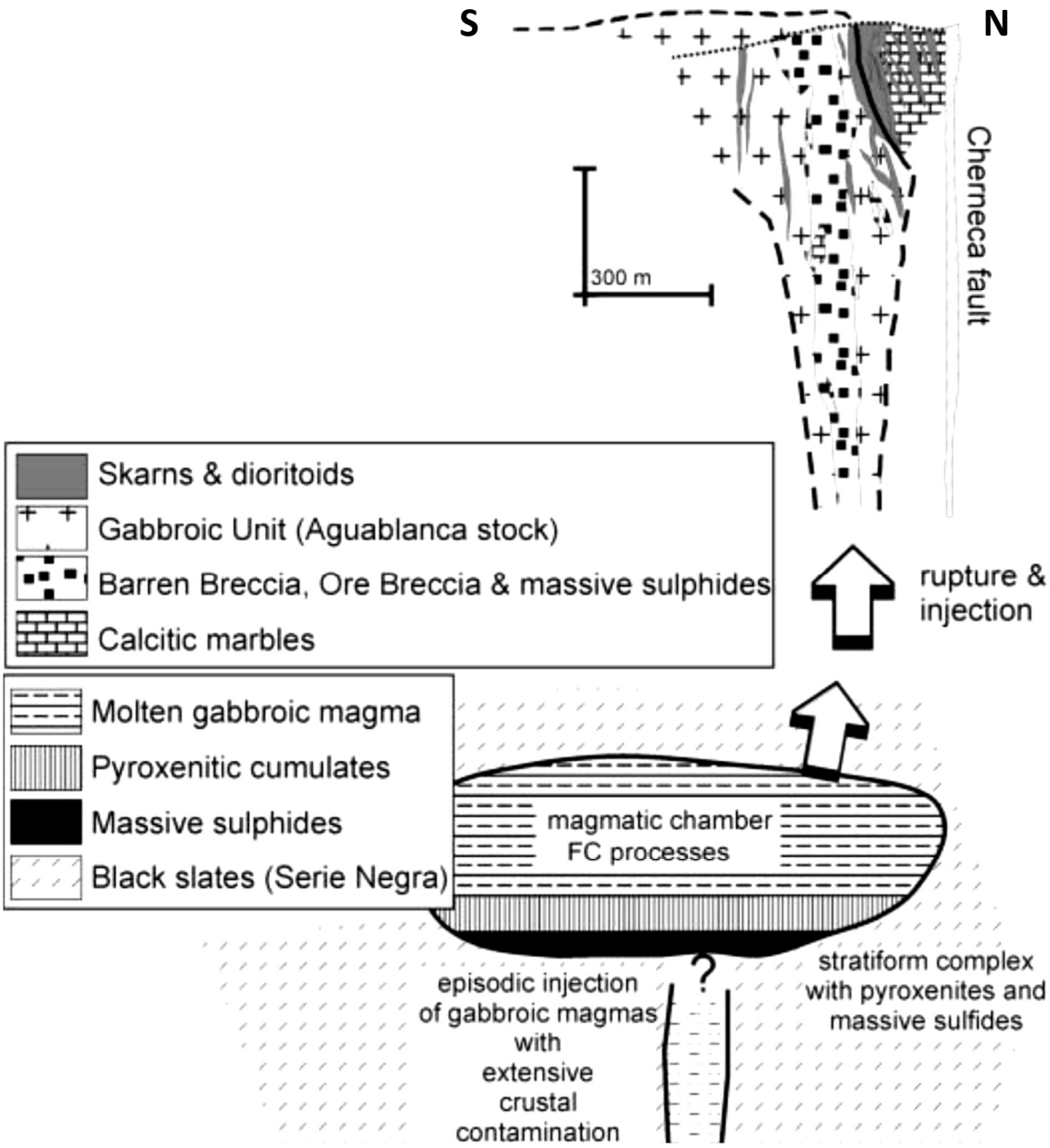

Figure 6. Geological model explaining the formation of the Aguablanca stock, according to Tornos et al. (2001).

References:

Casquet, C., galindo, C., Tornos, F., Velasco, F., Canales, A., 2001. The Aguablanca Cu-Ni ore deposit (Extremadura, Spain), a case of synorogenic orthmagmatic mineralization: age and isotope composition of magmas (Sr, Nd) and ore (S). Ore Geology Reviews, vol. 18, pp. 237-250.

Ortega, L., Lunar, R., García-Palomero, F., Moreno, T., Martín-Estévez, J. R., Prichard, H. M., Fisher, P. C., 2004. The Aguablanca Ni-Cu-PGE deposit, Southwestern Iberia: Magmatic ore-forming processes and retrograde evolution. The Canadian Mineralogist, vol. 42, pp. 325-350.

Piña, R., Gervilla, F., Barnes, S.-J., Ortega, L., Lunar, R., 2012. Distribution of platinum-group and chalcofile elements in the Aguablanca Ni-Cu sulfide deposit (SW Spain): Evidence from a LA-ICP-MS study. Chemical Geology, 302-303, 61-75.

Tornos, F., Casquet, C., Galindo, C., Velasco, F., Canales, A., 2001. A new style of Ni-Cu mineralization related to magmatic breccia pipes in a transpressional magmatic arc, Aguablanca, Spain. Mineralium Deposita, vol. 36, pp. 700-706.

11. Geology, geochemistry and formation of the giant Almadén Mercury deposit

Gabriela Ligeza

© Parque Minero de Almadén

Introduction

The giant Almadén area belongs to the main mercury district in the Iberian Peninsula. This mining district consists of the greatest accumulation of mercury in the world. In this area, there are 6 mines (Almadén, El Entredicho, Las Cuevas, Vieja Concepción, Nueva Concepción and Guadalperal) which account for more than 35% of worldwide Hg production (Palero-Fernandez et al.,2015). Out of these six mines, Almadén is known to be an unique deposit due to its giant size and geochemical variables. On a world-wide scale lies in the geological concentration process that has led to the accumulation of this huge amount of mercury, an element with a rather low average content at crustal level (about 67 ppb). Moreover, the Spanish deposits represent a unique geological context and show very different metallogenic characteristics from the rest of the world's mercury deposits, enabling us to speak of the "Almadén type"deposits.

Geological setting

The Almadén Mining District is located in central Spain, about 300 km SSW of Madrid and about 260 km to the NE of Seville. In the regional geological context, the Almadén Hg deposits lie in a great syncline near to the southern edge of Central-Iberian Zone (Fig. 1), according to the subdivision of the Variscan Iberian Massif made by Julivert et al. (1972). The rocks that crop out in the Almadén region are mainly siliciclastic, formed in diverse marine environments. Their original textures have not been altered by metamorphic processes (Saupé et al., 1977). The oldest rocks found in the anticlines (Late Precambrian) include the "Schist-Greywacke Complex" and they constitute a monotonous multilayered sequences of shales and greywackes formed in a turbiditic environment. On top of them there is a thick Paleozoic sedimentary sequences of rocks which were formed in a marine shelf basin and this sequence includes abundant volcanic intercalations. The different types of sediment are mainly the results of variations in the sea level in a stable basin, during Ordovician, Silurian and Lower Devonian times, allowing us to define several litho-stratigraphic units based the predominance of one of the following three lithologies: orthoquartzites, siltstones and black shales.

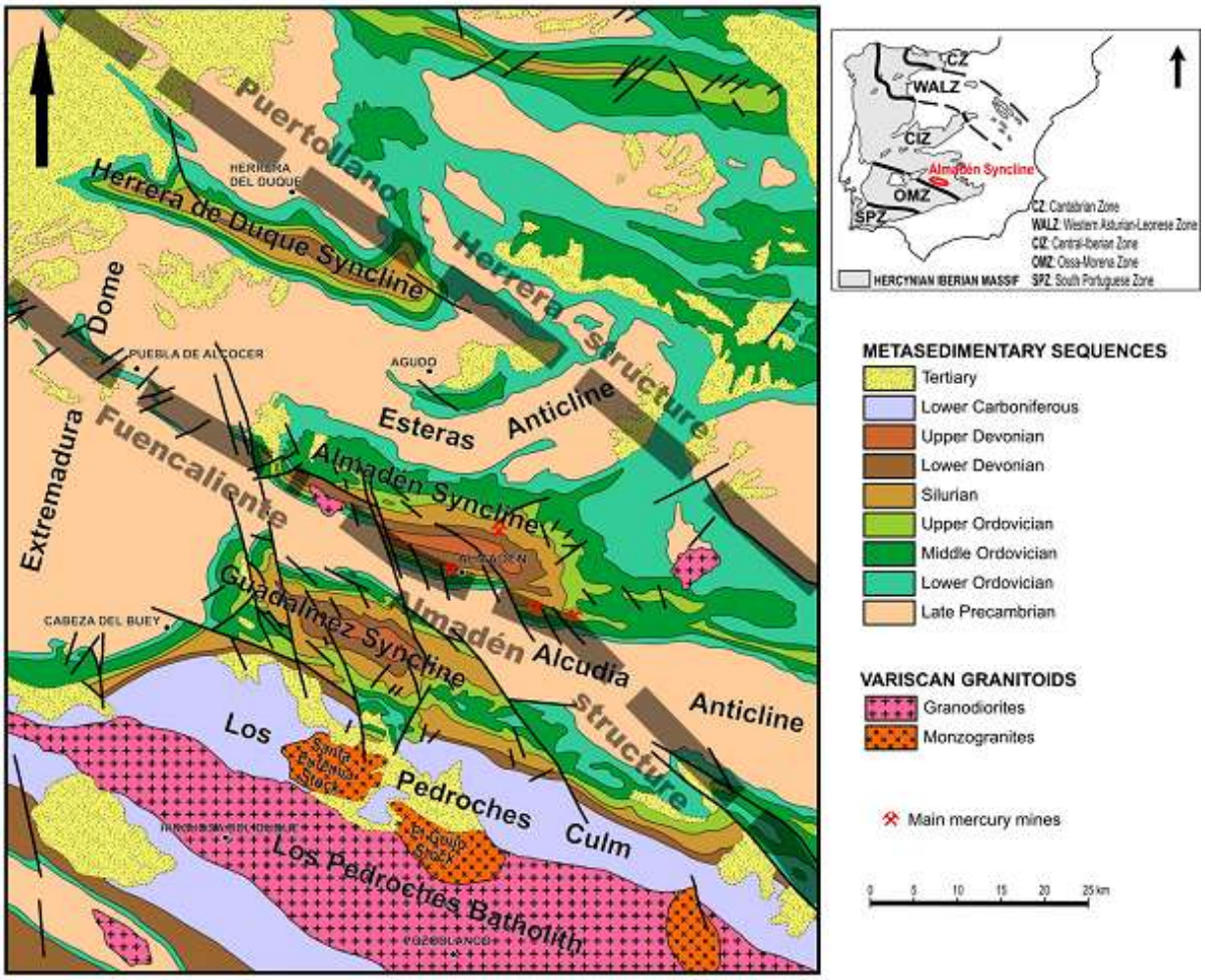

Figure 1: Geological map of Almaden area. Obtained from Palero-Fernandes et al. (2015).

The structural context and Variscan tectonism

Almadén Mining District is located in the the Almadén Syncline, which is 30 km long with a maximum width of 15 km, is an asymmetric WNW–ESE trending fold, wider in the east than in the west, since its south-easternflank is subvertical whereas its north-westernflank dips gently (Fig. 2). This is a peculiar feature of the fold, because its north vergence is opposite to that of the regional Variscan structures. This geometry was probably conditioned by the presence of the main NW–SE fracture system affecting the crust, which facilitated the Devonian basin subsidence and in turn facilitated the development of an asymmetric syncline during the Variscan shortening and the subvertical attitude of its southflank that was coincidentwith the crustal fractures.

The Variscan deformation around Almadén occurred in two stages (Ortega, 1992). Firstly, in the widespread stage (F1), due to near N-S shortening, the more important folds were formed on all scales and they were generated by buckling. Metamorphism was practically absent and only certain mafic volcanic rocks gave rise to neo-formed minerals in the zeolite facies (Higueras et al., 1995). The second tectonic stage (F2) consisted of a heterogeneous deformation produced by E–W shortening. The second Variscan stage (F2) affected the Almadén Syncline with variable intensity. It is mainly represented by fragile shear-bands, but conical geometry folds can be found too, resulting in interference between the E–W shortening and F1 folds.

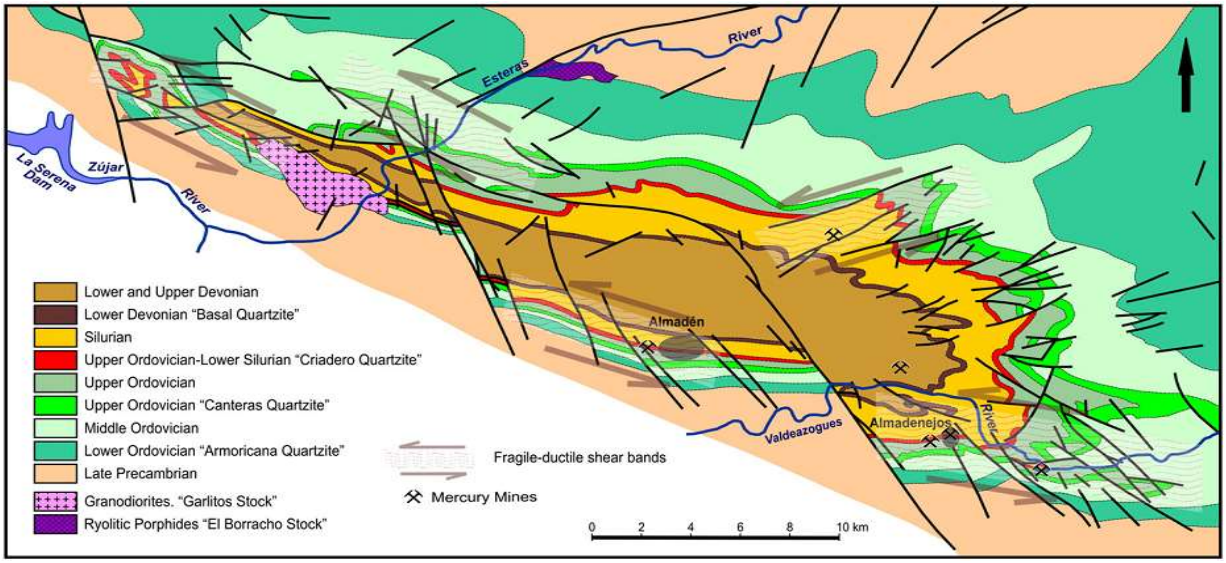

Figure 2: Geological map of Almadén syncline. Obtained from Palero-Fernandes et al. (2015).

Mineralization

The mercury deposits were found in the two different lithologies; a stratabound deposits (Fig.3a) and stockwork deposits (Fig.3 b/c/d). In the statabound deposits ore appears impregnating the rock and/or as fissure infilling the specific layers in the lower and upper parts og the orthoquartzite unit. The impregnation is the result of cinnabar filling the primary rock porosity, essentially the intergranular spaces or fissure in fillings (joints as described by Saupé, 1990).

The stockwork type deposits are mainly hosted in volcanic material, but minor amounts of mineralization can be found in detrital rocks, although in these cases the ores are always related to nearby volcanic rocks. The paragenesis is made up of cinnabar and pyrite as major minerals, accompanied by native mercury, pyrophylite, kaolinite, sericite, ankerite and quartz. A later mineralization with barite, siderite, dolomite–ankerite, chalcopyrite, pyrite and recrystallized cinnabar is also present. This later paragenesis is of little volumetric importance. The main mineralization infilled small veins and replaced volcanic rocks, the two processes being intimately related. Clear examples can be observed where the degree of replacement decreases with the distance from the massive cinnabar vein (Fig. 4). In detrital materials, the mineralization only infilled veins. The vein and replacement textures allow us to establish a sequence of crystallization of the main mineralization process. Pyrite was thefirst mineral to crystallize, followed by pyrophylite and kaolinite, then quartz, and finally cinnabar. The greater abundance of replacement mineralization in the volcanic rocks could be due to the fact that these rocks were easily altered, having previously undergone a strong carbonate alteration, in contrast to the lower susceptibility to alteration of the quarzites.

Geology of the Almadén Mine

The ore bodies in the Almadén mine have a stratabound character, with cinnabar located at very specific levels of the Criadero Quartzite unit. These ore bodies have been designated "San Pedro–San Diego Seam (SP)", San Francisco Seam (SF) and San Nicolas Seam (SN). The Criadero Quartzite in the Almadén mine is in a vertical position and subdivided into 3 intervals. From the lower to the upper parts, these are (Fig. 6):

1) "Lower Quartzite", with 8 to 15 m thick white orthoquartzite beds. This interval includes the San Pedro–San Diego Seam and is 3 to 8 m wide.
2) "Middle Black Shales", with 10 to 15 m of carbonaceous rich mudstones with frequent sandy pillow structures. This interval is always barren

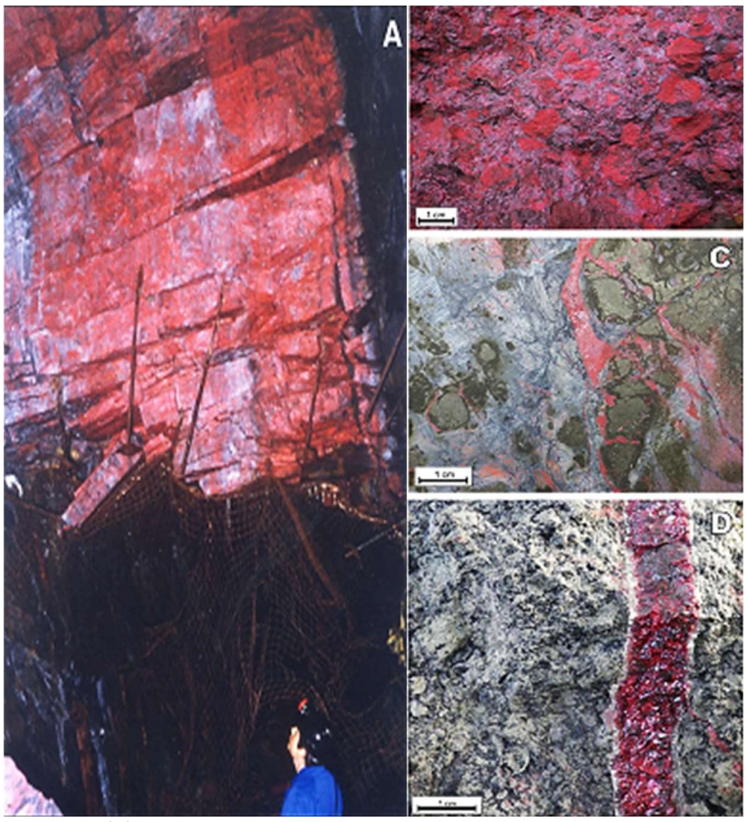

Figure 3: (a) Stratabound cinnabar in orthoquartzite beds, San Pedro Seam, 19th Level; (b) stockwork type; Massive replacement by cinnabar in breccia tuff rock. The replacement conserves the original volcanic rock texture; c) Replacement by pyrite and cinnabar in volcanic rocks. Pyritization is previous to cinnabrization. Hg ore is formed in absence of pyrite; (d) Cinnabar vein hosted in breccia tuff, with thinborders of pirophyllite and kaolinite. Obtained from Palero-Fernandes et al. (2015).

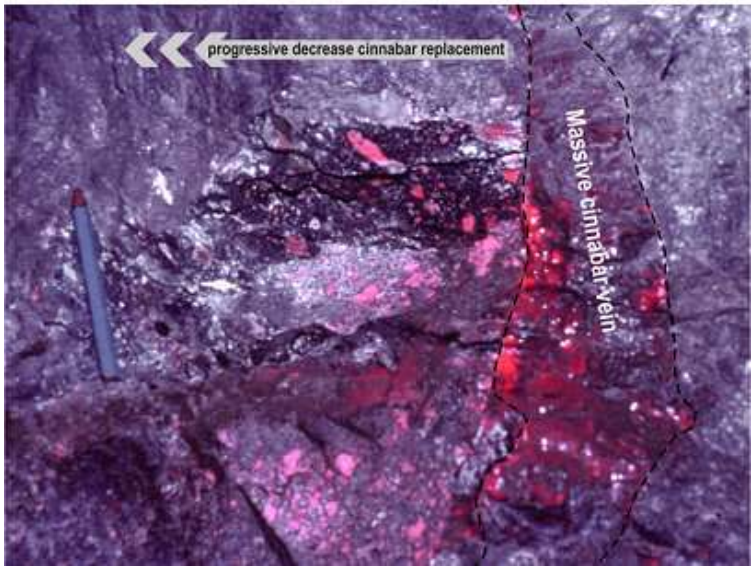

Figure 4: Progressive replacement by cinnabar in breccia tuff from a massive cinnabar vein. The replacement affects volcanic fragments and is strong near to the vein and decreases with increasing distance from the vein border. Obtained from Palero-Fernandes et al. (2015).

3) "Upper Quartzites", composed of 30 to 50 m of multilayered thin grey quartzite and fine micaceous siltstone beds. These beds become increasingly thicker and darker towards the top. San Francisco and San Nicolas seams are found in this upper part. These seams are from 2.5 to 5 m thick and separated by up to 8 m of fine-grained siltstone and carbonaceous mudstone beds. Tectonic wedging is responsible for the variation in thickness, or even absence, of this barren interbedded level.

Model of formation

Almadén deposit represents huge geochemical anomalies and its unique due to the lack of similar deposits of the same site and geological features worldwide (Palero-Fernandez et al., 2015). Therefore, it is challenging to establish a genetic model to explain their formation. Two hypotheses, which took into account the Paleozoic volcanic activity spatially related to Almadén area, have been postulated:

1) It is believed that mercury concentration was hosted in the shallow marine sediments that were later remobilized by the volcanic processed and then concentrated in a number of epigenetic structures (Saupe, 1990)
2) Mercury is believed to have a deep mantle origin, which rises to the surface together with the volcanic rocks, including ultramafic rocks of mantle affinity (Hernandez Sobrino et al., 1999; Higueras et al., 2013).

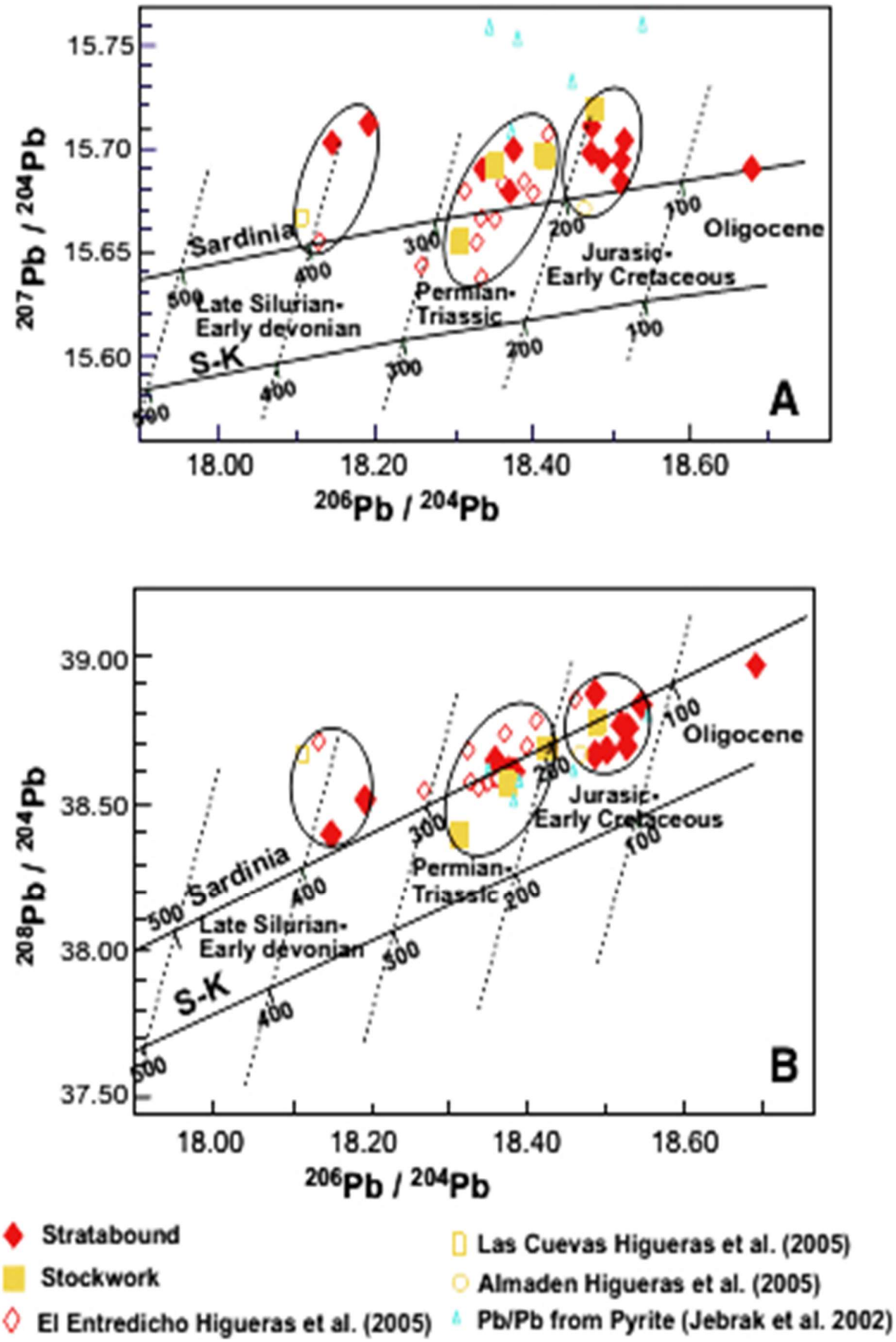

Figure 5: Pb isotopic ratios from the Almadén mines. SK is Stacey and Kramers (1975) growth curve and Sardinia is a two-stage Pb evolution curve proposed by Ludwig et al. (1989). Obtained from Palero-Fernandez et al. (2015).

The most recent studies of Palero-Ferndanez et al., 2015 report Pb isotopes from Almadén cinnabar deposits show a broad range of values, higher than those predicted for the Stacey and Kramers and Cumming and Richards crustal Pb evolution models but largely tallying with the Sardinia evolution line for this sector of the Variscan basement quite well (Fig.5). This shows that cinnabar is likely to have been mostly remobilized–crystallized during the regional extensional tectonic events, capturing lead from the host sedimentary sequence. This lead was mobilized by large scale, long term hydrothermal convective cells at various times, constituting a complex geotectonic history for the ore-forming processes.

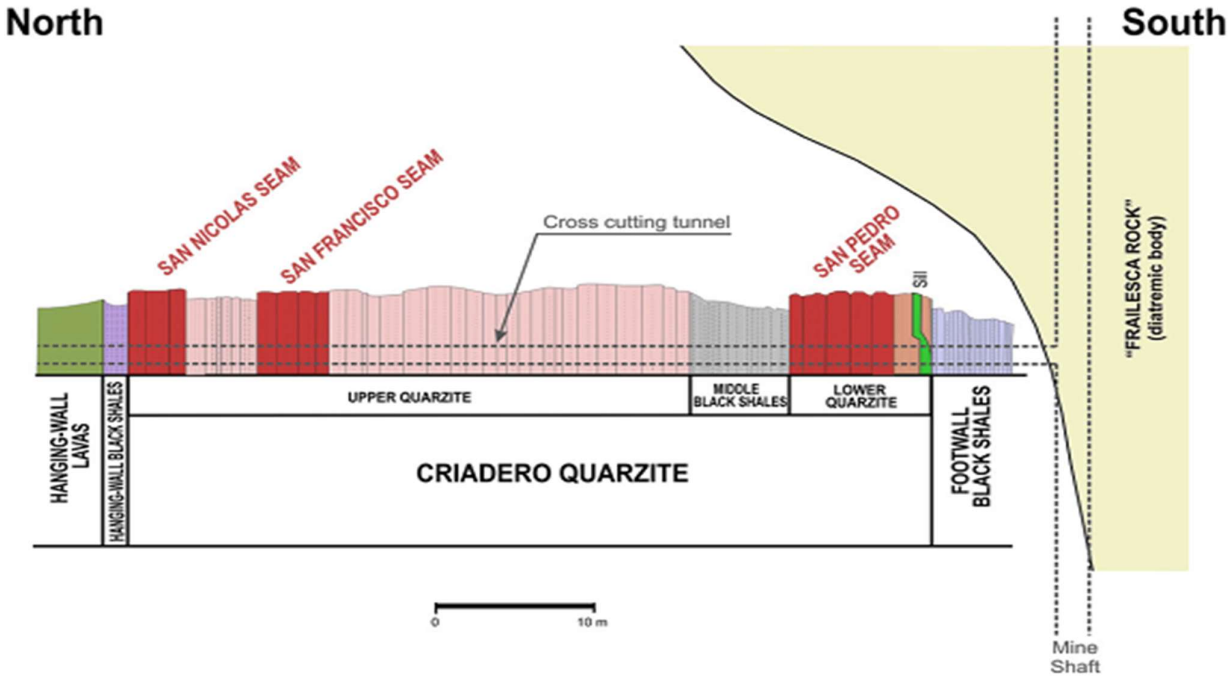

Figure 6: Typical lithostratigraphic section crossing Almadén Mine, including the three mined ore seams. Obtained from Palero-Fernandes et al. (2015).

References

Hernández Sobrino, A., Jébrak, M., Higueras, P., Oyarzun, R., Morata, D., Munhá, J., 1999.The Almadén mercury mining district, Spain. Miner. Deposita 34, 539–548.

Higueras, P., Oyarzun, R., Lillo, J., Morata, D., 2013. Intraplate mafic magmatism, degasification, and deposition of mercury: The giant Almadén mercury deposit (Spain) revisited. Ore Geol. Rev. 51, 93–102.

Julivert, M., Ribeiro, A., Conde, L., 1972. Memoria explicativa del Mapa Tectónico de la Península Ibérica y Baleares, Escala 1:100000. IGME, pp. 113.

Ludwig, K.R., Vollmer, R., Turi, B., Simmons, K.R., Perna, G., 1989.Isotopic constraints on the genesis of base-metal ores in southern and Central Sardinia. Eur. J. Mineral. 1, 657–666.

Palero-Fernández, F. J., Martin-Izard, A., Prieto, M. Z., & Mansilla-Plaza, L. (2015). Geological context and plumbotectonic evolution of the giant Almadén Mercury Deposit. *Ore Geology Reviews*, *64*, 71-88.

Saupé, F., 1990.The geology of the Almadén mercury deposit. Econ. Geol. 85, 482–510.

Stacey, J.S., Kramers, J.D., 1975.Approximation of terrestrial lead isotope evolution by a 2-stage model. Earth Planet. Sci. Lett. 26, 207–221.

Ortega, E., Hernández Sobrino, A., 1992.The mercury deposits of the Almadén syncline, Spain. Chron. Rech. Min. 506, 3–24.